

N O T I C E

THIS DOCUMENT HAS BEEN REPRODUCED FROM
MICROFICHE. ALTHOUGH IT IS RECOGNIZED THAT
CERTAIN PORTIONS ARE ILLEGIBLE, IT IS BEING RELEASED
IN THE INTEREST OF MAKING AVAILABLE AS MUCH
INFORMATION AS POSSIBLE

(NASA-CR-168421) EFFECTS OF HIGH ENERGY
RADIATION ON THE MECHANICAL PROPERTIES OF
EPOXY/GRAPHITE FIBER COMPOSITES Status
Report, 1 Jan. - 31 Dec. 1981 (North
Carolina State Univ.) 121 p HC A06/MF A01

N82-17267

Unclas
08895

G3/24



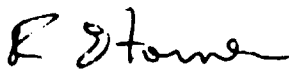
Status Report
on Grant Entitled

Effects of High Energy Radiation on the Mechanical Properties
of Epoxy/Graphite Fiber Composites

for the period January 1, 1981 - December 31, 1981

Grant No. NSG 1562-S4

Submitted by:



R. E. Fornes



J. D. Memory

Co-Principal Investigators
North Carolina State University
Raleigh, NC 27650



Table of Contents

	Page
I. Introduction	1
II. Mechanical Tests on Irradiated Samples	1
III. Mechanical Tests of Soaked Samples	3
IV. Preliminary ESCA (or XPS) Results	6
V. Electron Spin Resonance Studies	9
VI. X-Ray Diffraction Studies	12
VII. Appendices:	
A) Reprint of paper entitled "Effects of 1.33 Mev. Gamma Radiation and 0.5 Mev Electrons on the Mechanical Properties of Graphite Fiber Reinforced Composites" by R. E. Fornes, J. D. Memory and N. Naranong, <u>J. Appl. Polym. Sci. 26:2061-2066 (1981)</u>	
B) A copy of Master of Science thesis entitled "Characterization of a Cured Epoxy Resin Exposed to High Energy Radiation with Electron Spin Resonance" by Kevin R. Schaffer. This work was supported by funds from this grant.	
C) Copies of Abstracts of two papers presented at the American Physical Society Meeting in Phoenix, Arizona in March 1981.*	
1) "Effects of Ionizing Radiation on the Mechanical and Morphological Graphite Fiber Reinforced Composites," N. Naranong, K. Wolf, J. D. Memory, R. D. Gilbert and R. E. Fornes.	
2) "Electron Spin Resonance Studies of Epoxy Samples Exposed to 1/2 Mev Electrons," R. Schaffer, R. D. Gilbert, J. D. Memory and R. E. Fornes.	
*Other papers were presented at a seminar at the Polymer Group Meeting of the American Chemical Society in Raleigh, NC (January 1981); at Georgia Tech University (May 1981); and at the Fiber Science Gordon Research Conference (July 1981).	

I. Introduction

During the report period, work was continued on the effects of high energy radiation on graphite fiber reinforced composites. Included were studies of T300/5208 and C6000/PMR15 composites, T300 fibers and the resin system MY720/DDS (tetraglycidyl-4,4'-diaminodiphenyl methane cured with diaminodiphenyl sulfone). Radiation dose levels up to 8000 Mrads have been obtained with no deleterious effects on the breaking stress or modulus. The effects on the structure and morphology have been investigated using mechanical tests, electron spin resonance, X-ray diffraction, and electron spectroscopy for chemical analysis (ESCA or X-ray photoelectron spectroscopy). Details of these experiments and results are given below. In addition, we have continued studies of the fracture surfaces of irradiated samples with scanning electron microscopy and, at this time, our results indicate no differences in the morphology of irradiated and control samples.

II. Mechanical Tests of Irradiated Samples

The objective of this experiment was to examine the long-term effects of radiation on the mechanical properties, specifically ultimate stress and modulus measured by a three point bonding test, of unidirectional graphite fiber reinforced composites. Three different types of samples were used, namely T300/5208, C6000/PMR15 L, and C6000/PMR15 T. In the first two types the fiber axis is aligned to the longitudinal direction of the composite, whereas in the latter the fiber axis is aligned to the composite transverse direction.

The samples were placed in petri dishes and pre-vacuumed for one week in a heated desiccator at 80°C. They were placed in aluminum foil packages and

pre-vacuumed another week at 80°C. Immediately prior to irradiation, each foil package was vacuumed and heat-sealed through a glass tube. These packages were placed in nitrogen-filled Ziploc Baggies® during irradiation. Another set of samples was pre-vacuumed for one week in a heated desiccator at 80°C. These samples were attached inside Ziploc Baggies® using masking tape and were irradiated in air.

The samples were exposed to various levels of 0.5 MeV electron radiation with the maximum dose being 8000 Mrad. After irradiation, the samples were conditioned in a conditioned testing lab (70°F, 65% RH) for a minimum of two weeks before mechanical tests were performed. A three-point bending test was used to evaluate the ultimate stress and modulus of the composites. The samples were tested in rotating order to avoid machine bias in any given type.

The results of the mechanical tests are plotted in Figures 1-6 as a function of radiation dose for samples irradiated in air and in vacuum. For the T300/5208 samples, there was an increase in stress with radiation dose which was statistically significant. The value for the 8000 Mrad level was approximately 5-1/2% higher than the control value. The modulus values remained approximately constant with radiation dose for the T300/5208 samples. The stress and modulus data for the C6000/PMR15 L samples were somewhat variable and no trends were apparent. For the C6000/PMR15 T samples, the stress values showed an overall downward trend with increasing radiation dose; however, this decrease was not statistically significant. There were no significant differences between stress or modulus values of samples irradiated in air and those irradiated in vacuum.

One can conclude from this experiment that degradation due to radiation exposure is not apparent in longitudinal unidirectional samples until

extremely high doses, e.g. greater than 8000 Mrad, are reached. On the other hand, transverse samples exhibit slight degradation at low levels of radiation. These tests are essentially a measure of matrix and/or interface properties.

III. Mechanical Tests of Soaked Samples

The objective of these experiments was to study the effect of moisture on the mechanical properties of unidirectional graphite fiber reinforced composites. In the first experiment, six samples of each type were soaked in distilled water for one week at room temperature. The samples were taken from the water, surface dried, and tested with no laboratory conditioning. The ultimate stress and modulus values as determined by the three-point bending test are given in Table 1. The stress and modulus of the soaked T300/5208 samples showed a statistically significant increase over the dry samples. The C6000/PMR15 L samples exhibited a similar trend but the increase was not statistically significant. The stress and modulus values of the C6000/PMR15 T samples decreased upon soaking, but again this was not statistically significant.

Table 1
Results of Three-Point Bending Test

Composite Type	Stress ($\frac{Kg}{cm^2}$)		Modulus ($\frac{Kg}{cm^2}$)	
	Dry	Soaked	Dry	Soaked
T300/5208	21,700	22,400*	1,380,000	1,420,000*
C6000/PMR 15 longitudinal	19,900	20,200	971,000	993,000
C6000/PMR 15 transverse	981	807	74,800	73,500

*denotes significance at the 5% level but not at the 1% level

Note: Each value represents the mean of 6 samples.
Samples were soaked one week at room temperature.

To examine the effects of prolonged soaking, the above experiment was repeated with samples being soaked for four weeks at 80°C. The results of the three-point bending test are given in Table 2. The same trends were observed as in the previous experiment, but in this case the only statistically significant change was the decrease in stress for C6000/PMR 15 T.

Table 2
Results of Three-Point Bending Test

Composite Type	Stress ($\frac{Kg}{cm^2}$)		Modulus ($\frac{Kg}{cm^2}$)	
	Dry	Soaked	Dry	Soaked
T300/5208	21,700	22,000	1,380,000	1,350,000
C6000/PMR 15 longitudinal	19,800	21,000	971,000	1,060,000
C6000/PMR 15 transverse	981	751*	74,826	73,914

*denotes significant difference (at 5% and 1% levels)

Note: Each value represents the mean of 6 samples.
Samples were soaked 4 weeks at 80°C.

A third experiment was conducted to see if changes were time-dependent within the scope of the experiment. To ensure that all samples were completely dried out prior to soaking, the samples were pre-vacuumed. Nine samples of each type were placed in a vacuum desiccator at 80°C and vacuum pumped for three weeks. As before, samples were soaked in distilled water at 80°C. In this experiment, two exposure times were used--400 hours and 800 hours. Control samples remained in the heated desiccator during the soaking period. The results of the three-point bending test are given in Table 3. For both types of longitudinal samples, the stress and modulus for the control and soaked samples were approximately the same. For the C6000/PMR15 T samples, the stress values of the soaked samples were significantly lower. The modulus values were also lower.

Table 3
Results of Three-Point Bending Test

Composite Type	Stress ($\frac{Kg}{cm^2}$)			Modulus ($\frac{Kg}{cm^2}$)		
	Control	400 hr	800 hr	Control	400 hr	800 hr
T300/5208	20,900	21,100	21,000	1,340,000	1,310,000	1,300,000
C6000/PMR 15 longitudinal	20,500	19,200	20,400	1,100,000	914,000	1,060,000
C6000/PMR 15 transverse	1,020	842*	805*	79,700	73,300	75,100

*denotes significance at the 5% level but not at the 1% level.

Note: Each value represents the mean of 3 samples.
Samples were soaked at 80°C.

This experiment indicates that time is apparently not a factor in influencing changes in mechanical properties on a short-term scale. The increased stress and modulus observed when longitudinal samples were soaked probably are a result of internal stresses being relieved. The decrease in stress and modulus values upon soaking transverse samples is probably due to moisture absorption by the resin. It should be noted that similar trends are observed when composite samples are subjected to moisture and radiation.

IV. Preliminary ESCA Results

The objective of this experiment was to see if irradiation had an effect on the surface elements present in the graphite fiber composites, particularly since crosslinking of the resin was expected. The surface technique used to study composite samples was electron spectroscopy for chemical analysis

(ESCA) or x-ray photoelectron spectroscopy (XPS). This technique identifies elements with the exception of hydrogen, present on the surface of the specimen, and associates the binding energies detected to specific elements. By measuring the shift in binding energy of a particular element, one can assess the chemical bonding state of the element.

Three control samples of T300/5208 and three samples irradiated to 8000 Mrad were studied. The sample surfaces were washed with acetone prior to examination. For the control samples, the major elements were C and O and the minor elements were S, F, N, Cl, Na, and Si. For the irradiated samples, the major elements were C and O and the minor elements were S, N, Cl, Na, Si, and Al. Table 4 gives the atomic ratios of the elements present. Significant changes in concentration upon irradiation were seen for S, Cl, Na, and F. Possible changes in chemical state were observed for S, C, and Cl. Fluorine was probably eliminated as F_2 or HF. This phenomenon has been previously reported when fluorinated polymers were bombarded with electrons. There was an extremely large increase in surface oxidation as evident by the growth of the carbon 1s feature at 228 eV. This oxidation probably is manifested as a large increase in ketone or ester type carbons: $R-\overset{\text{O}}{\parallel}{C}-R'$ or $R-\overset{\text{O}}{\parallel}{C}-OR'$

Table 4

ESCA Analysis

Quantitative Analysis - Atomic Ratios Normalized to Carbon

<u>Element</u>	<u>Sample #</u>	<u>Control</u>	<u>Irradiated 8000 Mrad</u>	<u>Ratio Irradiated/ Control</u>
C	1	1	1	-
	2	1	1	-
	3	1	1	-
O	1	.264	.431	1.63
	2	.277	.443	1.60
	3	.295	.419	1.42
S	1	9.57×10^{-3}	1.96×10^{-2}	2.05
	2	1.92×10^{-2}	2.51×10^{-2}	1.31
	3	1.81×10^{-2}	2.04×10^{-2}	1.13
N	1	4.54×10^{-2}	4.62×10^{-2}	1.02
	2	4.26×10^{-2}	6.10×10^{-2}	1.43
	3	5.17×10^{-2}	4.59×10^{-2}	.888
Cl	1	1.89×10^{-2}	4.72×10^{-2}	2.49
	2	1.14×10^{-2}	4.08×10^{-2}	3.58
	3	1.55×10^{-2}	4.33×10^{-2}	2.79
Na	1	2.51×10^{-2}	4.95×10^{-2}	1.97
	2	3.68×10^{-2}	3.35×10^{-2}	.91
	3	3.19×10^{-2}	2.61×10^{-2}	.818
Si	1	6.01×10^{-2}	6.41×10^{-2}	1.07
	2	3.45×10^{-2}	8.49×10^{-2}	2.46
	3	6.26×10^{-2}	.126	2.01
F	1	5.79×10^{-2}	not detected	<0.1
	2	.130	not detected	<0.1
	3	3.86×10^{-2}	not detected	<0.1
Al	1	trace	2.07×10^{-2}	-
	2	trace	1.80×10^{-2}	-
	3	trace	2.05×10^{-2}	-

V. Electron Spin Resonance Studies**

Previous electron spin resonance (esr) studies have indicated that a large number of radicals are created in the epoxy resin matrix by high energy radiation, and that radical decay is fairly rapid due primarily to recombination. It was decided that esr characterization of epoxy resin samples varying in concentration ratio of hardener to epoxy might allow further insight into the nature of the radicals formed upon irradiation, as well as the mechanism of decay. Our earlier work** suggests that regions of high- and low-crosslink density are present in cured epoxy resins, and that the relative amount of these regions may depend on the percentage of hardener (crosslinking agent) present. Samples with a higher percentage of hardener would probably have a higher mole fraction of high-crosslink density regions.

Rod-like samples of Ciba Geigy Araldite (MY720) TGDDM (tetraglycidyl-4,4'-diaminodiphenyl methane) epoxy and Eporal DDS (4,4'-diaminodiphenyl sulfone) were prepared in various ratios as is shown in Table 5.

Table 5. Concentration Ratios of Epoxy and Hardener

<u>%DDS by wt.</u>	<u>%TGDDM by wt.</u>	<u>Molar Ratio DDS/TGDDM</u>
10	90	0.19
20	80	0.43
27	73	0.63
30	70	0.73
40	60	1.13

The percentage by weight ratio of TGDDM to DDS in composite samples currently being prepared by NASA is 73/27.

**See attached thesis for additional esr studies

Samples were prepared by slowly mixing in a jar the appropriate amount of DDS into the TGDDM while heating ($<110^{\circ}\text{C}$). In the sample containing 40% DDS by weight, considerable time was needed for all of the DDS to mix into the TGDDM. After mixing was complete, each jar was placed in a vacuum desiccator at 110°C allowing the sample to deaerate. Teflon tubes with an inside diameter of $3/32''$ were then pushed into each sample, and deaeration in the vacuum desiccator was continued. Each sample was then allowed to cool to room temperature while under a vacuum. The purpose of deaeration was to eliminate any air bubbles from the samples.

The Teflon tubes were then broken out of each jar and the ends were wrapped with Teflon tape. These samples were then cured in a vacuum desiccator under normal curing conditions: 137°C for 2 hours, then 160°C for 5 hours. Each rod-like sample was then pushed out of its Teflon tube.

Prior to irradiation, each sample was weighed, wrapped in aluminum foil, labeled, then vacuumed and flushed with nitrogen three times to remove any surface oxygen. Samples were placed in a dewar containing liquid nitrogen and then placed in the Cobalt 60 Gamma cell which irradiates with 1.17 and 1.33 MeV gamma radiation. The liquid nitrogen in the flask was replenished as necessary so that the samples would remain at cryogenic temperature, thus impeding the decay of radicals being formed.

After irradiation, radical concentration in each sample was obtained via a JEOL X-band ESR spectrometer. A sample holder which blows liquid nitrogen vapor over the sample while the reading is taken keeps the sample near $+77^{\circ}\text{K}$ and thus eliminates any radical decay. After the initial spectrum was obtained, each sample was allowed to decay at room temperature in an essentially oxygen free atmosphere for designated periods of time. Decay was

interrupted by placing the samples back into a dewar of liquid nitrogen, and additional spectra versus time at room temperature were obtained. This allowed the construction of a decay plot for each sample showing radical concentration versus time.

The initial experiments involved irradiation of samples in the gamma cell to a dosage of 5 Mrad's. Figure 7 shows the effect concentration ratio of epoxy to hardener has on radical decay behavior. Radical decay is much more significant the lower the percentage of hardener present. A lower percentage of hardener implies a low percentage of high-crosslink density regions, and this facilitates recombination. Thus, the lower the percentage of hardener, the more rapid the decay of radicals.

Samples containing 10% DDS by weight were rather brittle prior to irradiation. After irradiation, these samples were extremely brittle and crumbled upon mounting in the ESR sample holder. Data for 20/10 samples is therefore not available.

Our earlier work has shown that radical decay occurs according to two simultaneous second order reactions occurring in different zones. The initial portion of the decay curves in Figure 7 depicts the rapid decay which occurs in the zones of the low-crosslink density while the latter portion of the curves shows the slow decay occurring in the high-crosslink density zones.

The characteristics of the decay of these samples irradiated at 5 Mrad was found to be reproducible.

Radical decay data has also been obtained on samples irradiated with gamma radiation to a dose of 30 Mrad and is shown in Figure 8. As with the lower dose samples, decay is more significant with samples containing a lower percentage of hardener; however, the difference is not as significant with

the sample irradiated at higher dose as it is with the sample irradiated at lower dose.

It should be noted that the expected positions of the 73/27 and 70/30 curves in Figure 8 are reversed. This is most likely due to statistical variation since there is little difference between the percent hardener in each.

Continued investigation into the role of percent of hardener and radiation dose on radical decay is proposed. Also scheduled is the obtaining of decay data on samples of 100% TGDDM and 100% DDS irradiated with gamma radiation. This would test the hypothesis that the effects shown in Figures 7 and 8 are not merely due to an increase in the amount of DDS percent, but are due to the extent of crosslinking. (An alternate solution would be to prepare samples of 50, 60, 70, etc., percent by weight DDS, in which case the radical decay rate should progressively increase. However, mixing much more than 40% by weight DDS with TGDDM does not appear to be physically possible.)

VI. X-Ray Diffraction

Our work has demonstrated that graphite fiber reinforced epoxy resin composites show little change in stress and modulus when exposed to as much as 8000 Mrad's of 0.5 MeV electron radiation while under a vacuum. It was decided that X-ray diffraction should be used to look for any possible change in the crystallite dimensions or crystallinity of the fibers upon irradiation.

The most intense reflection in the X-ray pattern of graphite is an (002) reflection due to the staggered nature of the layered carbon rings. The reflection appears on the equator since the layers are parallel to the fiber

axis (due to the way the c-axis is defined as perpendicular to the fiber axis).

X-ray diffraction patterns were obtained for both irradiated and non-irradiated composite samples and graphite fiber samples of Thornel T-300/5208. $\text{Cu}_{K\alpha}$ radiation was used throughout. Figure 9 shows X-ray photographs of a control composite (left) and one irradiated with 8000 Mrad's with electron radiation.

Both diagrams show the (002) reflections on the equator and a halo caused by scattering from the amorphous epoxy-resin matrix (scattering patterns of graphite fibers alone show no amorphous halo). The bright spots on either side of the lead dot are caused by scattering of unfiltered white radiation and should be disregarded.

The (002) reflections in both samples correspond to a Bragg angle of $\theta = 12.46^\circ$ which indicates an interatomic spacing of 3.57\AA or a unit cell C-axis dimension of 7.14\AA . As expected, this is slightly larger than the interatomic spacing found in natural graphite.

The arc length of the reflection indicates the level of orientation in the fibers; however, it is the arc width that indicates the crystallite size and perfection--the wider the arc widths, the smaller the crystal.

Microdensitometer traces of X-ray negatives showed essentially no difference in arc widths between the irradiated and control samples as indicated by the width at half intensity of the peaks traced. Figures 10 and 11 show the microdensitometer equatorial and meridional traces respectively, for a control composite and one irradiated to 8000 Mrad's.

Diffractometer plots of irradiated and non-irradiated samples gave essentially the same information--that there was no difference in the arc widths. Both the microdensitometer and the diffractometer results show a line width of around 5° (in terms of 2θ) and this corresponds to values found in the literature.

In conclusion, $1/2$ MeV electron radiation up to 8000 Mrad's causes no disruption of crystallites in the graphite fibers as indicated by the constancy of the (002) reflection width measured with the microdensitometer and diffractometer.

Figure 1

T300/5208

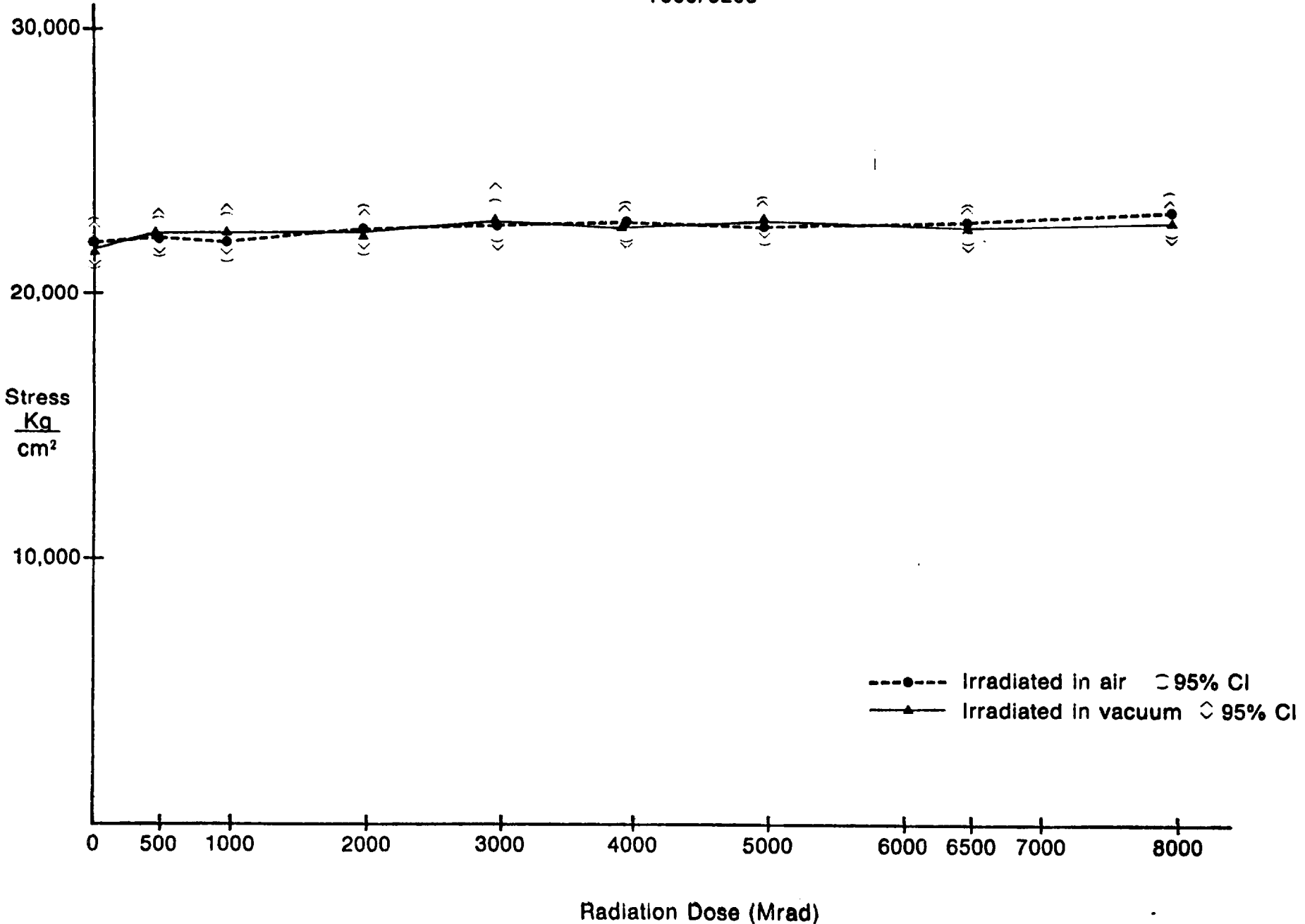


Figure 2
C6000/PMR 15 L

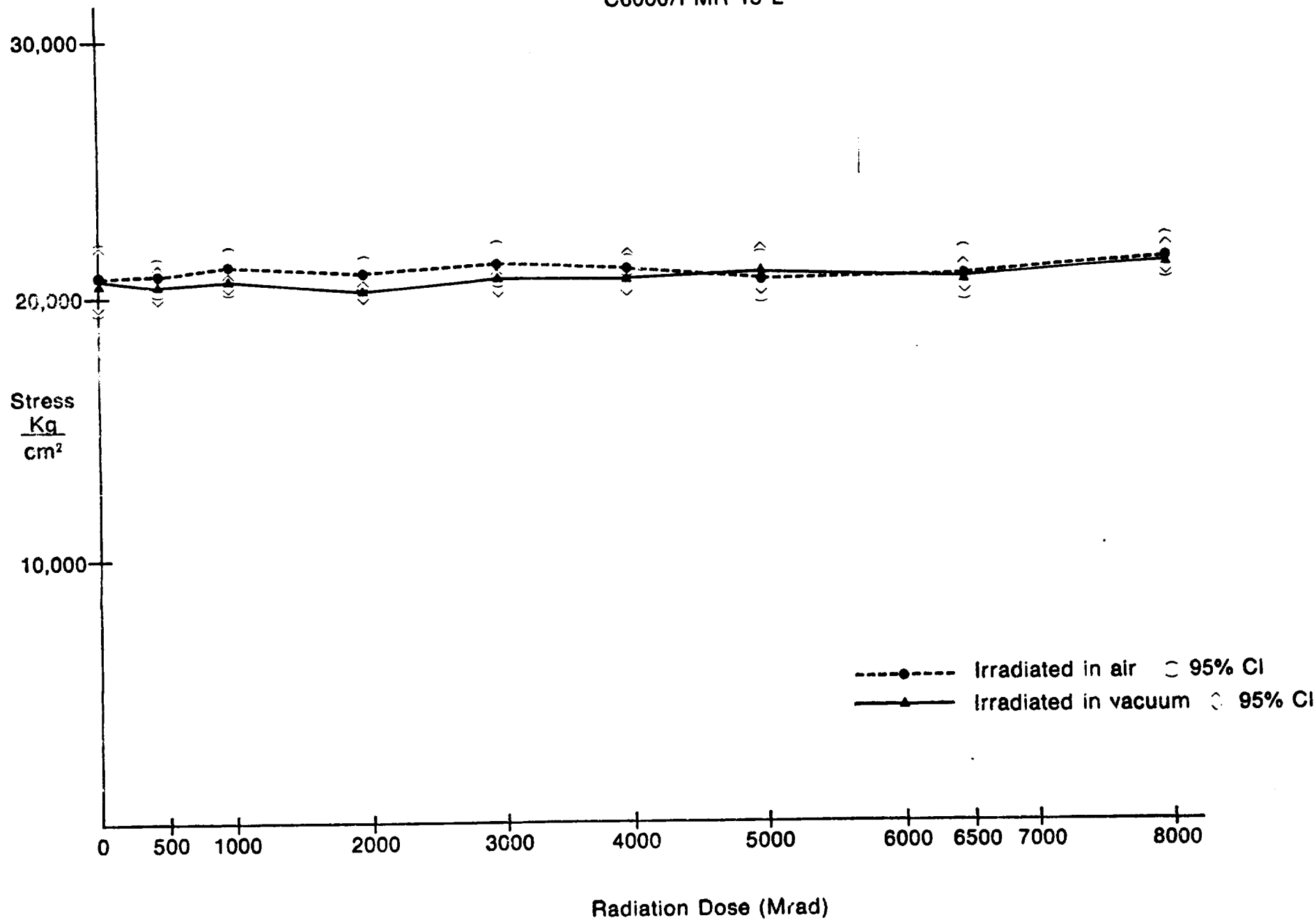


Figure 3

C6000/PMR 15 T

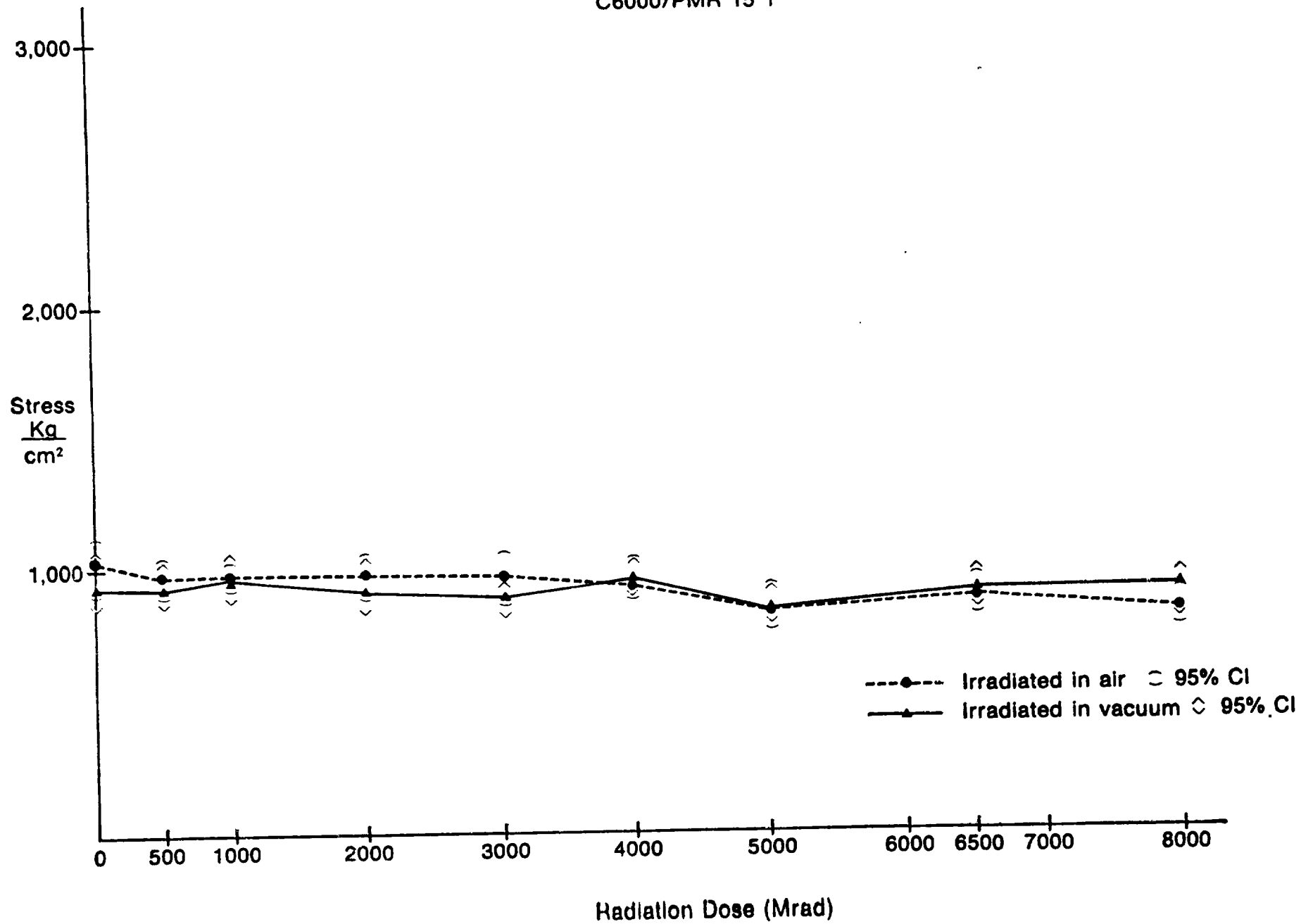


Figure 4

T300/5208

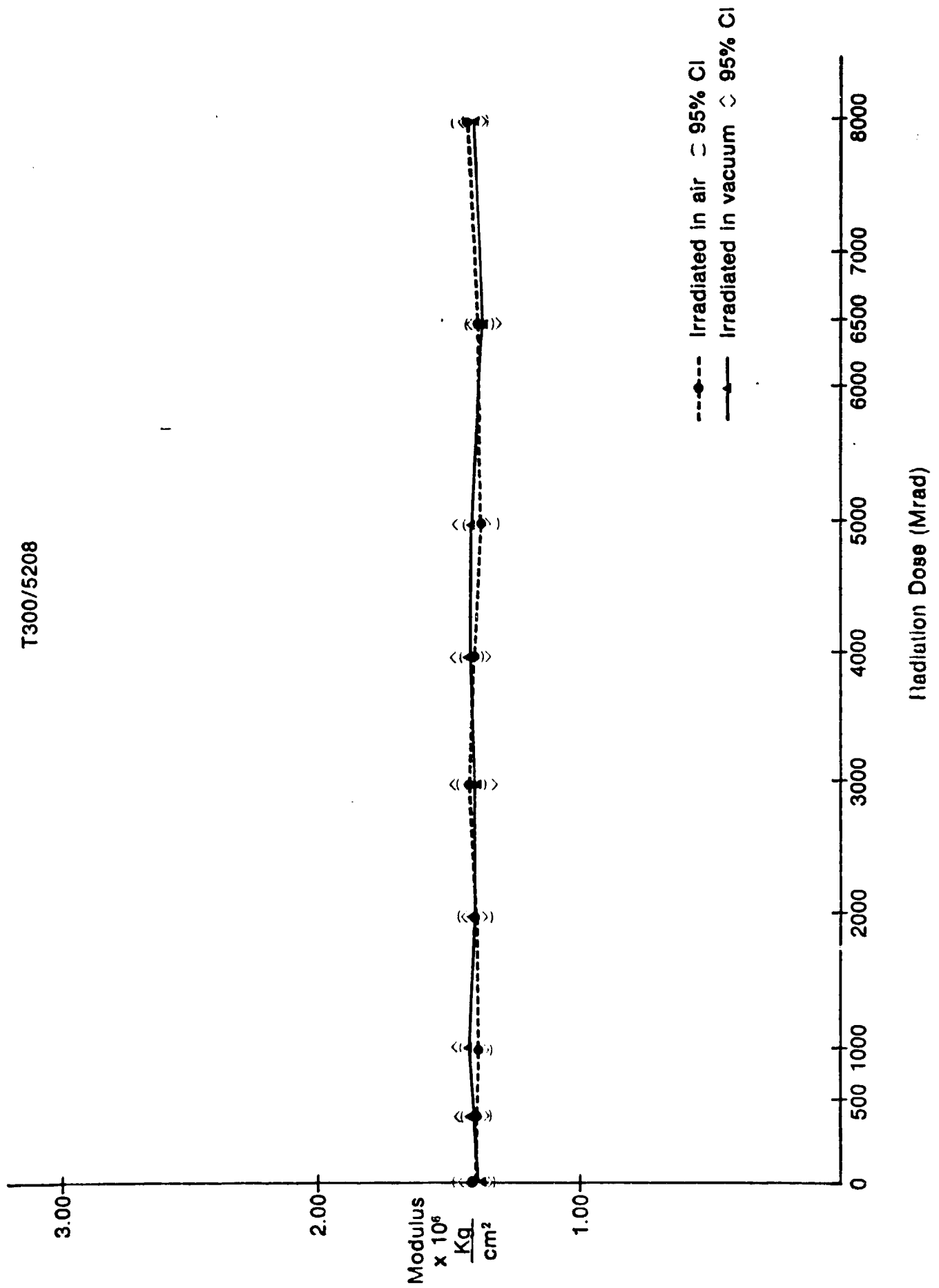


Figure 5
C6000/PMR 15 L

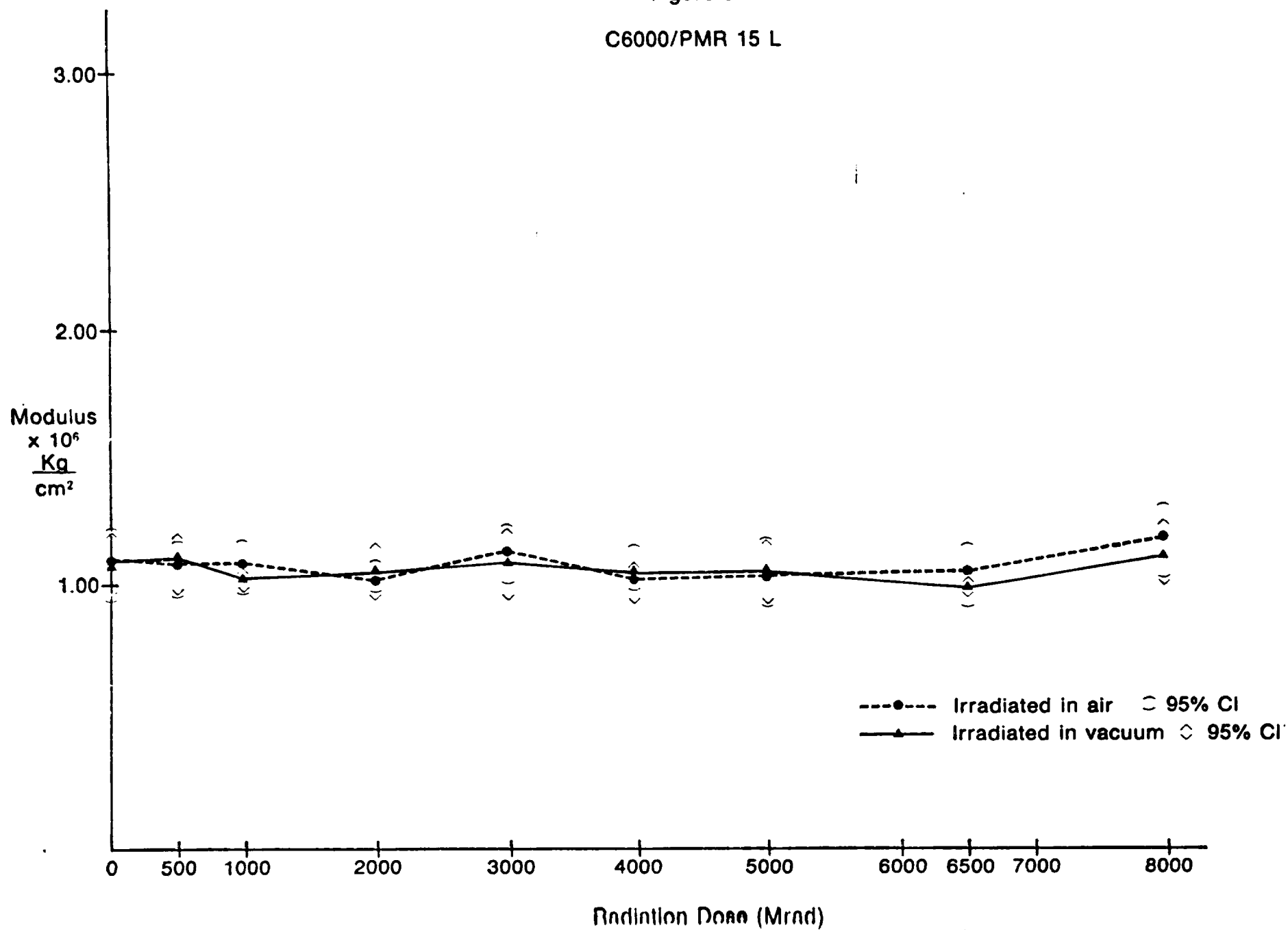
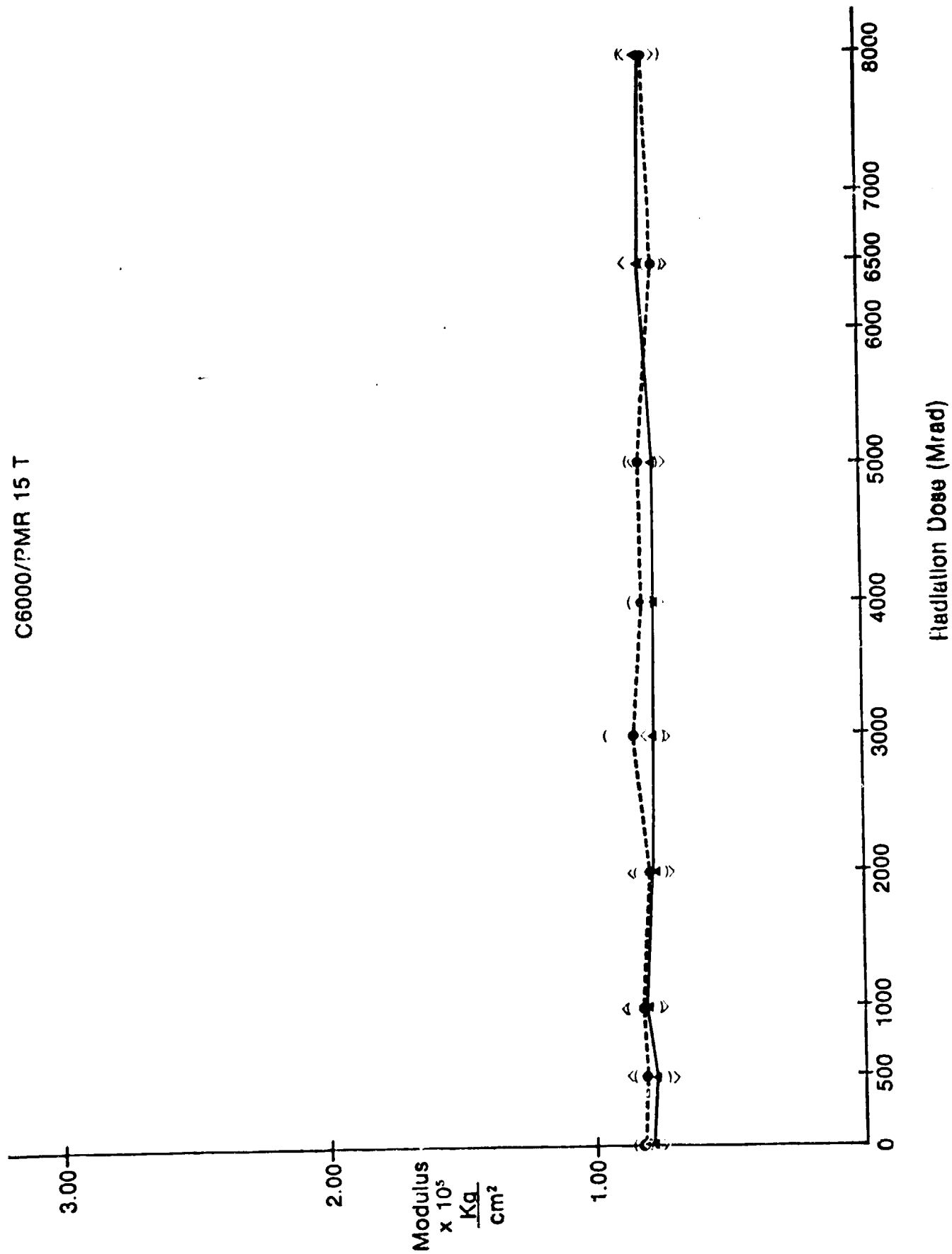
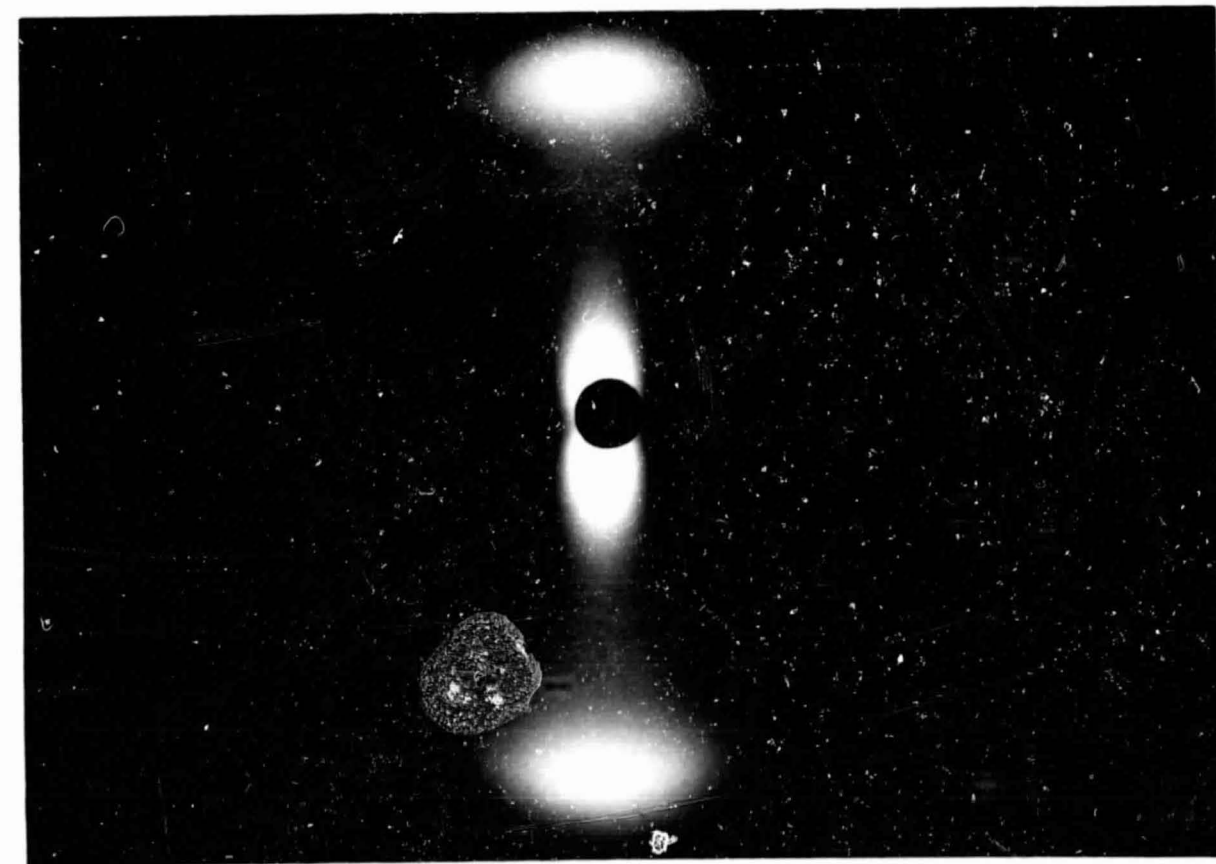


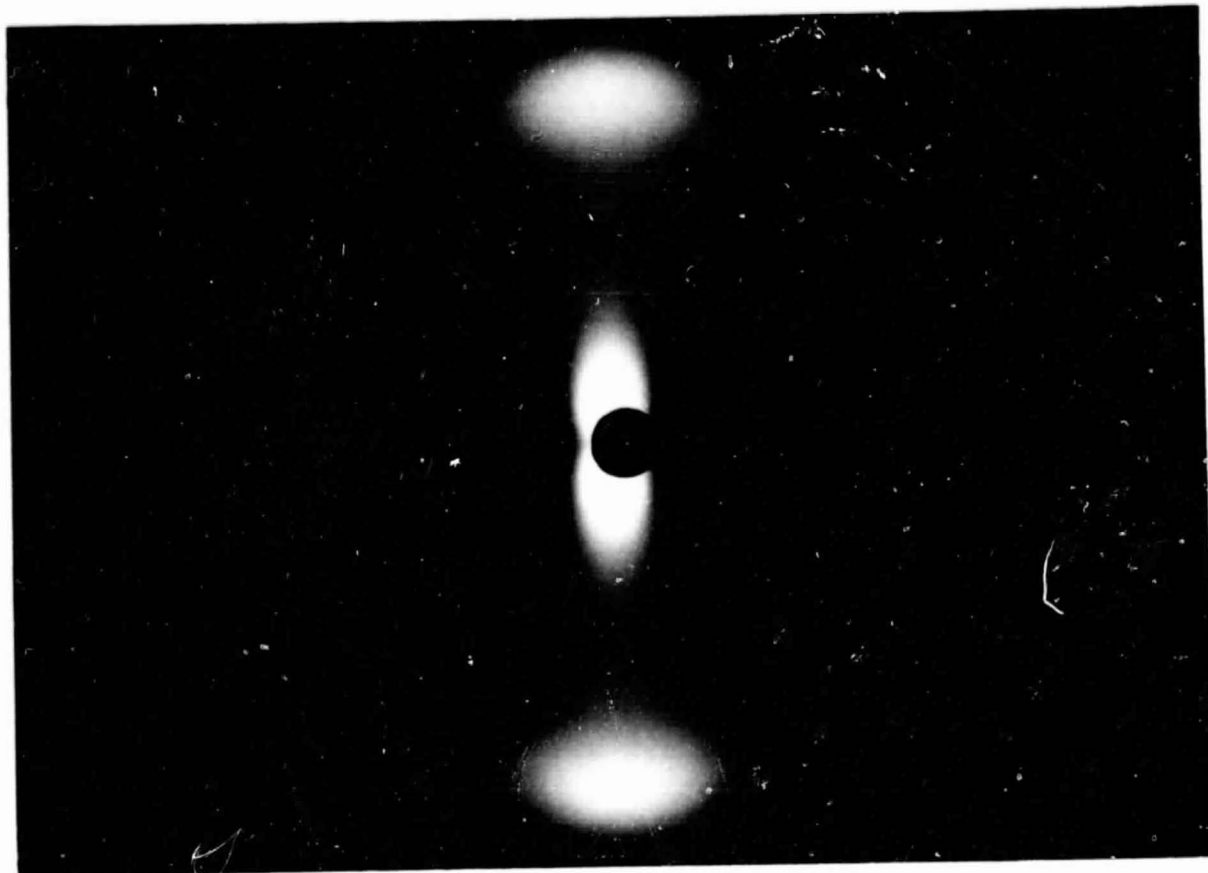
Figure 6

C6000/PMR 15 T





A. Control



B. 8000 Mrad of 1/2 Mev electrons

ORIGINAL PAGE
BLACK AND WHITE PHOTOGRAPH

Figure 9
X-Ray Diffraction Pattern of Uniaxial Graphite Fiber Composite (T300/5208)

Figure 10

X-ray Microdensitometer Trace
Equatorial Trace - T300/5208

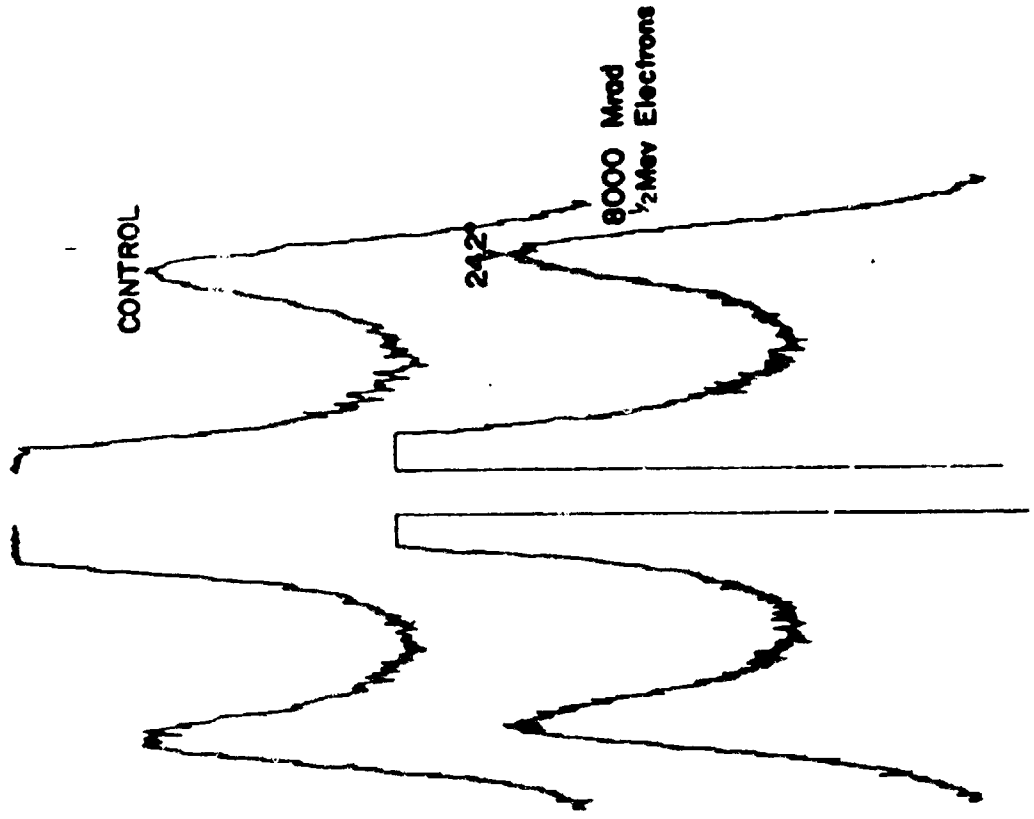


Figure 11

**X-ray Microdensitometer
Meridional Trace - T300/5208**

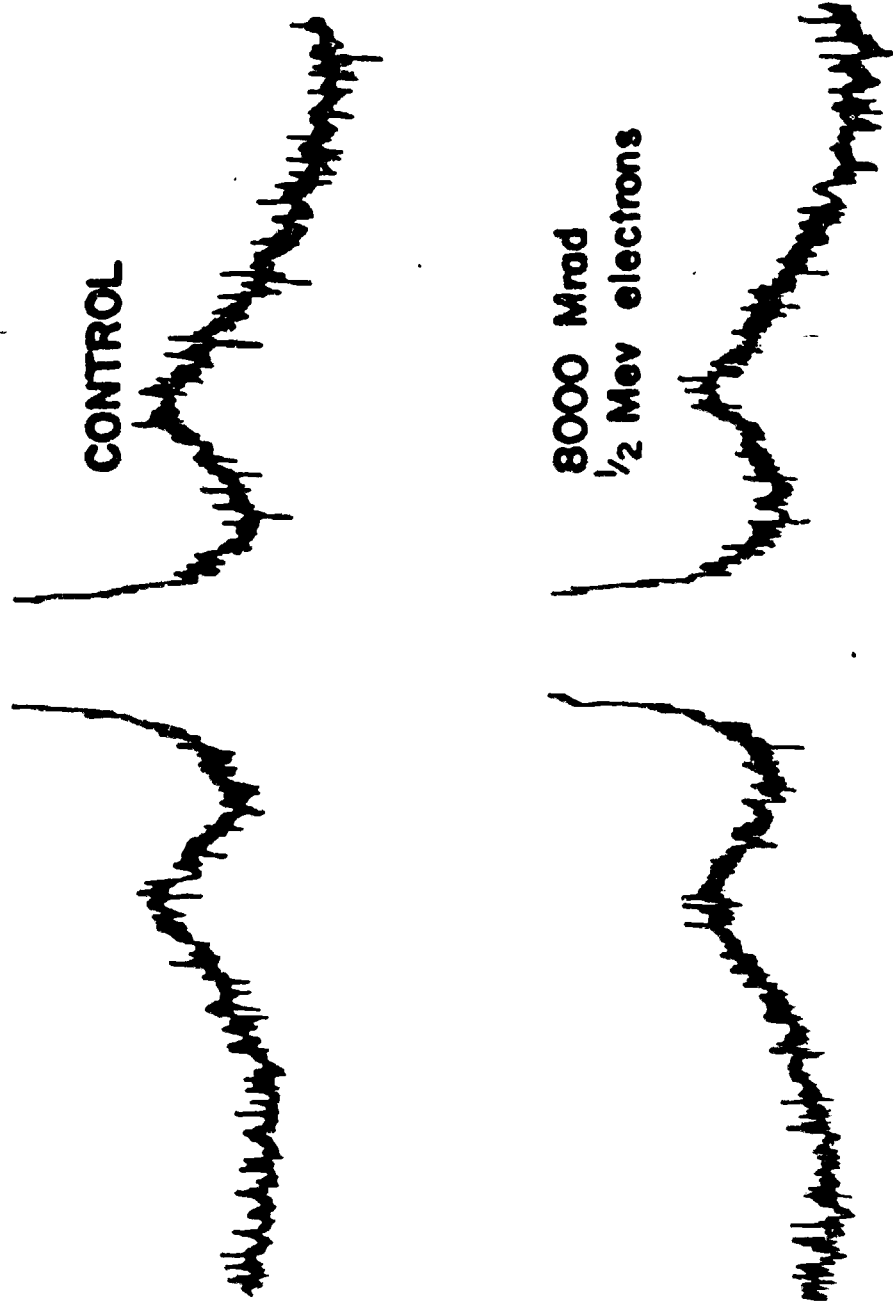


Figure 7

SPINS PER GRAM VS. DECAY TIME

at various epoxy/hardener ratios

Ratios of Epoxy/Hardener

- 60/40
- 70/30
- △ 73/27
- 80/20

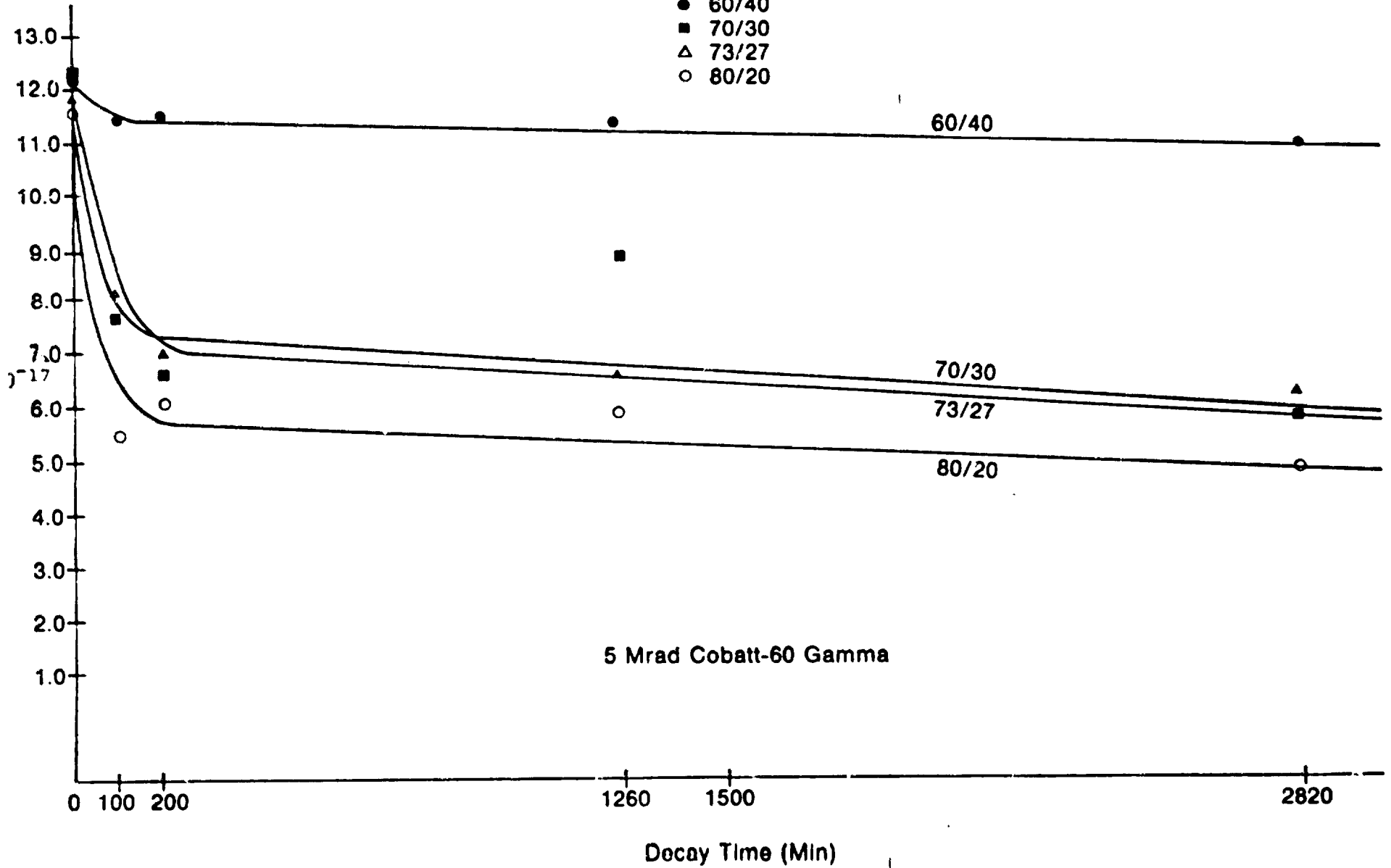


Figure 8

SPINS PER GRAM VS. DECAY TIME

at various epoxy/hardener ratios

30 Mrad Cobatt-60 Gamma

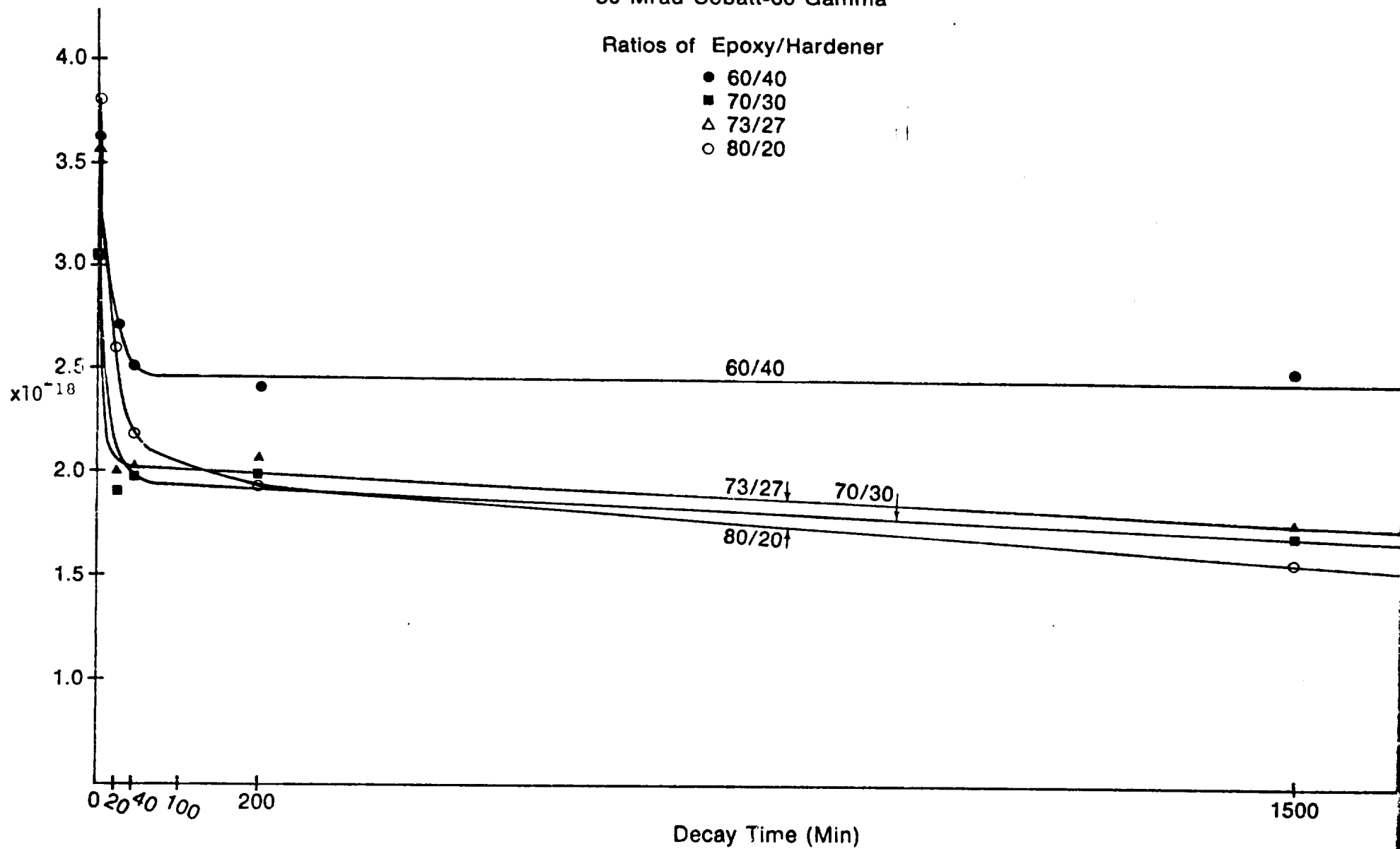
Ratios of Epoxy/Hardener

● 60/40

■ 70/30

△ 73/27

○ 80/20



Effect of 1.33 MeV γ Radiation and 0.5 MeV Electrons on the Mechanical Properties of Graphite Fiber Composites*

R. E. FORNES, J. D. MEMORY, and N. NARANONG, *North Carolina
State University, Raleigh, North Carolina 27650*

Synopsis

Epoxy/graphite fiber, polyimide/graphite fiber, and polysulfone/graphite fiber composites were exposed to 1.33 MeV γ irradiation and 0.5 MeV electron bombardment for varying periods of time. The effects of the irradiation treatments on the breaking stress and Young's modulus were studied by a three point bending test. Effects were small; indeed, both electron radiation up to 5000 Mrad and γ radiation up to 350 Mrad resulted in slight increases in both stress and modulus.

INTRODUCTION

Graphite fiber reinforced composites are light-weight high-strength materials that are particularly suitable for space vehicles. Since some space experiments are scheduled over a period of several years, materials used in space may be subjected to substantial quantities of high-energy radiation. For this reason, it is important that materials considered for use in these experiments be evaluated with respect to their response to high-energy radiation.

Several sets of composite samples, fabricated at NASA Langley Research Center and supplied to us, have been irradiated using 0.5 MeV electrons and 1.33 MeV γ radiation. The effects of the irradiation treatments on breaking stress and Young's modulus were determined by a three point bending test.

Most of the cosmic radiation in regions near the earth is due to protons.¹ However, significant numbers of both protons and electrons are trapped in the radiation belts around the earth^{2,3} and the predominant energy loss in matter of high-energy electrons found in geosynchronous orbit is by ionization.^{3,4} Similarly, 1.33 MeV γ radiation would lose most of its energy by ionization through Compton scattering and the photoelectric effect.⁵ Therefore, the experimental conditions of radiation exposure of materials to be investigated in this study should provide an excellent simulation of the actual effects of radiation on these materials when used in space applications. Moreover, it has been estimated⁶ that the radiation dose for geosynchronous orbit in a thirty year lifetime should be on the order of 1000 Mrad for the 0.056–0.081 cm thickness of the samples we used in the experimental work reported here. This, coupled with the observation that radiation effects on solid polymers are dose rate independent to first order,⁷ should indicate that the results described in this paper for doses up to 5000 Mrad should be applicable to the problem of estimating the radiation effects on space vehicles in geosynchronous orbit.

* Supported in part by NASA Grant No. NSG 1562-S2.

EXPERIMENTAL PROCEDURES

Studies were made on samples of cured graphite fiber/epoxy composite (T300/520B Thornel graphite fiber/Narmco 5208 epoxy and AS/3501 graphite fiber/epoxy by Hercules), graphite fiber/polyimide composite (C6000/PMR-15 Celion graphite fiber/polyimide matrix), and graphite fiber/polysulfone composite (C6000/P1700 Celion graphite fiber/polysulfone matrix). The samples were cured and cut at NASA Langley Research Center. Samples of each type were subjected for different periods of time to electron irradiation, and samples of graphite fiber/epoxy were γ irradiated for different periods of time.

The mechanical tests were made on an Instron using a "three-point bending tester" attachment.⁸ The specimens, 1.27 by 2.54 cm and 0.056–0.071 cm thick, were tested at a constant rate of elongation, perpendicular to the plane of the composites, at a speed of 0.254 cm/min (0.1 in./min) and with a span length of 1.40 cm (0.55 in.). The specimens were four-ply uniaxially oriented with the preferred axis aligned along the span direction during testing. The ultimate stress and average modulus at each exposure condition were determined by using the standard equations for small bending deformations of elastic bodies.⁸

The samples were treated in a vacuum desiccator at 80°C for 7 days, then sealed in aluminum foil (Reynolds Wrap, heavy duty, thickness of 0.025 mm) by first securing the ends of the samples in place with a thin layer of Scotch tape and sealing the edges of the folded aluminum wrap with an epoxy glue (Devcon 5 min Epoxy[®]). An open glass tube was inserted prior to sealing the foil to permit a vacuum line to be connected for further vacuum treatment. These packages were placed in a vacuum desiccator at 80°C for at least an additional 4 days; then the glass tube was attached to a vacuum line and heat sealed. The packages then were taken immediately to the electron accelerator and exposed to 0.5 MeV electrons at a current of 8.3 mA. Each package was placed in a ziploc baggie by Dow Chemical (10 by 10 in.) that was prefilled with N₂ to reduce oxidative degradation in case of pin hole leaks, the packages clamped to the conveyor on the accelerator, and passed through the electron beam. Each revolution of the conveyor through the beam resulted in a 10 Mrad dosage. Following the electron irradiation treatment in a 500 kV Electron accelerator made by High Voltage Engineering Corporation, the specimens were removed from the packages and placed in open petri containers in a controlled laboratory (relative humidity 65%, temperature 20°C) where they remained from 3 to 10 weeks prior to mechanical testing. Following each 400–500 Mrad exposure, the Ziploc baggies were replaced and refilled with N₂. After 2500 Mrad, the Al foil in regions of high stress concentrations (sharp bends) showed evidence of degradation and the Devcon epoxy seal on the aluminum foil showed evidence of appreciable discoloration, so the specimen were vacuumed and repackaged in new Al foil as described above.

Two sets of samples, T300/5208 and AS/3501, were exposed to 1.33 MeV γ radiation for periods up to 500 and 1070 h, respectively, in a Gamma Cell 220 made by Atomic Energy of Canada. These samples were vacuum desiccated at 80°C for a minimum of 3 days then placed in the vacuum chamber of the gamma cell (a $\frac{1}{10}$ Mrad/h ⁶⁰Co source), prevacuumed treated for 24 hr and exposed to γ radiation under a continuous vacuum (approximately 5×10^{-6} Torr). The samples, after γ exposure, were tested using the same procedures for equilibration and mechanical testing as described above.

RESULTS AND DISCUSSION

The theoretical prediction of stopping power of high energy electrons is given as by Segre.⁵

However, due to a secondary scattering, the effective irradiation dosage in a material will first increase and then is followed by a rapid monotonic decrease in radiation dosage.⁹ Since the electron accelerator used in our experiments is designed to pass samples across the beam twice during each revolution of the conveyor (once on the front side of the sample and once on the back side), the approximate dosage experienced by the composite specimens as a function of penetration depth is as shown in Figure 1. The density of the composite is about 1.55 g/cm³. The effective thickness of the baggie and aluminum foil is approximately 0.013 cm. Thus, the effective radiation dosage in the center of the specimen is approximately 40% higher than on the edge.

The load deformation curves of the three point bending tests were approximately linear in all cases and the deflections small so that equations for small bending deformations give excellent approximations of ultimate stress and Young's modulus.⁸ Effects of electrons and γ radiation on these parameters for the samples investigated are summarized in Figures 2-5. A minimum of ten replication measurements were made for each exposure condition. All samples exposed to 5000 Mrad of 0.5 MeV electrons showed a slight increase in both stress and modulus compared with the control. In each case, the increases were essentially monotonic. The increases at 5000 mrad to the control were 13%, 10%, and 11.5% in stress and 11%, 12%, and 12% in modulus for samples T300/5208, C6000/PMR15, and C6000/P1700, respectively.

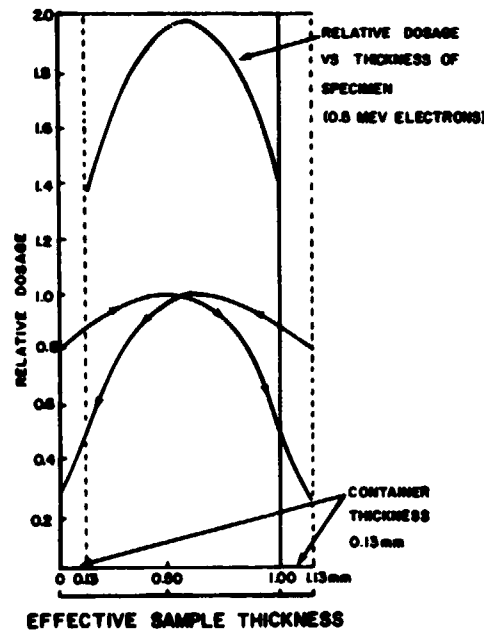


Fig. 1. Estimate of relative composite sample dosage vs. thickness when exposed to 0.5 MeV electrons in the sample holders when both sides of sample are exposed to the beam. The dose-distance relationship is adjusted to unit density material by multiplying thickness by specific gravity.

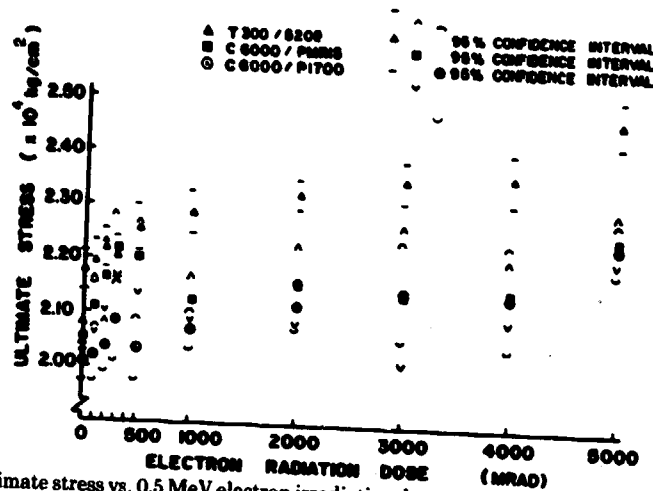


Fig. 2. Ultimate stress vs. 0.5 MeV electron irradiation dosage for graphite fiber composite samples.

Results are shown for the γ irradiated samples in Figures 4 and 5. At the dose levels applied in these experiments, no large changes were observed in either stress or modulus. (The maximum difference from the control for any of the treatments were $<10\%$.)

To test for significant difference in the stress or modulus as a function of irradiation dosage, analysis of variance was done using a statistical analysis system (SAS).¹⁰ In a sample set the data for two irradiation treatments were compared at the 5% confidence levels using the Duncan Multiple range test. In all cases, the 5000 Mrad treatment was significantly different from the control for both the stress and the modulus. Earlier work has been reported by Parkinson and Sisman¹¹ on the effects of radiation on the mechanical properties of a number of plastics. Their work suggests that polymers containing aromatic rings are highly resistant to radiation and they attribute this to the absorption and dis-

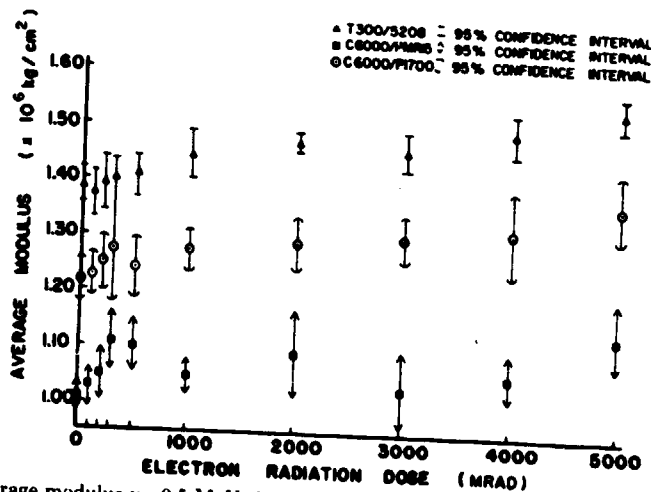


Fig. 3. Average modulus vs. 0.5 MeV electron irradiation dosage for graphite fiber composite samples.

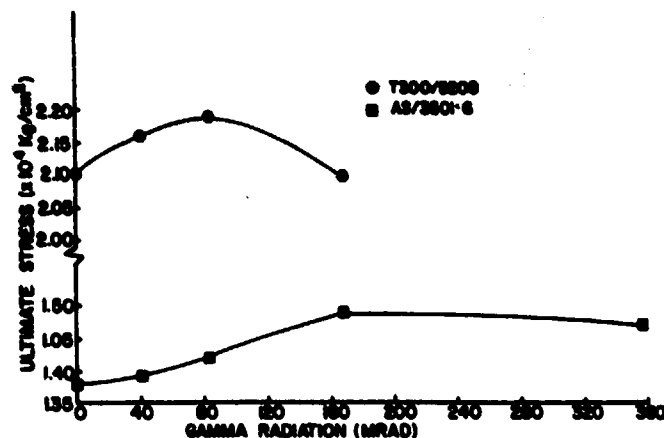


Fig. 4. Ultimate stress vs. 1.33 γ irradiation dosage for graphite fiber/epoxy composites.

sipation of energy, without bond disruption, of aromatic rings. Using neutron and γ radiation, they showed very little change in the mechanical properties of cured diaminodiphenyl methane epoxy and polyimide polymer at radiation dosages $\geq 10^9$ rad. Gamma irradiation experiments by Brown and O'Donnell¹² on aromatic polysulfone show that no deleterious effects occur in vacuum to dose levels of 600 Mrads. However, degradation of flexural properties did occur when irradiation of samples was done in air.

Bullock reported that fast-neutron irradiation of graphite fibers in air showed an increase in strength followed by a decrease (by as much as 25%) of the control.¹³ However, irradiation in an inert environment showed only an increase in the strength.¹⁴ Jones and Peggs¹⁵ show a small increase in both the strength and modulus of graphite when irradiated with fast neutrons at elevated temperature. In addition, they reported an increase in the crystallite dimension suggesting that the elevated temperature induced recrystallization.

Graphite fiber/epoxy composites irradiated in air at 75°C with a combination of γ , fast neutrons, and thermal neutrons showed a decrease in flexural strength and modulus.¹⁶ When samples were irradiated in liquid N₂, increases in the strength and modulus were observed when tested at liquid N₂ temperature while

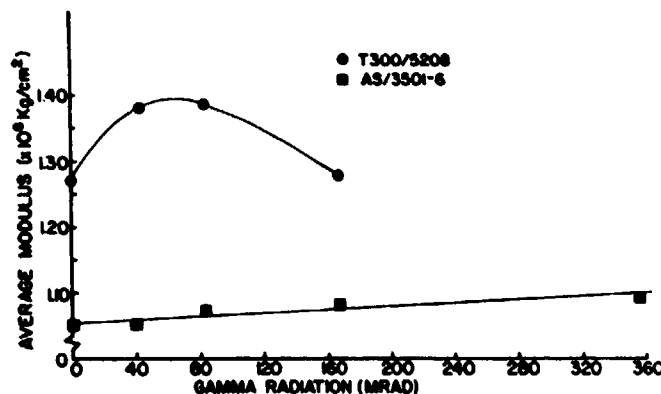


Fig. 5. Average modulus vs. 1.33 γ irradiation dosage for graphite fiber/epoxy composites.

a decrease in those parameters occurred when irradiated at liquid N₂ temperature but tested at room temperature.

The results reported here are consistent with earlier work on plastics, fibers and composites. All the composites that we have studied contain matrices which have an abundance of ring structures and none of the systems we studied showed any degradation in stress or modulus when subjected to ionizing radiation, under vacuum, to dose levels of 5×10^9 rad. The ring structures in the matrices and the fibers appear to protect the composite from radiation damage.

CONCLUSION

Graphite fiber/epoxy, graphite fiber/polysulfone, and graphite fiber/polyimide composites show no deleterious stress or modulus effects by the exposure of 0.5 MeV electron radiation in vacuum up to 5000 Mrad. At 5000 Mrad the stress and modulus increased by approximately 12% compared with the controls. Graphite fiber/epoxy composites show little change in stress and modulus when exposed to several hundred Mrad of γ radiation. Therefore, the results reported here indicate that graphite fiber composites would have a considerable lifetime in space (probably >30 years) before strength and stiffness properties would be affected significantly by high-energy radiation.

The authors gratefully acknowledge NASA for support of the research, Dr. E. R. Long of NASA Langley Research Center for supplying samples and helpful suggestions, Dr. W. K. Walsh for help with irradiation experiments, W. C. Stuckey for help with the mechanical testing, and to Dr. Vivian Stannett for his helpful comments.

References

1. K. M. V. Apparao, *Composition of Cosmic Radiation*, Gordon and Breach, New York, 1975, pp. 6-13.
2. E. R. Long, Jr., NASA Technical Paper 1568, National Aeronautics and Space Administration, Scientific and Technical Information Branch, November, 1979.
3. J. A. Ratcliffe, *Physics of the Upper Atmosphere*, Academic, New York 1960, Chap. 12.
4. E. Segre, *Nuclei and Particles*, Benjamin, New York, 1964, Chap. 2.
5. E. Segre, *Experimental Nuclear Physics*, Wiley, New York, 1953, Vol. 1, Part II.
6. K. C. Chang, K. Ki-Hong, J. W. Wilson, and E. R. Long, private communication.
7. A. Chapiro, *Radiation Chemistry of Polymeric Systems*, Wiley-Interscience, New York, 1962, p. 415.
8. *Annual Book of ASTM Standards*, Part 36, Method D790-71, American Society for Testing and Materials, Philadelphia, 1979.
9. W. K. Walsh and H. A. Rutherford, *Text. Res. J.*, **37**, 89 (1967).
10. A. J. Bass, J. H. Goodnight, J. P. Sall, and J. T. Helwig, *A Users Guide to SAS 76*, SAS Institute, Raleigh, N. C., 1977.
11. W. W. Parkinson and O. Sisman, *Nucl. Eng. Design*, **17**, 247 (1971).
12. J. R. Brown and J. H. O'Donnell, *Appl. Polym. Sci.*, **23**, 2763 (1979).
13. R. E. Bullock, *Radiat. Eff.*, **11**, 107 (1970).
14. R. E. Bullock, *Fiber Sci. Technol.*, **7**, 157 (1974).
15. B. F. Jones and I. D. Peggs, *Nature (London)*, **239**, 95 (1972).
16. R. E. Bullock, *Mater. Sci. Eng.*, **10**, 178 (1972).

Received July 25, 1980

Accepted January 19, 1981

Characterization of a Cured Epoxy Resin
Exposed to High Energy Radiation
With Electron Spin Resonance

by

Kevin R. Schaffer

A thesis submitted to the Graduate Faculty
of North Carolina State University in partial
fulfillment of the requirements for the
Degree of Master of Science

Department of Textile Chemistry

Raleigh

1981

Approved by

M. Keith De Anand

Richard W. Gilbert

Co-Chairman of Advisory
Committee

R. S. Hurre

Co-Chairman of Advisory
Committee

ABSTRACT

SCHAFFER, KEVIN R. Characterization of a Cured Epoxy Resin Epoxed to High Energy Radiation With Electron Spin Resonance." (Under the direction of Drs. Richard D. Gilbert and Raymond E. Fornes.)

This investigation dealt with irradiating a cured epoxy resin, tetraglycidyl-4,4 diamino diphenyl methane and 4,4' diaminodiphenyl sulfone, with 1/2 MeV electron and 1.17 and 1.33 MeV gamma radiations. Radical concentrations were estimated by comparison with a radical standard, 2-2 diphenyl-1-picryl hydrazyl, suspended in an ambient temperature cured epoxy resin. Radical concentration increase with irradiation dose and radical concentration decay at ambient temperature with time curves were plotted. The decay data obtained could be fit to a model which assumes two simultaneous second order reactions occurring in different zones.

BIOGRAPHY

Revin R. Schaffer was born in St. Louis, Mo. on August 5, 1956 the son of Mr. and Mrs. Albert Schaffer. As his older brother, Richard, and older sister, Cindy, and younger brother, Mark, he attended Corpus Christi Elementary School in Jennings, Mo. for eight years.

After attending Jennings Senior High School for two years, his father was transferred to Henderson, North Carolina, where the author graduated from Vance Senior High School in 1974.

He entered North Carolina State University in 1974 and graduated with honors in 1978 with a Bachelor of Science in Textile Chemistry. He entered the Master of Science program in the fall of 1978. Upon completion of graduate work, he will begin a career at Dow Chemical Corporation in Freeport, Texas.

ACKNOWLEDGEMENTS

I wish to express my sincere appreciation to Drs. R. D. Gilbert and R. E. Fornes for their guidance, advice, encouragement, patience, and extreme understanding which made the execution of this study possible. Also, I would like to thank Drs. M. R. DeArmond and J. D. Memory for discussions concerning this study.

I wish to thank Mr. Lynell Williamson and Mr. Gene Floyd for their assistance in the experimental portion of this research.

I also wish to thank my fellow students, Linda, Joe, Jerry, Greg, Sudhir, Rochana, Penny, Marshall, Frank, and Sam, for they have helped in ways one reading this cannot comprehend and the one writing this cannot express enough appreciation.

And I also wish to thank my family for their patience and assistance during the past three years.

TABLE OF CONTENTS

	Page
LIST OF TABLES	vi
LIST OF FIGURES	viii
1. INTRODUCTION	1
2. LITERATURE REVIEW	2
2.1 High Energy Photons	3
2.2 Electrons	5
2.3 Heavy Charged Particles and Neutrons	7
2.4 Energy Deposition in Matter	7
2.4.1 High Energy and UV Radiations	7
2.4.2 Tracks and Spurs	10
2.5 Radical Reactions	13
2.6 Radical Yields	15
2.7 Electron Spin Resonance	16
2.7.1 General Theory	16
2.7.2 Boltzmann's Distribution	18
2.7.3 Power Saturation	19
2.7.4 The ESR Spectrum	20
2.7.4.1 Line Shapes	20
2.7.4.2 Hyperfine Splitting	23
2.7.4.3 Anisotropic Interaction	25
2.7.4.4 Isotropic Interaction	25
2.7.4.5 Exchange Interaction	25
2.7.5 Radical Concentration	26
2.8 Radiation Damage in Polymers	27
2.8.1 Crosslinking and Scission	28
2.8.2 Aromatics	29
2.8.3 Polyethylene	30
2.8.3.1 Free Radical Reactions	30
2.8.3.2 Decay of Alkyl Radicals	31
2.8.3.3 Decay of Allylic Radicals	36
2.8.4 Polyamides	36
2.8.5 Poly(ethylene terephthalate)	42
2.8.5.1 Radical Decay	44
2.8.6 Polysulphones	46
2.8.7 Epoxy Resins	48
3. EXPERIMENTAL PROCEDURE	50
3.1 Materials	50
3.1.1 Epoxy Resin Samples	50
3.1.2 Radical Standard	51

	Page
3.2 Equipment	51
3.2.1 Radiation Equipment	51
3.2.2 ESR Spectrometer	52
3.3 Procedure	52
3.3.1 Epoxy Sample Preparation	52
3.3.2 Standard Samples	53
3.3.3 Electron Irradiation Exposure	53
3.3.4 Gamma Irradiation Exposure	54
3.3.5 ESR Measurements	54
3.3.6 Decay Experiments	55
4. RESULTS AND DISCUSSION	56
4.1 ESR Spectra	56
4.2 Radical Build-up	59
4.3 Spur Size	62
4.4 Radical Decay	63
4.4.1 The Q Function	63
4.4.2 Radical Decay Constants	68
5. SUMMARY	70
6. RECOMMENDATIONS	71
7. REFERENCES	72
8. APPENDICES	76

LIST OF TABLES

	Page
2.1 Linear Energy Transfer and Distance Between Spurs for Various Radiations	11
2.2 Nuclear Spins for Different Nuclei	23
4.1 Calculated Values of the Q Function	66
A Experimental Data of Radical Concentration Build-up and Decay for 1/2 MeV Electron and 1.33, 1.17 MeV Gamma Irradiated Samples	76

LIST OF FIGURES

	Page
Literature Review	
1. The Compton Scattering Process	4
2. Modified diagram for the important processes involving electronically excited states and preionizing states	9
3. Schematic representation of processes leading to charge separation in the condensed state	9
4. Absorption by matter of a) ultraviolet light photons and b) alpha-particles	11
5. Distribution of spurs and primary events along particle tracks of a) alpha particle b) fast electron	12
6. The two orientations of an electron magnetic moment (M_e) with respect to a magnetic field H . . .	17
7. Basic principle of ESR	17
8. Basic principle of phase detection	22
9. Identification of Lorentzian and Gaussian curves by slope method	22
10. The hyperfine of Zeeman splittings for an electron ($S=1/2$) and a proton ($I=1/2$)	24
11. Schematic of the reaction of oxygen with allyl radicals in polyethylene	32
12. Fraction of pure second order kinetics in one reaction zone plotted as a function of the number of pairs of free radicals per zone	32
13. Decay of optical density @ 300 $m\mu$ of irradiated nylon (MXD-6) films at various temperatures	39
14. Initial reaction rate constants from ultraviolet absorption studies for nylon (MXD-6) films at various temperatures	39

15. Transient optical density versus radiation dose for irradiated polyamide films (0.1 mm thick) 1) Nylon 6,6 2) Nylon 610, and 3) Polyoxamide . . .	41
16. Variation in distribution of spurs with radiation dose, the change of the boxes containing different numbers of spurs	41
17. The initial accumulation of radicals with dose	43
18. Schematic of mechanism for dose rate dependence based on available evidence	43

Results and Discussion

1. Relative absorption versus thickness in sample 94 mils in diameter taken along a) diameter parallel to irradiating electron beam and b) along diameter perpendicular to irradiating electron beam	57
2. ESR spectrum of gamma irradiated TGDDM/DDS sample . . .	58
3. ESR spectrum of electron irradiated TGDDM/DDS sample . .	58
4. ESR spectrum of gamma irradiated sample after 6 minutes at ambient temperature	60
5. ESR spectrum of electron irradiated sample with superimposed spectrum of DPPH suspended in epoxy resin	60
6. Build-up of radical concentration with dose of Cobalt 60 (1.33 and 1.17 MeV) in TGDDM/DDS samples .	61
7. Build-up of radical concentration with dose of 1/2 MeV electrons in TGDDM/DDS samples	61
8. Radical concentration versus time at room temperature for TGDDM/DDS samples irradiated at various dosages with 1/2 MeV electrons	64
9. Radical concentration versus time at room temperature for TGDDM/DDS samples irradiated at various dosages with 1/2 MeV electrons	64

10. $Q = \frac{t}{\bar{c} - \bar{c}_0}$ versus time for radical decay data of
Figure 9 65
11. $Q = \frac{t}{\bar{c} - \bar{c}_0}$ versus time for radical decay of Figure 8 65

Appendix

- A. Radical build-up curve for 1/2 MeV electron
radiation as alternate experiment 77

1. Introduction

Graphite reinforced composite materials are highly promising for space structural applications such as solar panel supports, solid fuel rocket motors, and hot air ducting [1,2] because of their high modulus and strength, low thermal expansion, and light weight. Due to large amounts of ionizing radiation in space environment, the effect of gamma, electron, proton, and other radiations upon the mechanical properties of graphite reinforced composites is an important consideration [3]. The matrices into which graphite fibers were embedded in composites in completed studies [3] were highly aromatic polymers, primarily epoxy resins, polysulfones, and polyimides.

The purpose of this thesis is to investigate the immediate chemical effects of ionizing radiation on the epoxy resins, specifically the formation of free radicals and their character employing electron spin resonance spectroscopy (ESR).

2. Literature Review

Ionizing or high energy radiation is a broad term which defines radiation that is composed either of charged particles that directly produce ions, excited molecules, or free radicals in the irradiated medium, or photons or fast moving neutral particles that produce these species in the medium indirectly by charged particles ejected from the absorbing molecules [4]. High energy radiations whether fast electrons, β particles, fast protons, neutrons, α particles, or electromagnetic radiation of short wavelengths lose their energy by reacting with electrons and nuclei of the medium. This may give rise to displaced or excited nuclei, free electrons, ionized atoms or molecules, and excited atoms or molecules in which an electron has been raised to a higher energy level [5].

X-rays, electrons, and positive ions are produced mainly by accelerators. Gamma rays, beta particles, alpha particles, and neutrons are obtained from nuclear reactions in radioactive isotopes and nuclear reactors [6]. These different sources of radiations give an energy range of nearly ten orders of magnitude [7].

One can group the different types of radiations used in radiation chemistry by their physical nature [4]:

- (1) high energy photons (gamma rays and X-rays)
- (2) accelerated high energy electrons
- (3) accelerated ions
- (4) neutrons.

The first two are emphasized in this study.

2.1. High Energy Photons

Photons tend to lose energy whenever they interact with matter. Only a portion of incident photons will interact with a finite thickness of matter. The remainder of the photons which do not interact are transmitted with no change in direction or energy. The intensity, defined as the radiation energy passing through a sphere of unit cross-sectional area in unit time at the point of interest may be expressed by the equation [8]:

$$I = N \times E \quad (1)$$

where I is the intensity (ergs/cm²sec), E is the average energy of photons in ergs, and N is the flux of photons (number of photons/cm²sec).

An infinitesimal reduction in intensity, dI , through an infinitesimal thickness of matter or absorber, dx , is given by the equation:

$$dI = -I\mu dx \quad (2)$$

where I is the incident beam intensity. μ is the total linear absorption coefficient which is the fraction of incident photons diverted from the incident beam by a unit thickness of absorber [8].

Equation 2 can be integrated to apply to large thicknesses to give:

$$I = I_0 e^{-\mu x} \quad (3)$$

The total absorption coefficient is the sum of the absorption coefficient of the three processes in which high energy photons can transfer energy to matter, namely, a "photoelectric process," "Compton scattering," and "pair production" [6].

In photoelectric absorption the entire energy of the photon is transferred to an electron; which is ejected with a kinetic energy, E , equal to the photon energy, $h\nu$, less the electron binding energy, E_b [9].

$$E = h\nu - E_b \quad (4)$$

The distribution of angles at which electrons are ejected is dependent upon the energy of the incident photons. At lower photon energies the ejection of the electrons are 90° to the incident photons' path while at higher photon energies the electrons take a more forward direction [8].

Compton scattering involves an elastic collision of high energy photons ($h\nu$ above 10 kev) with electrons giving scattered photons of energy $h\nu'$. This energy $h\nu'$ is represented by the equation

$$h\nu' = \frac{h\nu}{1 + \frac{h\nu}{mc^2}} \quad (1 - \cos \theta) \quad (5)$$

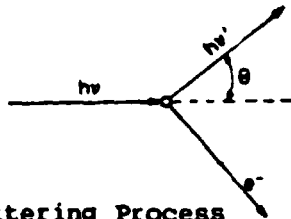


Figure 1 The Compton Scattering Process (6)

where m is the electron mass, c is the velocity of light, and θ is the angle between the incident and scattered photon illustrated in Figure 1 [6].

Pair production involves the absorption of a photon and the production of a pair of particles, a positron and an electron [9]. This

process involves the annihilation of the photon in the field of a nucleus of high atomic weight and constitutes a significant fraction of photon energy loss only in the case of very high energy photons so it is of little importance in radiation chemistry of polymers which are composed of atoms of relatively low atomic weights [6].

X-rays are photons produced by the decay of electrons to empty low energy states of an atom. Electronic states may be excited by bombarding the atom with high energy electrons. Gamma rays are identical in nature (i.e. electromagnetic radiation) to X-rays but their source is emission from the nuclei of natural or artificial radioactive isotopes. They occur at discrete frequencies. Cobalt-60, for example, gives two sharp lines of approximately equal intensity at 1.17 and 1.33 MeV [4]. About the region of photon energy of 1 MeV, the mass absorption coefficient μ is due primarily to Compton scattering which is the major mechanism of ionization [10].

2.2 Electrons

High energy electrons, 10 MeV or higher generally lose energy by radiation electromagnetic energy (Bremsstrahlung) resulting from deceleration of electrons in the fields of nuclei [8]. In the irradiation of polymers, electrons mainly lose energy by transfer to the molecular electrons of the stopping material by collisions called Coulomb interaction [9]. The approximate ratio of energy loss by radiation to energy loss by collision is [9]

$$\frac{\left(\frac{dE}{dx}\right)_{\text{rad}}}{\left(\frac{dE}{dx}\right)_{\text{coll}}} = \frac{E Z_2}{800} \quad (6)$$

where E is the energy in MeV and Z_2 is the atomic number of the absorber. This ratio illustrates that energy loss by Bremsstrahlung emission is significant for electrons of high energy and for high atomic weight absorbers [9].

The energy loss per centimeter by ionization and excitation at relativistic velocities of high energy electrons is

$$-\left(\frac{dE}{dx}\right)_{\text{coll}} = \sum_i \frac{2\pi N_i e^4 Z_i}{mv^2} \left[\ln \frac{mv^2 E}{2I^2 (1-B^2)} - (2\sqrt{1-B^2} - 1 + B^2) \right. \\ \left. \log 2 + 1 - B^2 + \frac{1}{8} (1 - \sqrt{1-B^2})^2 \right] \quad (7)$$

where E is the kinetic energy of the incident electron.

x is the distance into the scatterer.

N_i is the number of the i th type atom in scatterer.

Z_i is the atomic number of the i th type atom.

e is the electron charge.

I_i is the average ionization potential of the i th atom.

m is the electron rest mass.

v is the incident electron velocity.

$B = v/c$

C is the speed of light in vacuum.

Electrons follow erratic paths through matter, whereas some electrons escape large energy loss over a long distance; others undergo numerous large deflections [9].

The range in aluminum of electrons of energies of 0.5 to 3 MeV has been empirically found to be [9]

$$R = AE - B$$

where R is the range in g/cm², A = 0.5 g/erg cm² and B = 0.16 g/cm². This formula fits data for aluminum best but can reasonably fit other materials containing light atoms since the range (g/cm²) varies little with atomic number [8].

2.3 Heavy Charged Particles and Neutrons

Heavy charged particles such as protons and alpha particles interact with matter in the manner of electrons by elastic collisions with the Coulomb electrons of the stopping material [8].

The major mechanism of ionization of neutrons is similar to beams of charged particles because the main ionization species are protons and heavier positive ions produced by the interaction of the neutrons with atomic nuclei [8].

2.4 Energy Deposition in Matter

The energy lost per unit path length ($-\frac{dE}{dx}$) (given for Coulomb collisions in equation 6) is termed the "linear energy transfer" (LET) (may be expressed keV per micron of path) [4]. LET is the linear rate of energy loss by an ionizing particle penetrating a material medium and can be roughly calculated by dividing the total energy loss by the particle by its path length [8].

2.4.1 High Energy and UV Radiations

Several differences exist between the irradiation process with high energy radiations and the photo process with UV light.

One difference is the energy levels to which molecules or atoms are excited by the incoming radiation as mechanisms for energy dissipation

[6]. Ultraviolet light cannot excite molecules to ionization or preionization levels as high energy radiation does. Preionization states can either proceed to form radicals, radical ions, or through a process of internal conversion convert the electronic excitation energy to vibrational energy, and with further molecular collisions, to the ground state [6,9] as illustrated in Figure 2 [6].

The existence of preionization and ionization states in radiolysis leads to a second difference compared to photolysis. Electromagnetic radiations transfer energy to electrons and positrons and energy is then dissipated along the tracks of these particles [8]. For most high energy radiation, the energy transmitted through the stopping material by secondary or fast electrons [12]. The motions of these electrons are tracks punctuated by ionization and molecular or atomic excitations. These excitations or preionization states are created through direct radiation chemical interaction with secondary electrons [6]:



and are similar to corresponding excitation states produced in photolysis (illustrated in Figure 3):



Through products obtained from radiolysis and photolysis are similar, differences may arise in the types of products due to the mechanism available in the latter of charge separation and energy transfer to a molecule D of lower ionization potential [12]. Figure 3 summarizes the processes which lead to charge separation and excitation state formation

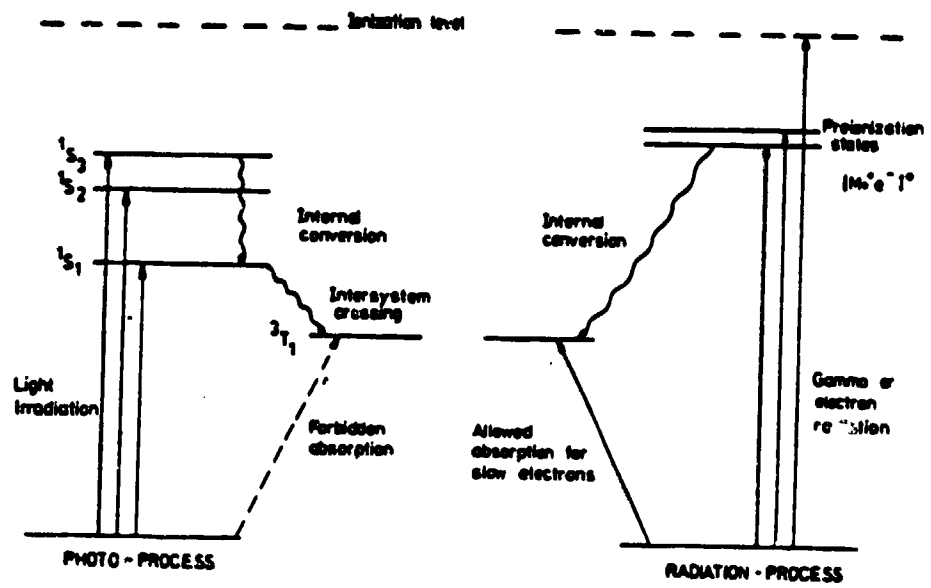


Figure 2. Modified diagram for the most important processes involving electronically excited states and preionizing states (6).

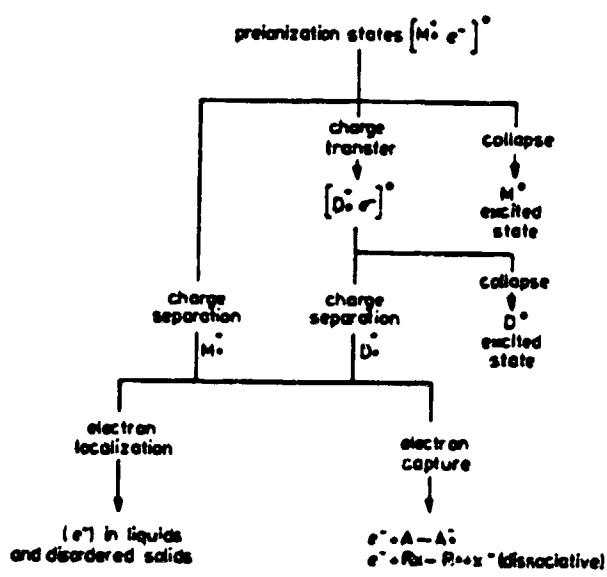


Figure 3. Schematic representation of processes leading to charge separation in the condensed state (12).

in liquids and solids as a result of collisions with the lower energy secondary electrons [2].

A third difference is the geometries in which the reaction species are formed [8]. As seen in Figure 4, in the photo process excited molecules are formed more homogeneously in the material. In other words for an equivalent amount of energy absorbed, the lower energy particles lose energy more homogeneously throughout the material. However, there may be a great difference in penetration depth, so Figure 4 applies only to thin samples or to thicker samples on a microscopic level.

2.4.2 Tracks and Spurs

The excitations and ionizations formed in radiolysis will be the same for a particular material independent of the type or energy of radiation [8]. However, high energy radiations of different types and intensities lose radiation at different rates and leave different distributions of ions and excited species in the medium [8]. These various distributions effect the quantities and proportions of chemical products obtained from radiation sources [8].

A major assumption in the radiation of solids is that the structure of tracks will resemble those observed in the gases, but reduced in proportion to the relative density of the phases [4]. Along the tracks are ions and excited molecules which are a direct result of the incident particle and of secondary electrons. The energy distribution of secondary electrons is not dependent upon radiation type [13].

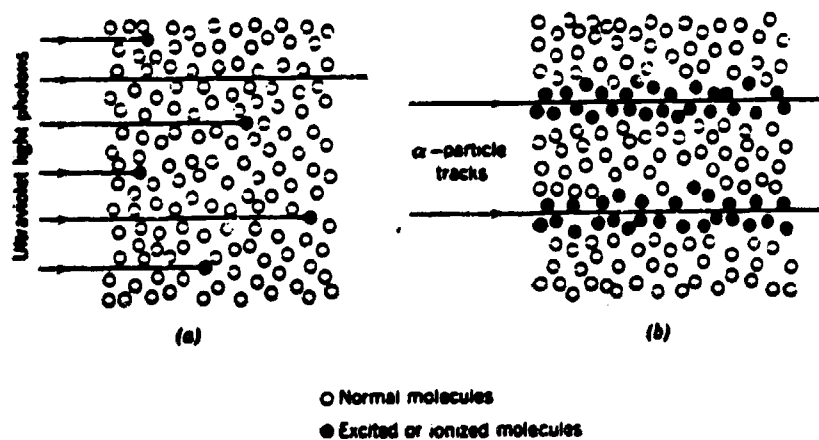
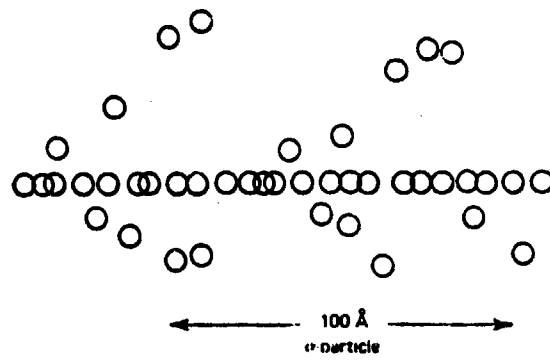


Figure 4. Absorption by matter of a) ultra violet light photons
 b) alpha-particles (8).

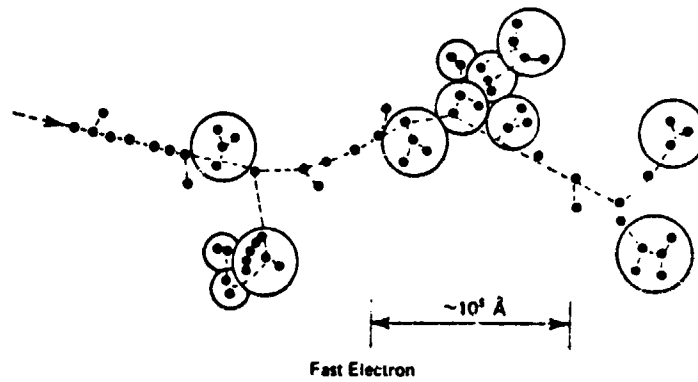
Table 2.1 Linear Energy Transfer and Distance Between Spurs for Various Radiations (13).

Radiation	L.E.T. in eV/Å	Spur separation Å
γ rays	0.8 to 3.0	75 to 20
0.01 MeV electrons	0.23	260
0.1 MeV electrons	0.04	1400
1 MeV electrons	0.02	3000
⁶⁰ Co γ	0.02	3000
1 MeV protons	2.8	21
10 MeV protons	0.47	130
1 MeV α-particles	26.4	2.3
10 MeV α-particles	5.6	11

Mean energy per spur taken as 60 eV.*



(a)



(b)

Figure 5. Distribution of spurs and primary events along particle tracks of a) alpha particle b) fast electron (9).

The fast or secondary electrons can be divided into two groups; those that form delta rays (small side tracks) and those that produce small clusters of ions and excited molecules called spurs [13].

The distance between spurs varies with different types of radiation as can be seen in Table I. High energy electrons and gamma radiation have comparable spur distances (about 3000 Å) in liquid water. How the distance between spurs is dependent upon the rate in which the energy is deposited is illustrated in Figure 5 [9], a schematic diagram of assumed spur distribution along the track of a fast electron and of an alpha particle. A high rate of energy deposition as in alpha particles will produce densely ionized cylindrical columns. A low rate of energy deposition will produce isolated spurs analogous to beads on a string.

The most immediate processes of ionization, excitation and electron capture in Figure 3 are not influenced by the materials viscosity. Experimental evidence suggests that charge separations over 50-100 Å can exist in a rigid matrix if mechanisms for electron capture and localization are inherent [12]. Thus so ions and preionization states can surely exist in spurs formed in polymers.

2.5 Radical Reactions

Although other active chemical species such as ions or excited states are present in tracks of ionization particles, free radical reactions are considered to be the predominate events [4].

Chapiro [4] gives three observations as evidence for this assumption.

- 1) Products derived from radiation of organic compounds are similar, though not exactly the same as products arising from photolysis.
- 2) Some classical free radical reactions can be initiated by ionization radiation and show a great similarity to reactions initiated by ultra-violet light or chemical initiators.
- 3) Free radical inhibitors are effective in many cases when a reaction is initiated by ionizing radiation.

Once free radicals are formed with high energy radiation their lifetimes vary with species in the immediate area; for instance whether it is isolated or located in a spur, the viscosity of the medium, and stabilization due to the amount of resonance energy available [12].

After formation, free radicals can undergo numerous reactions [6]:

- 1) Atom transfer reactions such as hydrogen abstraction by a free radical:



- 2) Addition reactions to a double bond:



these include addition reactions observed in aromatic compounds [4]:

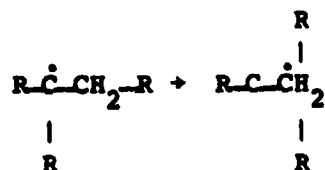


where ϕ is an aromatic molecule and $R\phi\cdot$ is an addition complex having a quinone radical structure [6]:

- 3) Fragmentation reactions involving a dissociation into an unsaturated product molecule and another free radical:



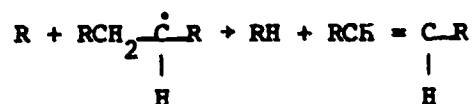
- 4) Rearrangement reactions in which the free radical changes position within the molecule:



- 5) Combination of two radicals:



- 6) Disproportionation which also involves two radicals but results in two molecules one of higher unsaturation:



2.6 Radical Yields

In radiolysis of liquid hydrocarbons, the only reactive species that can be quantitatively determined are free radicals [9]. Radical chemical yields or "G" values are the absolute chemical yield of a chemical species or products denoted as the number of chemical events occurring 100 eV of absorbed energy [9]. For example,

$G(R\cdot)$ = the number of radicals produced per 100 eV absorbed

Another important term in radiation chemistry concerns the unit of absorbed dose, the rad, which is 100 ergs per gram [8].

One technique to determine radical yields best in the gas or liquid phase is through radical scavengers. These are chemical species or stable free radicals that readily react with the free radicals produced.

A problem with radical scavengers is the radicals detected cannot be those radicals which react within the spurs, but only the radicals which diffuse from the spurs [9].

2.7 Electron Spin Resonance

Electron spin resonance (ESR) or electron paramagnetic resonance (EPR) spectroscopy is the most sensitive and informative method of determining the presence of unpaired electrons in the solid phase [8].

2.7.1 General Theory

ESR spectroscopy utilizes the magnetic properties of the unpaired electrons of free radical molecules. Electrons are characterized in orbitals of the molecule with a spin quantum number $+1/2$ or $-1/2$. Two electrons in the same orbital have matched spin quantum numbers and give no total magnetic moment.

The unpaired electron in a free radical can be approximated as a free electron with spin $\vec{S} = 1/2$ and vector magnetic moment, \vec{M}_s ,

$$\vec{M}_s = ge \sqrt{s(s+1)} \beta \quad (9)$$

where g is the electron g factor, a dimensionless number, the value depending upon the environment of the electron [14]. The g value of a free electron is 2.00232 and $\beta = eh/2Mc$ is the Bohr magneton, the unit of magnetic moment having the value of 9.274×10^{-21} erg G^{-1} .

According to quantum theory a particle with spin has two possible orientations in an external magnetic field termed parallel and antiparallel [14]. Figure 6 illustrates how the magnetic moment vector can be oriented in a magnetic field [6]. The two states are of slightly different energies, the antiparallel direction being of higher energy [14].

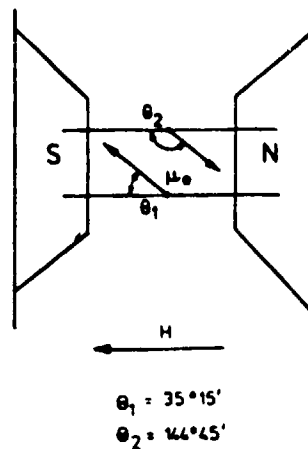


Figure 6. The two orientations of an electron magnetic moment (μ_e) with respect to a magnetic field H (6).

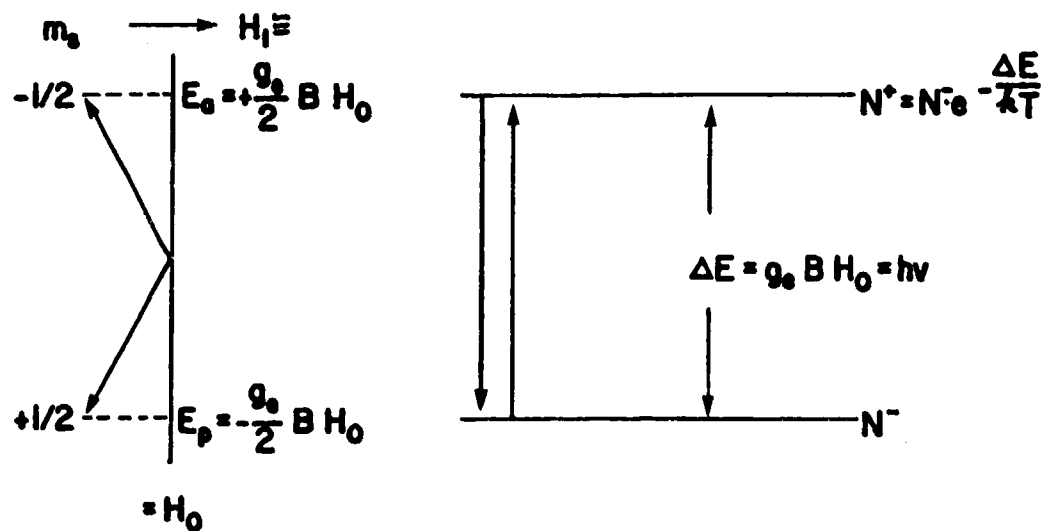


Figure 7. Basic principle of ESR (14).

given by [14]

$$E = -\vec{M}_s \cdot \vec{H}_0 = -M_0 |\vec{H}| \cdot \cos(\vec{M} \cdot \vec{H}_0) \cdot 10 \quad (10)$$

Figure 7 shows the energy difference (ΔE) between the energy parallel

$$E_p = -\left(\frac{ge}{2}\right) \beta H_0 \text{ and the energy antiparallel } (E_a = +\left(\frac{ge}{2}\right) \beta H_0) \text{ is } g\beta H \quad [14].$$

When the electrons are subjected to a radio frequency magnetic field such that a resonance condition

$$h\nu = \Delta E = g\beta H$$

is established, where ν is the frequency, transitions between the parallel and antiparallel orientations occur. In classical terms, the electron magnetic moment vector axis precesses about the static magnetic field vector at a precise frequency called the Larmor frequency. The

The energy of a magnetic dipole \vec{M}_s in a static magnetic field is electron is able to absorb energy at this frequency to cause transitions between the parallel-antiparallel states.

2.7.2 Boltzmann's Distribution

A net absorption of energy from radio frequency field, ν , can be observed if there exists a difference in probabilities of transition or in the populations of the two orientation states [14].

At thermal equilibrium where there is no net transfer of energy within the system, the ratio of populations of parallel and antiparallel states is given by the Boltzmann equation [14]:

$$\frac{N_a}{N_p} = e^{-\Delta E/kt} = e^{ge\beta H/kt} \quad (12)$$

where k is the Boltzmann constant ($k = 1.38044 \times 10^{-16} \text{erg K}^{-1}$). The

signal intensity increases with an increasing N_a/N_p ratio, so from this equation one can conclude that signal intensity increases with decreasing temperature [6].

A basic assumption of ESR is that radiation fields do not effect the thermal distribution of electrons in the two energy states [15].

2.7.3 Power Saturation

The ESR signal intensity is proportional to the microwave energy density from the onset, but with increasing microwave power levels the ESR signal increases until maximum is attained after which the intensity decreases until disappearance [6]. The nonlinear dependence of signal intensity or microwave power is called power saturation [16].

If the resonance condition is to be maintained the electron must have mechanism to dissipate the absorbed energy so that saturation of the higher energy state does not occur [17].

The processes in which electrons lose energies are termed relaxation processes and involve the sharing of the energy of the electron spin with thermal vibrations of the solid, generally termed spin-lattice interactions [17]. The strength of spin-lattice interactions are characterized by the spin-lattice relaxation time, T_1 , with the stronger interactions causing a shorter T_1 and thereby reducing the chance of power saturation [17].

Spin-spin interactions are energy transfer mechanisms which occur between electron and nuclear spins of neighboring atoms and also between unpaired electrons of different molecules [17]. Spin-spin interactions

do not dissipate energy but can transport energy to positions with strong spin-lattice interactions, thereby shortening T_1 [6].

2.7.4 The ESR Spectrum

Most spectra obtained on an ESR Spectrometer are the first derivative of energy absorption curves, because of the use of phase sensitive detection. Phase sensitive signal detection uses a signal frequency sine-wave modulation to carry information through changes in amplitude of that modulation [15]. Figure 8 gives a schematic of the variation in amplitude of the magnetic field modulation as the absorption curve is scanned and recorded [17].

2.7.4.1 Lineshapes

The lineshapes of ESR signals are determined by interaction of free radicals with their local environments while line widths depend upon the strength of the interaction and relaxation times [5].

There are two main types of line shapes generally used to characterize absorption curves, namely Lorentzian and Gaussian [6].

In a homogeneous system of a single radical, where relaxation depends on spin lattice interactions, and on the condition that thermal equilibrium is maintained, theory predicts a Lorentzian lineshape of the ESR curve [15]. An inhomogeneous system where the electrons are in different local environments results in resonance not occurring simultaneously for all spins. If spin-spin interactions occur more slowly than spin-lattice interactions, the spin system will not attain equilibrium and the lineshape will be Gaussian [15].

Many spectra are a combination of Gaussian and Lorentzian features; which predominates can be identified by the slope method as illustrated in Figure 9 [6,15].

Ingram give four important parameters to define any ESR spectrum [17]:

- 1) The "g-value" or spectroscopic splitting factor
- 2) The value of any splitting in electronic levels
- 3) The value of any hyperfine splittings
- 4) The width of absorption lines.

The g-value gives an indication of the difference in the two energy levels of the parallel and antiparallel states of the radical electrons [17]. Anisotropies caused by local magnetic field differences in the free electron environment in single crystals can give information on the structure of the radical if an understanding of the nature of the anisotropic interactions is possessed [6].

The determination of the g-values of randomly oriented radicals in an amorphous solid or crystalline powder gives a less detailed picture of radical structure and electron distribution because the anisotropies are averaged spatially in the sample [6].

The splitting of electronic levels occurs with the existence of diradicals and triplet states. Due to line broadening, these electronic level splittings are difficult to observe in a noncrystalline solid [17].

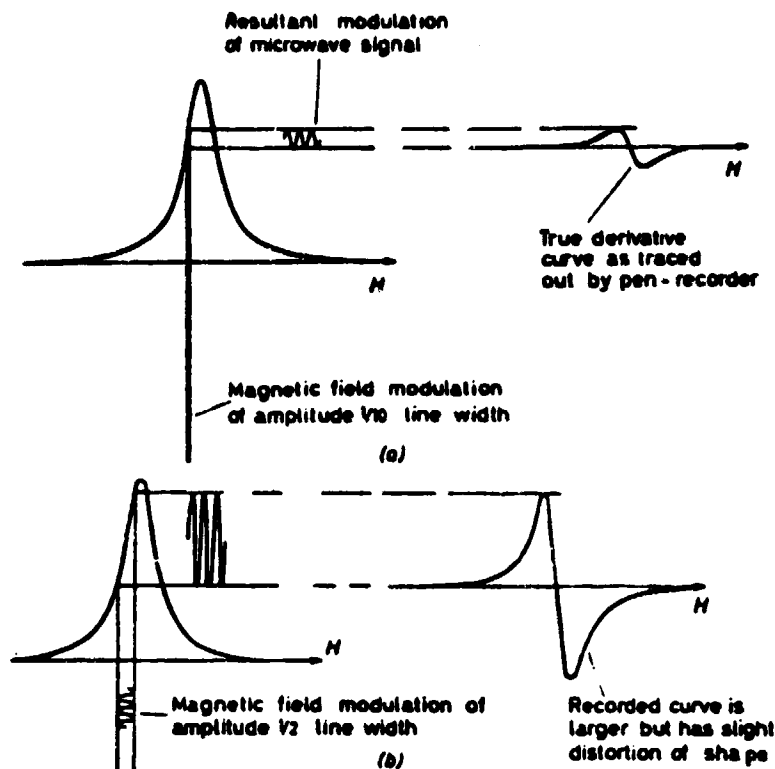


Figure 8. Basic principle of phase detection (17).

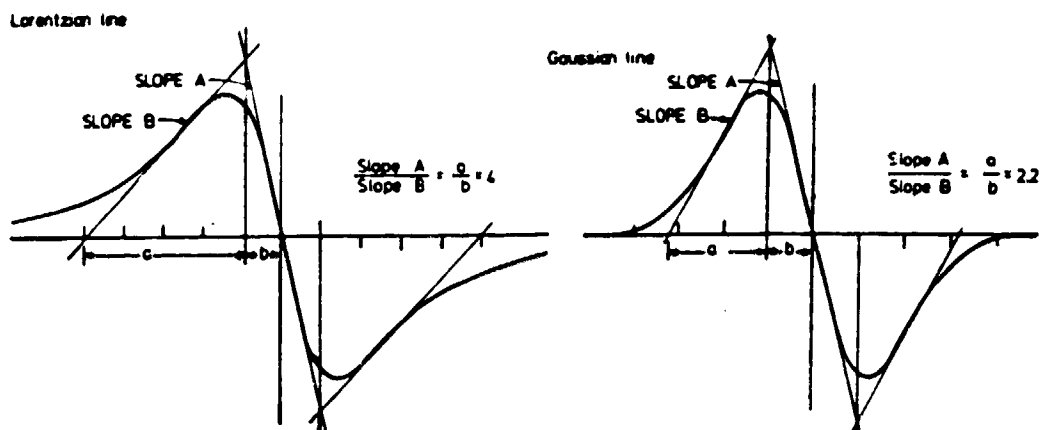


Figure 9. Identification of Lorentzian and Gaussian curves by slope method (15).

2.5.2 Hyperfine Splitting

Hyperfine splittings are due to interactions of impaired electrons with magnetic fields due to nuclei present in the same radical [8].

Nuclear spins of various element are given in Table 2.

Table 2.2
Nuclear Spins for Different Nuclei

^1H	I $1/2$	^{13}C	I $1/2$	^{16}O	I 0
^2H	1	^{14}C	1	^{32}S	0
^{12}C	0	^{15}N	$1/2$	^{33}S	$3/2$

In a spin system immersed in an external magnetic field in which the electrons are adjacent with nuclei which have spins, $I = 1/2$, the magnetic field experienced by a particular electron will either be shifted to a higher or lower energy by a value "A" called the hyperfine splitting constant. Figure 10 diagrams the hyperfine or Zeeman splittings of an electron ($s = 1/2$) and a proton ($I = 1/2$) [6].

Probabilities for energy transitions due to changes in electron spin and nuclear spin with relation to the magnetic field may be determined. The only transitions allowed involve either the electron or nucleus but not both. [6].

The magnetic interaction between electron and nuclear spins of the same molecule is called hyperfine coupling and is most readily observed in dilute solution where interactions with nuclei of other molecules is minimized.

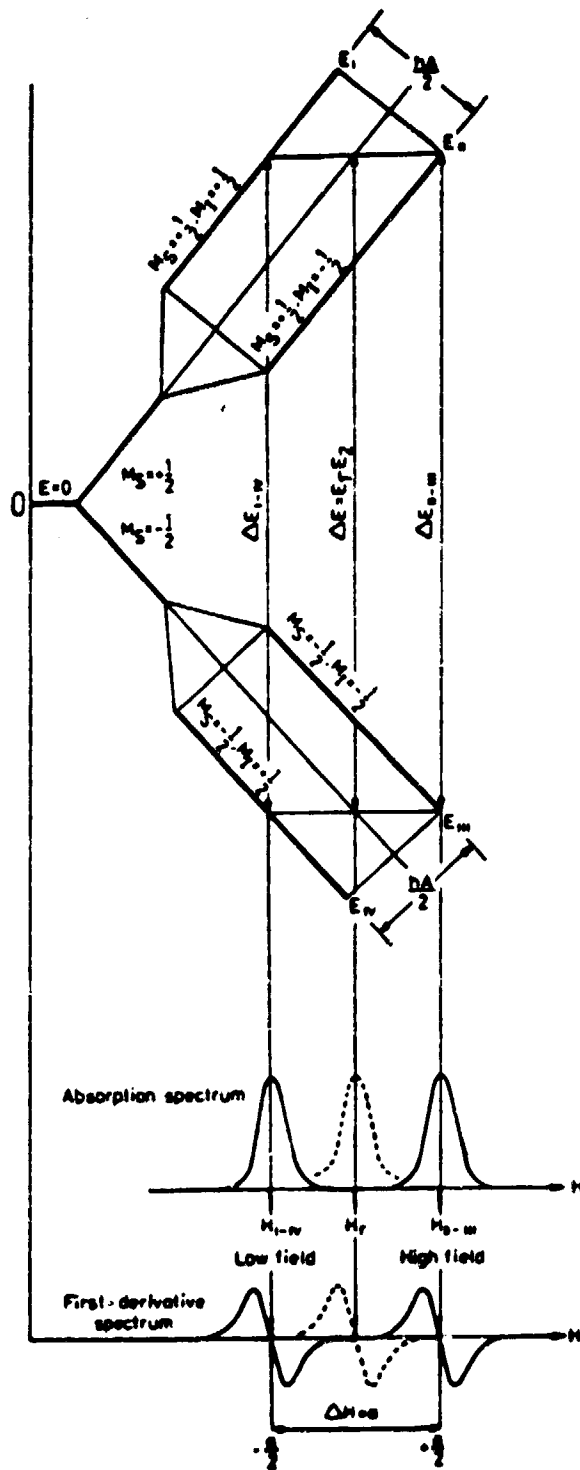


Figure 10. The hyperfine or Zeeman splittings for an electron ($S = 1/2$) and a proton ($I = 1/2$) (δ).

2.7.4.3 Anisotropic Interaction

The hyperfine interaction may be broken into an isotropic and an anisotropic term. The isotropic term is the Fermi-contact interaction which originates from electron nuclear electrostatic interaction. The anisotropic term is due to dipole-dipole interactions.

Anisotropic hyperfine splitting can be studied in detail in crystalline material by rotation of the crystal in the magnetic field [17]. In amorphous crystalline powder, and viscous liquids solids this anisotropic hyperfine splitting causes broadening of the signal thereby smearing out hyperfine structure of any type [14].

2.7.4.4 Isotropic Interaction

Isotropic interaction is proportional to the electron density at the nucleus [17]. It can only be observed if the orbital in which the electron is present gives a finite electron density at the nucleus [17].

In aromatic free radicals the unpaired electron occupies molecular orbitals which theoretically have zero electron density at the nuclei. If excited states are admixed with the ground states of the orbitals this condition is not observed and a hyperfine constant of 28 gauss can be calculated, which is close to experimental values [17].

2.7.4.5 Exchange Interaction

Exchange interaction occurs in samples of high radical concentration and is caused by radicals being in such close vicinity with each other that there is orbital overlap [14]. The result of this overlap is that the ESR absorption line is much sharper than would be obtained in the presence of just anisotropic interaction. Since the electron does

not exist in the local magnetic field of any particular nuclei long enough, hyperfine interaction is not observed [14].

2.7.5 Radical Concentration

The absolute radical concentration can be obtained from spectrometer parameters and the relation between spin concentration and the magnetic susceptibility of the free electron [15]. Due to the number of independent measurements required a comparison method is more often, if not always, employed.

In the absence of power saturation, the area under an ESR absorption curve is proportional to the number of spins in the sample [15]. Assuming a relatively small linewidth and that reflections in the waveguide do not effect measurements, a sample with an unknown spin concentration can be compared with a sample with a known number spin using the derived equation [19]:

$$N_x = N_s \frac{g_s}{g_x} \frac{s(s+1)}{s_x(s_x+1)} \left(\frac{V}{\eta}\right)_x \left(\frac{V}{\eta}\right)_s \frac{(T-\theta)_x}{(T-\theta)_s} \frac{K_s}{K_x} \frac{V_s}{V} \frac{Q_s}{Q_x} \cdot \frac{\dot{H}_x^2}{\dot{H}_s^2} \frac{f_s}{f_x} \frac{Hm'_s}{Hm'_x} \frac{F_s}{F_x} \frac{2_x}{2_s} \frac{A_x}{A_s} \quad (13)$$

where x relates the unknown sample and s to the standard. $\dot{H} = \frac{dH}{dt}$ is the magnetic field sweep rate, g is the Landé factor, s is the spin quantum number, v is the sample volume, η is the filling factor, V the crystal voltage, Q the loaded quality factor of the cavity, Hm' the modulation amplitude, $f = 1/2 Hm' \int Hmdv$ a correction for modulation field inhomogeneity, F_u the amplitude factor, 2 is the microwave frequency, T the absolute temperature in Kelvin degrees, θ is the Weiss constant, and A is the area under the absorption curve [19].

If the same crystal voltage, microwave frequency, and temperature are used for samples and the values $S = 1/2$ and $\theta = 0^\circ\text{K}$ inserted with

the substitution of $(\frac{V}{h})_x (\frac{V}{h})_s \frac{f_s}{f_x} = K$ equation B becomes [19]:

$$N_x = N_s \frac{g_s}{g_x} \frac{\dot{H}_x^2}{\dot{H}_s^2} \frac{Hm_s'}{Hm_x'} \frac{F_s}{F_x} K \frac{Q_s}{Q_x} \frac{A_x}{A_s} \quad (14)$$

Samples of approximate equal g value, filling factor, and recording parameters, \dot{H} , Hm , and F this equation is further simplified:

$$N_x = N_s \frac{A_x}{A_s} \frac{v_x}{v_s} \quad (15)$$

Methods to determine absorption curve areas include an analogous method developed by Burgess [20], direct electronic integration [15], and numerical integration method such as reported by Wyard [21].

2.8 Radiation Damage in Polymers

Experimental evidence indicates that equal amounts of absorbed energy by polymers cause equivalent changes in the polymer properties independent of radiation type [4]. Practically, the most important effect of high energy radiation has upon polymers is induced changes in mechanical properties.

Polymers can be divided into two groups, thermoplastic which consist of long chain molecules and thermosetting which exist as three dimensional networks. Radiation effects of chain scission and cross-linking show up more dramatically in thermoplastic materials than in intrinsically crosslinked materials such as thermosetting resins [4,22].

The radical chemical reactions discussed in Section 2.3 are the same for radicals as in polymers. Many radiation induced reactions have low molecular weight analogies [22]. Unlike low molecular weight

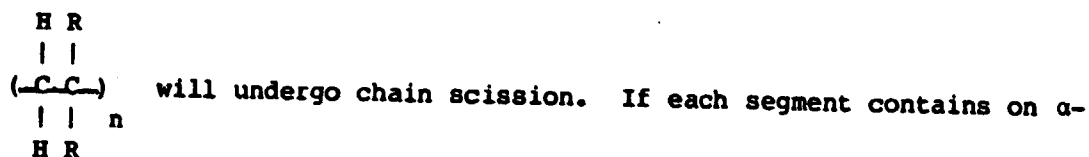
compounds, mechanical and physical properties can be greatly altered by a very small amount of reaction [22].

The addition, fragmentation, rearrangement, combination, and disproportionation reactions may take place with ionic species as well as with free radicals [23].

2.8.1 Crosslinking and Scission

These reactions ultimately change the chemical structures of the polymer molecules which either results in crosslinking or scissions and in turn, alters the physical properties of the material [23]. The reactions which take place are very much a function of chemical structure of the structure units.

For example, polymers constructed of vinyl units of the form



hydrogen or is of the structure $(-\text{CH}_2-\text{CH}_2-)_n$ or $(-\text{CH}_2-\overset{\text{H}}{\underset{\text{R}}{\text{C}}}-)_n$ crosslinking

will predominate [24.]

Dole [25] states that due to steric hindrance of the more substituted monomer the heat of recombination is higher, making recombination less probable. Radiation damage is minimized when the damage in the form of biradicals is repaired by recombination [25].

Charlesby states polymers that degrade by main chain fracture show no crosslinking and there appears to be no competition between the processes of crosslinking and scission.

Crosslinking with radiation increases the molecular weight of the polymer to the limiting value being that sample is comprised of one molecule. Increased crosslinking will bind the polymer into material whose properties are a function of crosslink density [23].

Scission results in the reduction of molecular weight which means an increase in solubility, a lowering of the glass transition temperature, and a decrease in tensile and impact strength [23,4].

Side reactions to scission and crosslinking are the production of low molecular weight fragments and gases and also the formation of unsaturation [23]. The gases formed either escape readily or if higher molecular weight plasticize the polymer eventually causing swelling, cracking, or even foaming at high temperature [4].

2.8.2 Aromatics

Another example of the importance of the chemistry of the structural unit is that aromatic polymers exhibit a resistance to radiation [3,23]. These compounds can absorb energy by raising to excited states and then dissipating the energy that does not disrupt the chemical structure [23].

The G (crosslinking), G (main chain scission), and G (gas production) are all considerably less for polymers that contain aromatic structures than those that do not [26].

More specific examples of the effect of radiation upon solid phase polymers will now be reviewed. The relationship between free radicals generated and mechanical property effect will be accentuated.

2.8.3 Polyethylene

Polyethylene is a polycrystalline polymer, whose physical and mechanical properties have been extensively studied. Its radiation chemistry has also been widely investigated using ESR.

At low doses properties sensitive to interlamella, amorphous area activity in the polymer are the most effected [27]. Changes in time-dependent properties as creep, stress relaxation, and stress cracking are a result of crosslinks which decrease viscous flow in the amorphous regions [27].

Higher dosages cause loss of crystallinity which decrease the strength and modulus of polyethylene [27].

2.8.3.1 Free Radical Reactions

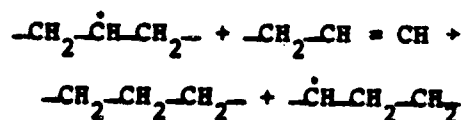
The free radicals generated in the radiolysis of polyethylene at liquid nitrogen temperatures are the alkyl radical $(-\text{CH}_2-\overset{\cdot}{\underset{\text{H}}{\text{C}}}-\text{CH}_2-)$, G (alkyl) = 1.4 - 6.0, the allyl radical, $(-\overset{\cdot}{\text{C}}\text{H}-\text{CH}=\text{CH}-)$, G (allyl) = .023 - 0.4, and the polyenyl free radical, $(-\overset{\cdot}{\text{C}}\text{H}-(\text{CH}=\text{CH})_n-)$, the latter is only produced in significant yields at higher doses [28].

In linear, unbranched polyethylene main chain scission reactions do not occur, recombination is the major mechanism leading to the formation of crosslinks [28].

The production of allyl radicals is thought to be the product of the initial reaction [9]



and then the reaction



The probability for such reactions occurring is enhanced by the mechanism of abstraction type radical transfer causing a net migration of the free electrons [28]:



Oxygen reacts readily with polymer radicals to form peroxide radicals in chain reactions. Approximately five oxygen molecules per radical react to cause chain scission, carboxyl formation, and hydroxyl formation (9).

Figure 10 gives a schematic of possible routes of reaction of oxygen with allyl radicals, the predominate radical at room temperature (28). The last reaction of each sequence continues as a chain reaction.

2.8.3.2 Decay of Alkyl Radicals

By separation of the ESR spectrum of irradiated polyethylene into components Charlesby, et al (18) found that alkyl radicals decay according to the second order rate law:

$$\left[\frac{1}{R\cdot}\right] + \left[\frac{1}{R\cdot}\right] = kt \quad (16)$$

This equation results from the integration of the second-order rate equation:

$$\frac{d[R\cdot]}{dt} = k_1 (R\cdot)^2 \quad (17)$$

and one assumes that the reaction occurs in a uniform medium (47).

Smith and Jacob (47) found that the initial rate of disappearance of alkyl radicals does follow a second-order rate law and after a transition period a different second-order law. Assuming that the alkyl radicals exist in isolated spurs with an initial specific volume, Smith and Jacob found their data could be fit with the equation

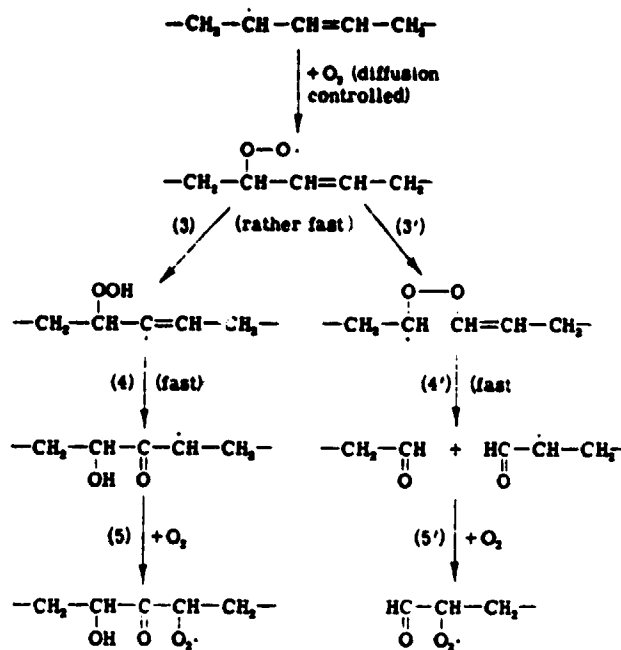


Figure 11. Schematic of the reaction of oxygen with allyl radicals in polyethylene (28).

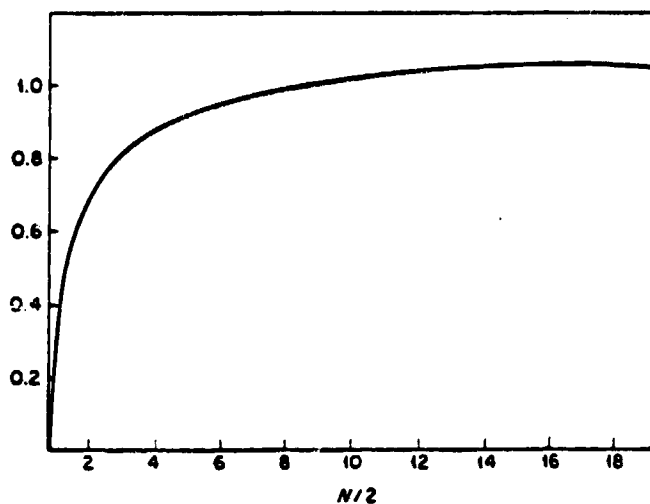


Figure 12. Fraction of pure second order kinetics in one reaction zone plotted as a function of the number of pairs of free radicals per zone (29).

$$\frac{N}{N_0} - 1 = \frac{n}{n_0} - 1 = (2\tau_D / \bar{\tau}) \{1 - [t/\tau_D + 1]^{-1/2}\} \quad (18)$$

where N/N_0 is the ratio of the overall radical concentration at time t to the initial concentration. n/n_0 is a similar ratio except pertains to a single spur. τ_D is the time required for the square of the radius of a spur to increase by an amount equal to the initial value, and $\bar{\tau}$ is the average lifetime of the radical.

Johnson, Wen, and Dole (48) found no second order decay, but quantitatively interpreted the kinetics in terms of fast and slow first order processes following the equation:

$$C = C_s^0 e^{-k_s t} + C_f^0 e^{-k_f t} \quad (19)$$

where c_s and c_f are the concentration of slow decaying and rapidly decaying radicals, respectively, k_s and k_f are the decay constants, and C_s^0 and C_f^0 the initial concentrations of these two radicals.

It is possible that the different conclusions on the order of alkyl radical decay in polyethylene results from differences in the nature of the solids, the time range of the experiments, or the initial radical concentration (30).

Dole and Inokiti (30) developed a mathematical model in which the radicals are isolated among a number of physically separated zones and the reaction rates are considered from the standpoint of the transition from second to first order kinetics as the concentration of reacting species becomes small (on the order of ten or less) and also from the standpoint of an initial nonuniform distribution of reactants in the zones. The radicals are assumed to be inhomogeneously dispersed in a number of zones or spurs, s , all of equal volume V_i , each containing a number of radicals N_i ($i = 1, 2, 3, \dots, s$). The regions exterior to the

zones are excluded from free radical diffusion and reaction. C is the overall average concentration of free radicals.

If the reactions in each zone were strictly first order then

$$-\sum_i s_i (dc_i/dt) = k_i \sum_i s_i c_i = s(dc/dt) = k_i sc \quad (20)$$

and the overall reaction observed will be first order.

If the overall reaction were ideally second order in each zone the rate equation in the above terms would be

$$-[d \sum_i s_i N_i/dt]_{\text{ideal}} = (s/v_i) k_2 (\bar{N}_i)^2 \quad (21)$$

where

$$\bar{N}_i = \frac{1}{s} \sum_i s_i N_i \quad (22)$$

The actual, observed reaction rate is expressed

$$-[d \sum_i s_i N_i/dt]_{\text{obs}} = (s/v_i) k_2 (N_i^2)_{\text{AV}} \quad (23)$$

where

$$(N_i^2)_{\text{AV}} = \sum_i s_i N_i^2 / s \quad (24)$$

The ratio, R_b , of the rate observed to the ideal is given by

$$R_b = \frac{-d[\sum_i s_i (N_i/dt)]_{\text{obs}}}{-d[\sum_i s_i N_i/dt]_{\text{ideal}}} = \frac{(N_i^2)_{\text{AV}}}{(\bar{N}_i)^2} \quad (25)$$

The observed second order reaction rate will appear faster or equal to the ideal because the term $(N_i^2)_{\text{AV}}$ will always be greater or equal to the term $(\bar{N}_i)^2$.

The number of ways two radicals can be chosen to react out of the number N_i is given by the following binomial coefficient:

$$C_2^{N_i} = N_i! / (N_i - 2)! 2! = N_i (N_i - 1) / 2 \quad (26)$$

When $N_i \gg 1$, their equation reduces to a strictly second order proportionality.

Iwasaki, et al (31) detected the presence of radical pairs in polyethylene that do not increase in concentration with dose rate. They concluded these radical pairs do not form by occasional overlapping of spurs but are formed in intrinsic ratios indicating a saturation limit. They also concluded these radical pairs were two alkyl radicals



If a radical is situated so that it can only react with one other radical, as can be assumed with these alkyl radical pairs, the number of ways in which these radicals can react is $C_1^{N_1/2}$ and is equal to $N_1/2$. The ratio of second order to first order reactions would be

$$\frac{C_2^{N_1}}{C_1^{N_1/2}} = N_1 - 1 \quad (27)$$

The true second-order rate is proportional to N_1^2 and the first order would be proportional to N_1 , so the above ratio is proportional to N_1 .

Restoring the assumption of no overlap of reaction zones and introducing the assumption that radicals exist in the zones only as even numbers, (i.e., only radical pairs are produced) the results of the preceding analysis can be illustrated in Figure 11(30). Recombination rates will be predominately first order if only one free radical pair occurs in each zone, and the fraction of second order kinetics observed will increase as more radical pairs are assigned to each spur.

If the radical distribution is multinomial (random), then the overall observed reaction rate constant would be strictly second order (28). If the radical concentration in the zones is random (nonuniform) and the restriction to even numbers of radicals in each zone is

neglected, the reaction rate should be exactly second order (30). If the concentration in the spurs are equal, a deviation to first order kinetics would result.

2.8.3.3 Decay of Allylic Radicals

The decay of allylic radicals in the crystalline and amorphous areas of polyethylene can be mathematically described as a second order decay process occurring simultaneously in different zones (32). One must assume two spatially separated second-order reactions occurring with and without diffusion control in each zone for the best interpretation of the experimental data. The application of this technique will be reviewed in section dealing with poly(ethylene terephthalate).

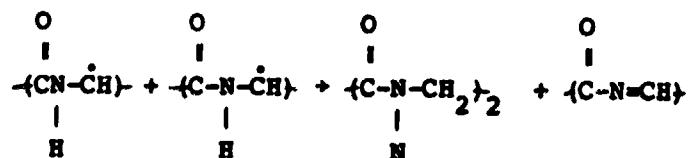
2.8.4 Polyamides

Polyamides are semicrystalline polymers that, when containing aromatic groups, exhibit good radiation resistance (33,34). Nylon 6,6, a nonaromatic polymer, exhibits significant loss in tensile strength and breaking elongation due to chain scission yields being greater than crosslinking yields (34).

The predominate free radical in nylon 6,6 is at the α -carbon to amide nitrogen ($C-N-\dot{C}$) (34). Disproportionation results in an amide

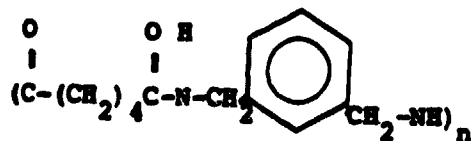


group and one ($CON=CH$) group which decomposes to produce a chain scission (34).



Meta-xylylenediamine and adipic acid form an aromatic polymer,

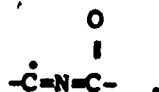
MXD-6, of the structure



which shows resistance to gamma radiation (33).

Radical Decay

Krasnansky observed changes in optical density at 300 m μ of a UV-visible spectrum was the result of colored species (33):



Krasnansky (35) derived the following empirical equation to describe experimental decay curves in Figure 13:

$$-\frac{dA}{dt} = A^2 (c_3 e^{k_1 t} + c_4 e^{-k_2 t}) \quad (28)$$

This is derived from the equation for the straight line in Figure 12:

$$\ln\left(\frac{A_0}{A_F}\right) = k_F t + a \quad (29)$$

and figure 14:

$$\ln\left(\frac{A_0}{A_F} - \frac{A_0}{A_i}\right) = -k_i t + b. \quad (30)$$

These two equations combine to give

$$\frac{A_0}{A_i} = e^a e^{k_F t} - e^b e^{-k_i t} \quad (31)$$

where F means final, i the initial time of the reactions, and A is the absorption. Equation 19 can be written

$$\frac{A_0}{A} = (c_1 e^{k_1 t} - c_2 e^{-k_2 t}) \quad (32)$$

and differentiated to give equation 28 which describes a second order process dependent upon two catalytic species, one increasing and the other decreasing with time (35).

Zimmerman (36) obtained a negative deviation from linearity in radical concentration versus dose rate curve for various polyamides as shown in Figure 14 (36).

The polymers, nylon 66, nylon 610, and the polyamide from 2 methyl hexamethylene diamine and oxalic acid, were irradiated with 2 MeV electrons at 78°C where the decay termination rate is assumed negligible (34,36). Zimmerman (36) also found that the radical termination rate constants decrease as dose increases. He associated these phenomena with the overlap of free radical spurs at higher doses.

The dose at which linear dependence ceases indicates the placement of new clusters of radicals at sites of previous spurs. Assuming spurs distribute randomly in an irradiated solid during the radiation process and that the polymer is divided spacially into N boxes each having the average volume of a spur, a model can be constructed.

Let f_0 be the fraction of boxes containing no spurs, f_1 and one spur, f_2 two spurs, etc., while r is the ratio of spurs to boxes. The change in f per unit change in r is:

$$-\frac{df}{dr} = f_0 \quad (33)$$

similarly,

$$\frac{df_1}{dr} = f_0 - f_1 \quad (34)$$

$$\frac{df_n}{dr} = f_{n-1} - f_n \quad (35)$$

These equations are solved as those developed by Flory (37) for

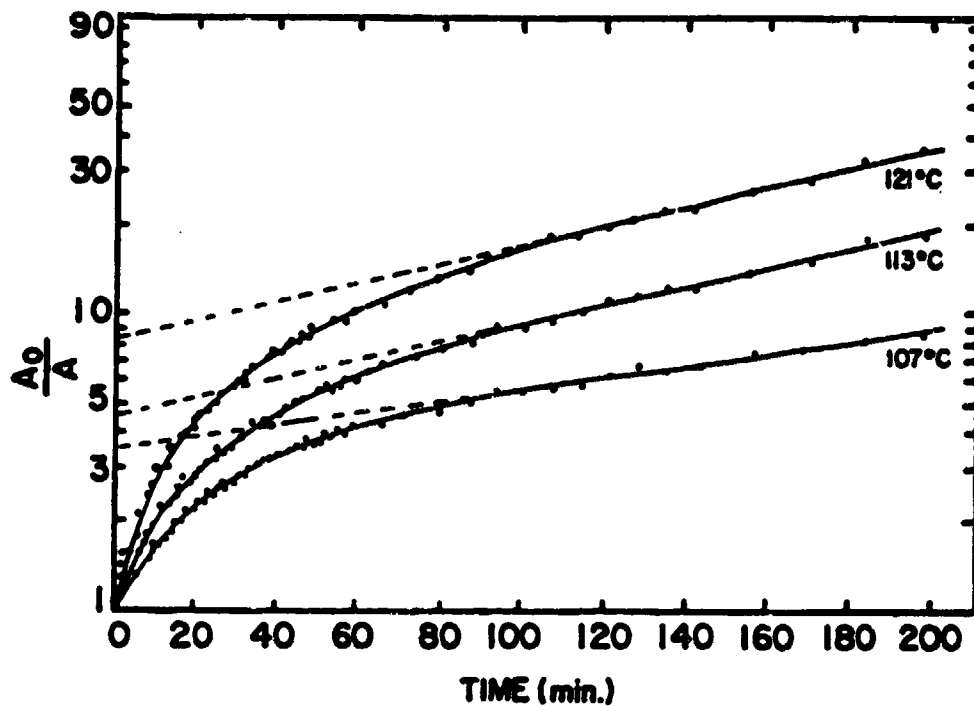


Figure 13. Decay of optical density @300 $m\mu$ of irradiated nylon (MXD-6) films at various temperatures (33).

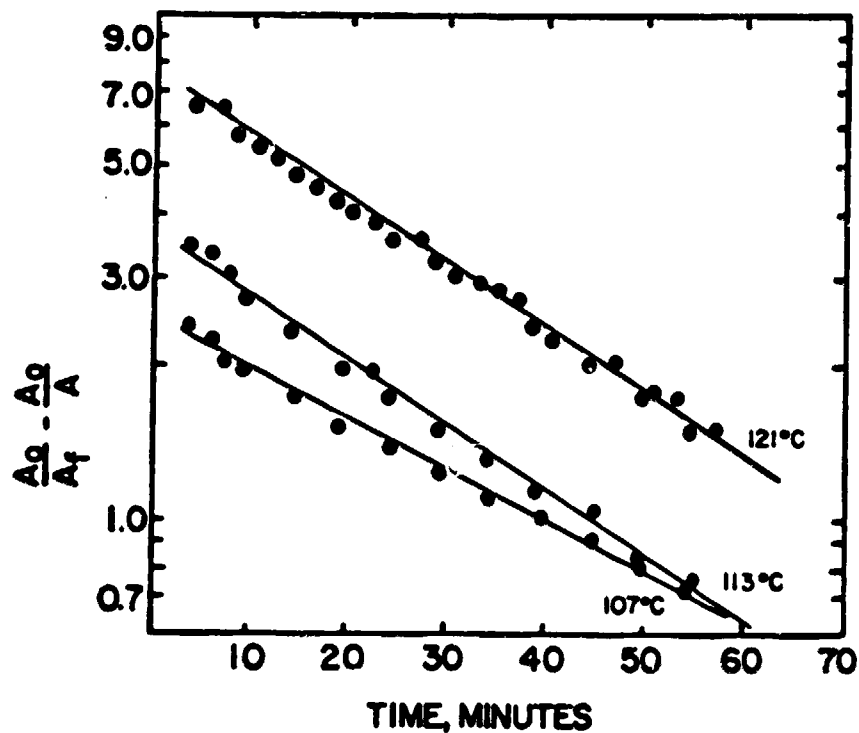


Figure 14. Initial reaction rate constants from ultraviolet absorption studies for nylon (MXD-6) films at various temperatures (33).

calculating molecular weight distributions formed by addition polymerization of monomers to a fixed number of chains. The solution involves rearranging and integrating equation 33

$$\int \frac{df_0}{f_0} = \int_0^r -dr \quad (36)$$

$$\ln f_0 = -r \quad (37)$$

$$f_0 = e^{-r} \quad (38)$$

inserting into equation 34

$$\frac{df_1}{dr} + f_1 = e^{-r} \quad (39)$$

and solving the resulting first order linear differential equation giving

$$f_1 = re^{-r} \quad (40)$$

For equation 35 placing the value of $n = 2$, the solution is

$$f_2 = r^2 e^{-r} / 2 \quad (41)$$

The general solution can be deduced to be

$$f_n = r^n e^{-r} / n! \quad (42)$$

which is a form of Poisson's distribution formula. Figure 16 illustrates the changes of fractions of boxes containing different numbers of spurs, f_0 , f_1 , f_2 , f_3 , and f_g which is the fraction of polymer occupied by more than one spur, with increasing r which is proportional to radiation dosage (36).

From Figure 15 marked deviation from linearity for nylon 66 and nylon 610 occur at 5 Mrads and at 10 Mrads for polyoxamide. From this fact, these doses correspond to $r = .2$ in equation 29 and the number of spurs is equal to the number of boxes ($r=1$) at 25 and 50 Mrads, respectively. The diameter of a spur can be calculated as 38Å for 66 and 610 nylons and 30Å for polyoxamide, assuming for each spur 100ev are dissipated (36).

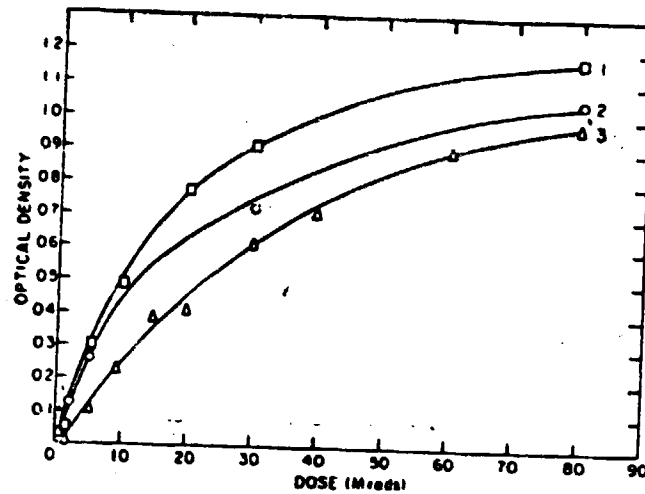


Figure 15. Transient optical density versus radiation dose for irradiated polyamide films (0.1 mm thick), 1) Nylon 6,6, 2) Nylon 610, and 3) Polyoxamide (34).

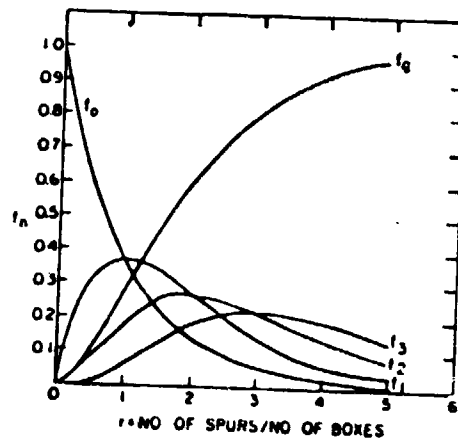
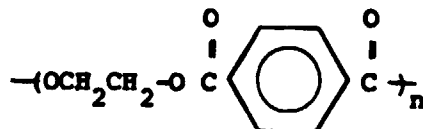


Figure 16. Variation in distribution of spurs with radiation dose, the change of the boxes containing different numbers of spurs, F_0 , F_1 , F_2 , F_3 and F_4 which is the fraction of polymer occupied by more than one spur, with increasing r which is proportional to radiation dose (34).

2.8.5. Poly(ethylene terephthalate)

Poly(ethylene terephthalate), PET, is a condensation polymer of the regular structure



that leads to a high degree of crystallinity.

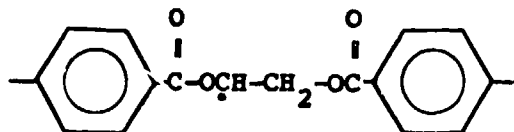
When exposed to high energy radiation the elongation at break decreases for PET. It decreases at the same rate as polyethylene, but the tensile strength which is initially much higher decreases faster (23). The radiation stability of PET is viewed as lower than polyethylene (23).

Chapiro (4) states that an increase in modulus is always observed at low radiation doses, but decreases to below the original value at higher doses.

The ESR spectra of PET irradiated and recorded at -196°C gives a strong singlet with g equal to that of a free electron (38). The signal can be photo bleached and saturates with power easily so Nemetea and Stannett (38) concluded the peak was due to trapped electrons (38).

Araki et al (39) irradiated biaxially oriented film in vacuo and then exposed the sample in air to oxidatively degrade the free radicals in the amorphous regions.

The resulting spectra of six or eight lines, depending upon sample orientation was assigned the structure:



An extra center line was tentatively assigned by Araki et al (39) to this structure:

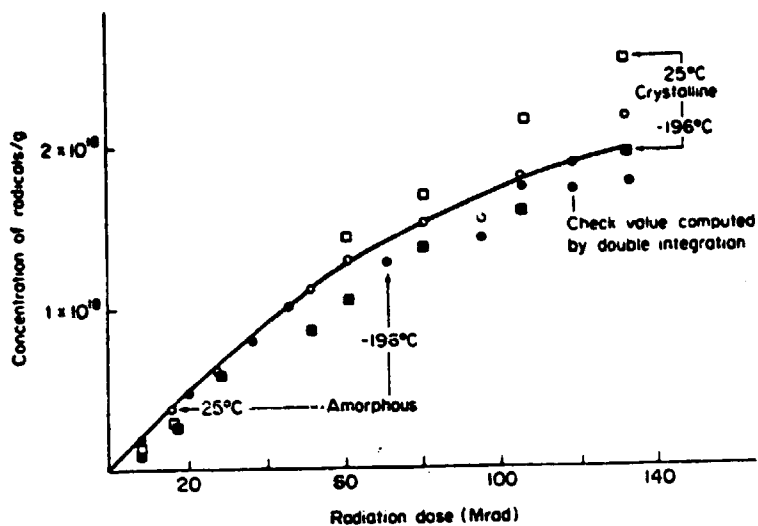


Figure 17. The initial accumulation of radicals with dose (40).

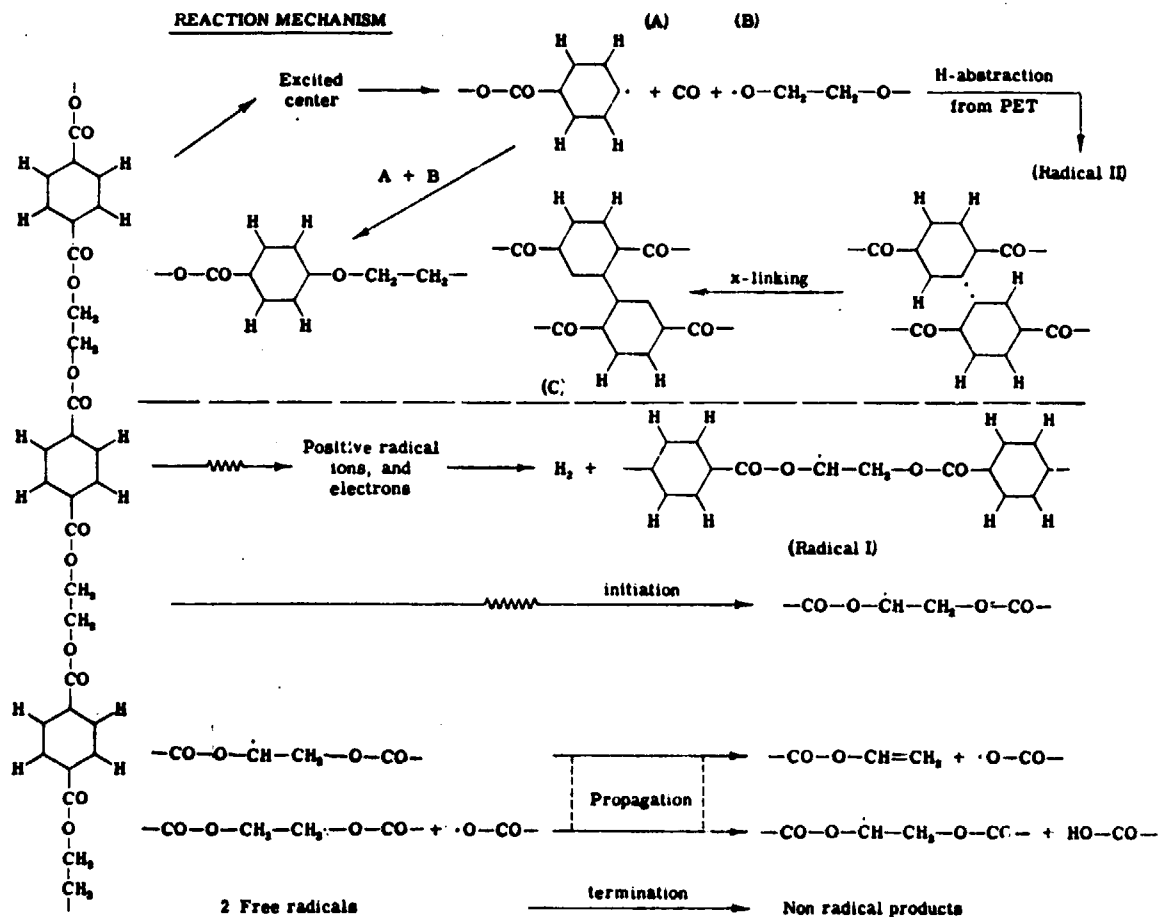
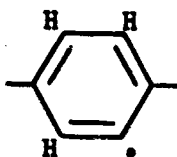


Figure 18. Schematic of mechanism for dose rate dependence based on available evidence (19).



Completely amorphous PET yields poorly resolved spectra that have not been analyzed (40). Figure 17 shows that the initial accumulation of free radicals with dose exhibits little difference whether irradiated at 196°C and allowed to warm to room temperature for examination or examined after irradiation at room temperature by ESR spectroscopy (40).

The effects of radiation on PET are dependent upon dose rate. Specifically, under high dose rates the polymer gels because of cross-linking, but under low dose rates at the same dose levels solubility is maintained (40). PET appears to be more susceptible to chain scission at low dose rates.

Figure 18 (40) gives Turner's (40) mechanism for the dose rate dependence based on the available evidence. The probability of termination of the propagation reaction at the bottom of Figure 17 (40) would be greater at higher dose rates because more radicals would be available for termination (40).

2.8.5.1 Radical Decay

Stannett, et al (41) demonstrated that the Q function developed by Dole et al (32) for the kinetics of two simultaneous second-order reactions occurring in different zones can be applied to semicrystalline PET.

This model considers two reaction zones whose second order reaction constants are K_f for fast decay in one zone and K_s for slow decay in

the second. The assumption that there is no interdiffusion between zones is made, for if rapid diffusion between zones occurred the overall reaction would be observed as simple second order with a reaction rate constant equal to $K_F + K_S$.

With the condition that no exchange occurs between zones, the following equations can be written:

$$C = C_f + C_s \quad (43)$$

$$C_o = C_{o,F} + C_{o,S} \quad (44)$$

$$C_f = \frac{C_{o,F}}{1 + C_{o,F} K_{Ft}} \quad (45)$$

$$C_s = \frac{C_{o,S}}{1 + C_{o,S} K_{St}} \quad (46)$$

where equations 45 and 46 are the usual integrated second-order equations, t is time, and C_o the total observed concentration at zero time. From these equations a Q-function is derived,

$$Q = \frac{t}{\frac{1}{C} - \frac{1}{C_o}} = \frac{1 + C_o X_F X_S (k_F + k_S) t}{X_F^2 K_F = X_S^2 K_S + C_o X_F X_S K_F K_S t} \quad (47)$$

where X_F and X_S are mole fractions of the fast and slowly decaying species at zero time; eg $X_F = C_{o,F}/C_o$.

When $K_S \ll K_F$, $X_S \neq 0$, and $K_S = 0$,

$$Q = \frac{1}{X_F^2 K_F} + C_o \frac{X_S}{X_F} t \quad (48)$$

and when a plot of Q vs. t is linear with a non zero slope the conclusion can be made that only one of two types of radicals present is reacting at a measurable rate.

For the more general case the following equation is used:

$$Q = \frac{1 + Kt}{A + Bt} \quad (49)$$

where

$$A = X_F^2 K_F + X_S^2 K_S \quad (50)$$

$$B = C_o X_F X_S K_F K_S \quad (51)$$

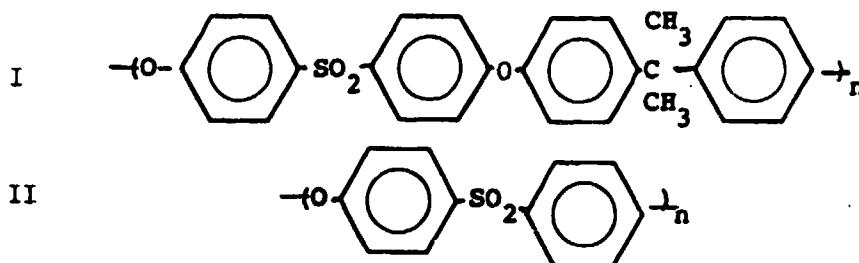
$$K = C \times X_F \times X_S (K_F + K_S) \quad (52)$$

Stannett et al (41) state that their present calculations with the Q function indicate that the radical decay rate constant is greater for a sample irradiated with a 15.0 Mrad dose than a sample irradiated with a 7.5 Mrad dose. In polyethylene the opposite is true. This discrepancy was tentatively explained by the fact that crosslinking is the predominant reaction in polyethylene and scission is predominant in PET at low dose rates. Crosslinking constricts the chain probability while scission should have the converse effect.

2.8.6 Polysulphones

Aromatic polysulphones form commercial plastics possessing a high glass transition temperature and a high thermal stability in both inert and oxidizing atmosphere (26).

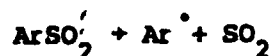
Two polysulphones studied by Brown and O'Donnell (43) are poly(oxy 1,4 phenylene sulfonyl 1,4-phenylene-oxy 1,4 phenyleneisopropylidene-1,4 phenylene) (I) and poly (oxy-1,4-phenylenesulfonyl-1,4-phenylene) (II) of the structures



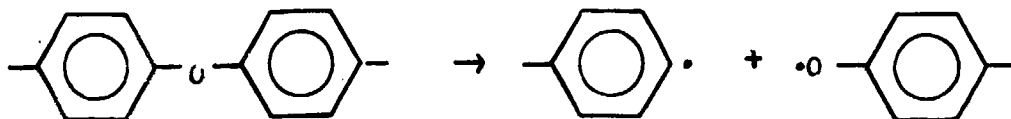
When irradiated with cobalt-60, γ rays at dose rates of 2-4 Mrad/hr in a vacuum, flexural strength of polysulfone I dose not decrease, however after irradiation in air flexural strength diminishes by fifty percent. Polysulfone II shows good retention of flexural strength with

radiation in the same manner under vacuum but in air an initial decrease in flexural strength is evident followed by a decrease with increasing dose.

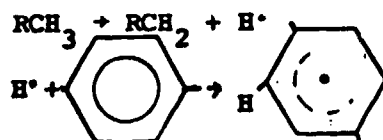
Irradiation of both sulfones produces SO_2 g, indicating the carbon sulfur bond chain scission is an important first step followed by SO_2 liberation (43).



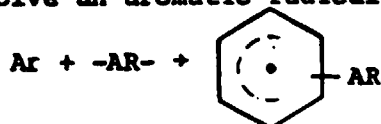
This reaction is supported by the ESR experiment of Lyons et al (44) in which he identified the presence of phenylenesulfonyl radicals in γ -irradiated polysulfone II. Also from his work Lyons concluded both oxy- and sulphony- linkages are susceptible to breakage.



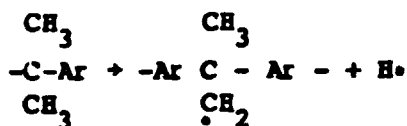
At liquid nitrogen temperatures, the major radicals present are cyclohexadienyl radicals formed by the process (44):

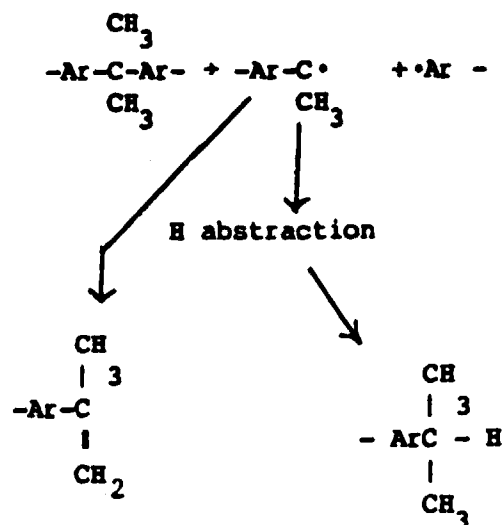
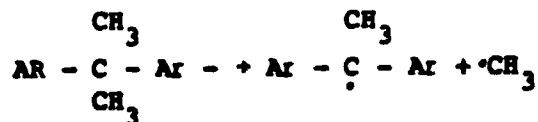


Crosslinking and scission reactions are possible for both the polysulphones could involve an aromatic radical:



A possible reaction sequence that leads to chain scission in polysulfone I at the isopropylidene linkage is given below (44)

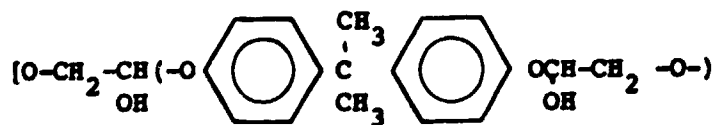




The decrease in flexural strength was shown by Brown and O'Donnell to be dependent upon the diffusion of oxygen. Increases in chain scission at the surface manifested by the lower viscosity of polymer removed from the surface relative to regions in the center of the sample, illustrated that the decrease in flexural strength would be observed in air only if oxygen is allowed to diffuse far into the sample (26).

2.8.7 Epoxy Resins

Epoxy resins are thermosetting polymers. A widely used epoxy is based on polyethers formed in condensation reactions between bisphenol A and epichlorohydrine (23).



Epoxies required large portions of amines for curing, and the use

of aromatic amines enhance radiation resistance to relatively high doses (45).

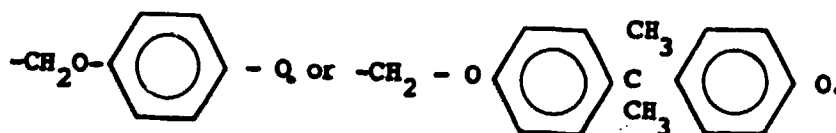
Oxygen plays an intricate role in the degradation of epoxies and at high dose rates it may be depleted faster than diffusion can occur making sample thickness pertinent (23).

There are few ESR studies of irradiated epoxy resins. Overall (46) reported the generation of radicals in epoxy rods which darkened upon heating to 130°C in air. Heating in vacuum of the sample caused a decay of radicals and a decrease in the initial line width from 8-10 gauss to 7 gauss after 17 days.

Heating new samples in vacuum at 180°C produced no radicals.

The disappearance of radicals on heating the epoxide rods in vacuum shows this process occurs through molecular diffusion rather than through interaction with oxygen. The necessity of air to produce radicals is probably due to diffusion controlled oxidation.

The ESR spectra is unresolved, but the most probable radical is the result of oxidative scission of the polymer chains:



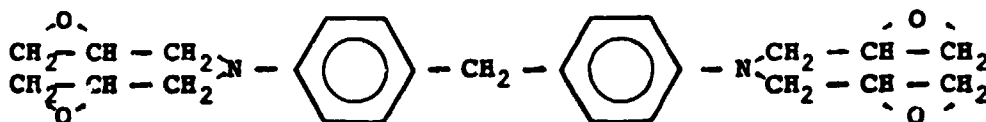
3. Experimental Procedure

Ciba Geigy MY720 Alradite Epoxy Resin was cured with Eporal Hardener (Ciba Geigy) and irradiated with 0.5 Mev electron radiation at room temperature and with ^{60}Co (1.33 and 1.17 Mev) gamma radiation at liquid nitrogen temperature. Free radical concentration in the samples were estimated by comparison with a free radical standard by double integration of the ESR spectra. Radical build up with dose and radical decay curves with time were analyzed and the results compared with those of other polymers.

3.1 Materials

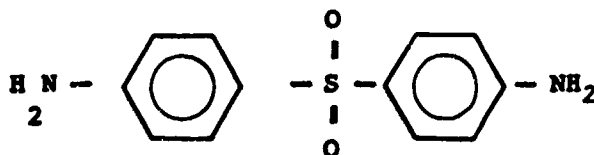
3.1.1 Epoxy Resin Samples

Ciba Geigy MY720 Alradite Epoxy Resin is named tetraglycidyl-4,4' diaminodiphenyl methane (TGDDM) and Ciba Geigy Eporal Hardener is 4,4' diamino diphenyl sulfone (DDS). The structures of the epoxy resin and curing agent are given below (50):



Tetraglycidyl - 4,4' diamino diphenyl methane

(TGDDM)

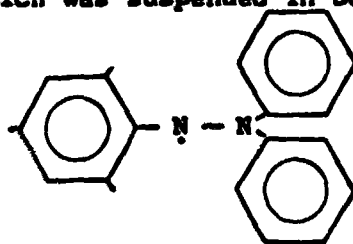


4,4' - diamino diphenyl sulphone

(DDS)

3.1.2 Radical Standard

The radical standard used was 2,2 - diphenyl - 1 - picryl hydrzyl (DPPH) (MW = 394.32) which was suspended in Scotch brand 3M epoxy amide resin.



2-2 diphenyl - 1- picryl hydrazyl
(DPPH)

3.2 Equipment

3.2.1 Radiation Equipment

Radiation from an electron accelerator and Cobalt - 60 gamma source were used in this study. The electron accelerator, manufactured by High Voltage Engineering Corporation, was operated at 8.3 milliamperes beam current and 500,000 volts from an insulated core transformer. This equipment utilizes a horizontal beam scanned 48" by 6". The samples were hung vertically on a conveyor, which carried them in front of the beam twice each revolution through equipment so that samples received half of their total dose on each side. All radiations were carried out in nitrogen filled ziploc polyethylene bags from Dow Chemical Corporation. Dosimetry measurements performed by Naranong (3) were used for dosage determination in this investigation. The gamma radiation was obtained from a Gamma Cell 220 cobalt - 60 source with a known dose rate of approximately 0.24 Mrad per hour.

3.2.2 ESR Spectrometer

The radicals generated by irradiation were observed on a Japan Electron Optics Laboratory (JEOL) JES - ME - 1X ESR spectrometer. Measurements were made at liquid nitrogen temperature in an immersion dewar.

3.3 Procedure

3.3.1 Epoxy Sample Preparation

The samples were in the form of cylindrical rods which were 3/32" (0.238 cm) in diameter and were composed of 73% (w/w) TGDDM and 27% (w/w) DDS.

The resin was mixed by first weighing the TGDDM in a tared container and heating to 100 - 110 °C on a hot plate agitated with an overhead mechanical stirrer. The calculated amount of DDS was slowly added to the TGDDM at 110°C continuing stirring until the DDS was completely dissolved.

The mixture was placed in a heated vacuum desiccator at 110°C and deaerated. To avoid excessive overflow of the mixture from the container the vacuum was shut off at three five minute intervals (and the system flushed with nitrogen). The desiccator's heater was then shut off and the desiccator and contents were maintained under vacuum for 48 hours at room temperature. The mixture was stored in a desiccator until use.

The epoxy resin was reheated under vacuum to 110°C and then placed under a nitrogen atmosphere. Teflon tubing with a 3/32" inner diameter cut into lengths of 3 cm were inserted lengthwise into the TGDDM/DDS

mixture and allowed to sink. The solution was allowed to cool. The container was then broken and the excess resin was easily taken off the surface of the teflon. The ends of the tubes were sealed with teflon tape. The resin was then cured at 137°C for 3 hours and then 160°C for 5 hours.

The cured epoxy rods were removed by either cutting the top of the tubing lengthwise and peeling it off or by pushing the rods out with a small metal rod. The samples were weighed, wrapped in aluminum foil, labeled, placed in a desiccator, and stored under vacuum.

3.3.2 Standard Samples

DPPH was weighed out into a tared container and then Scotch brand 34 epoxy resin and amide hardener were added to the container, weighed, and mixed in the same manner as the TGDM/DDS system except at ambient temperature. The mixture was deaerated for 15 minutes and teflon tubes inserted into the resin mixture. The resin was allowed to partially cure at ambient temperature before the teflon tubes were removed and the resin allowed to fully cure for 24 hours.

3.3.3 Electron Irradiation Exposure

The samples which were wrapped with aluminum foil and placed in nitrogen filled ziploc bags were placed on the conveyor belt of the electron accelerator and passed through the resulting in a nominal 10 Mrad exposure per pass. Each pass took approximately 3.5 minutes.

The samples were removed from the conveyor after the desired dosage and immediately immersed into a Dewar containing liquid nitrogen (-196°C), stored until ESR measurement was made.

3.3.4 Gamma Irradiation Exposure

The labeled, aluminum foil wrapped samples were placed at various intervals of time in a Dewar containing liquid nitrogen which was located in the irradiation chamber of the gamma cell so a range of 10-50 Mrad dosages could be obtained. The samples were stored until ESR measurement was made.

3.3.5 ESR Measurements

The samples were measured on the ESR spectrometer at liquid nitrogen temperature with an ESR quartz nitrogen immersion dewar. The typical settings on the spectrometer were as follows:

Magnetic field	:	~ 3700 - 3740 ± 100 Gauss
Gain	:	~ 1 x 1 - 1 x 1000
Response	:	0.1 - 0.3 sec
Modulation width	:	.63 - 1.6 Gauss
Power	:	0.2 - 0.6 mw
Crystal Current	:	0.5 - 0.7 mA
Frequency	:	~ 9.35 GHz
Scan time	:	5-10 minutes

The first derivative spectra were doubly integrated by the numerical method of W yard (21). the equation used was:

$$A = 1/2 h^2 \sum_{r=1}^n (2n - 2r + 1) y_r$$

where h is the width of the interval into which the spectra were divided, n is the number of intervals, and y is the height of the rth interval at the middle of the interval. A is the area of the absorption

C-2

curve of the spectra and is proportional to the radical concentration in the sample.

The areas of the DPPH sample with known spin concentration were compared with areas of the unknown TGDDM/DDS samples to estimate the radical concentration of the unknown samples. Using the formula:

$$\frac{A_U}{W_U} \times \frac{C_D}{A_D} \times W_D \times \frac{F_D}{F_U} = C_D$$

where A is the area of the absorption spectra, C is the concentration (spins/g), F is the amplitude setting, and w the weight in grams while U and D are subscripts denoting the unknown and DPPH samples, respectively.

3.3.6 Decay Experiments

Radical decay was measured by exposing the sample to room temperature for a period of time and then recording the ESR spectra at liquid nitrogen temperature. It was determined that the sample took about 1/2 minute to reach 17°C and 2-3 minutes to reach room temperature. This time was counted with the time of decay. It is negligible at long times.

4. Results and Discussion

Using an empirical estimate developed by Walsh and Rutherford (50) and applied to a thin film by Naranong (3), the curve that approximates the dosage experienced by a TGDDM/DDS sample which has an effective thickness of 122 mils (93.8×1.3 specific gravity) along the sample thickness parallel to the electron beam is shown in Figure 1A. This curve illustrating the dosage experienced as a function of distance along the diameter perpendicular to the beam as shown in Figure 1B. The effective radiation dosage at the center of the sample can be seen to be a fractional percentage of the dosage toward the edges. The actual average dosage across the cross section is calculated to be 0.57 of the dosage delivered by the beam. All the results hereafter are based on the normal dosage and are not corrected for variation over the cross section.

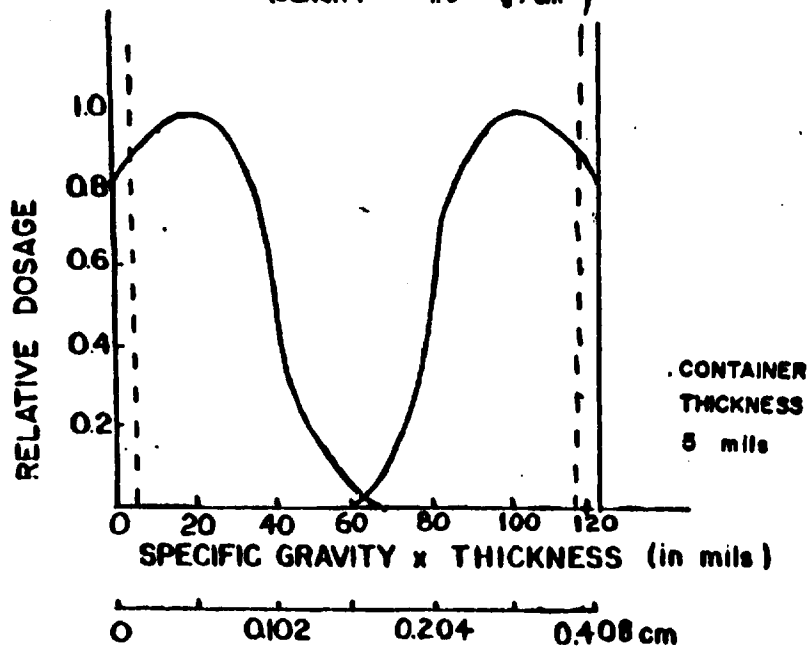
In the gamma experiments, the high penetration of the gamma radiation into samples allows one to assume a homogeneous deposition of energy into the material.

4.1 ESR Spectra

Figures 2 and 3 show the ESR spectra of TGDDM/DDS samples; gamma irradiated at 196°C and an electron irradiated at ambient temperature, respectively. The major difference in these spectra is the presence of long wings in the spectrum of the gamma irradiated sample (Figure 2) which are not present in the spectrum of the electron irradiated sample (Figure 3). The radical concentration of the sample irradiated with

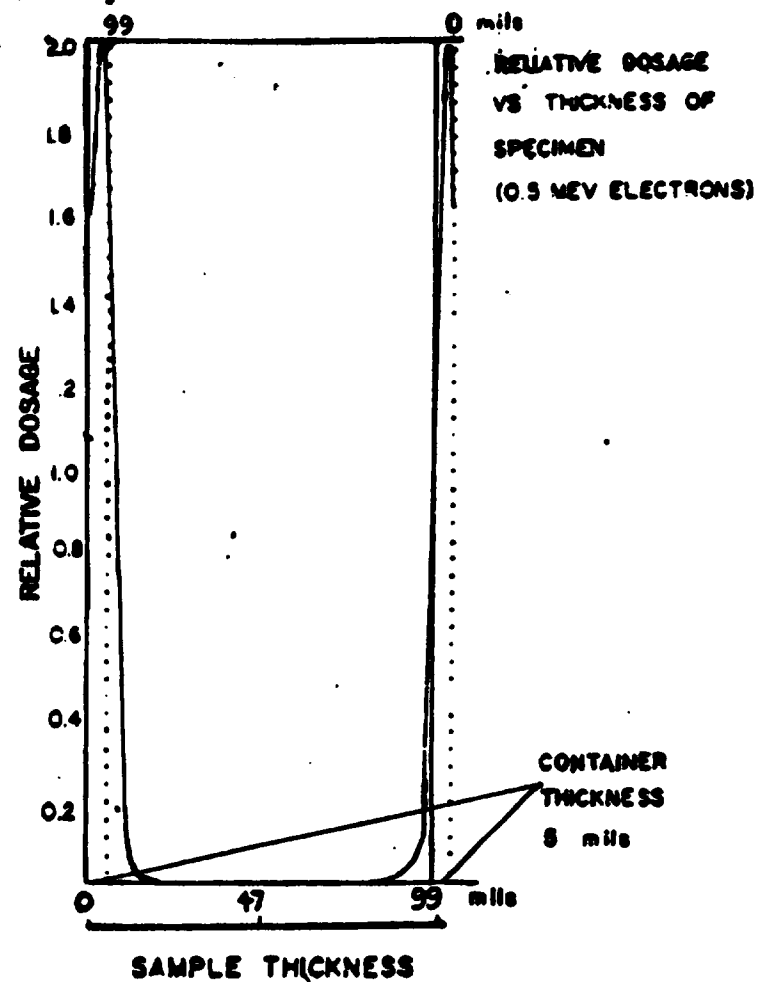
ORIGINAL PAGE IS
OF POOR QUALITY

RELATIVE ABSORPTION VS THICKNESS FOR 1/2 MEV
ELECTRONS IN EPOXY (DENSITY $\approx 1.3 \text{ g/cm}^3$)



A

RELATIVE ABSORPTION VS THICKNESS FOR
TGDDM/DDS SAMPLE



B

Figure 1. Relative absorption versus thickness in sample 94 mils in diameter taken along (a) diameter⁵ parallel to irradiating electron beam and (b) along diameter perpendicular to irradiating electron beam.

ESR of CURED EPOXY
 γ IRRADIATED 53.73 Mrad at 77°K
ESR at 77°K
 2.4×10^{19} radicals/gm

58

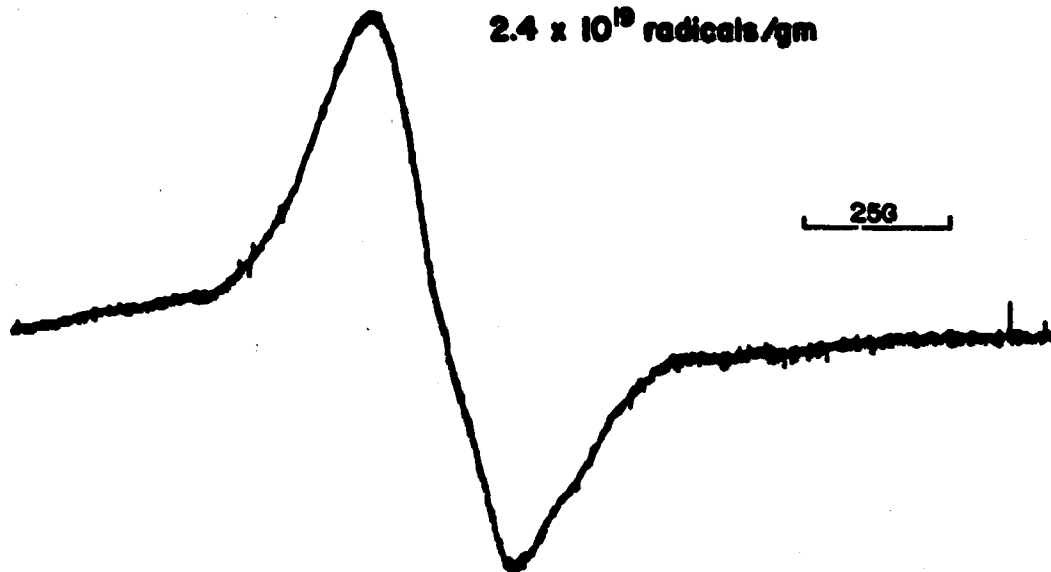


Figure 2. ESR spectrum of gamma irradiated TGDDM/DDS sample.

ELECTRON IRRADIATED EPOXY 60Mrads
IRRADIATED AT ROOM TEMP
STORAGE, RADICAL MEASUREMENT AT 77°K
 1.7×10^{19} radicals/g

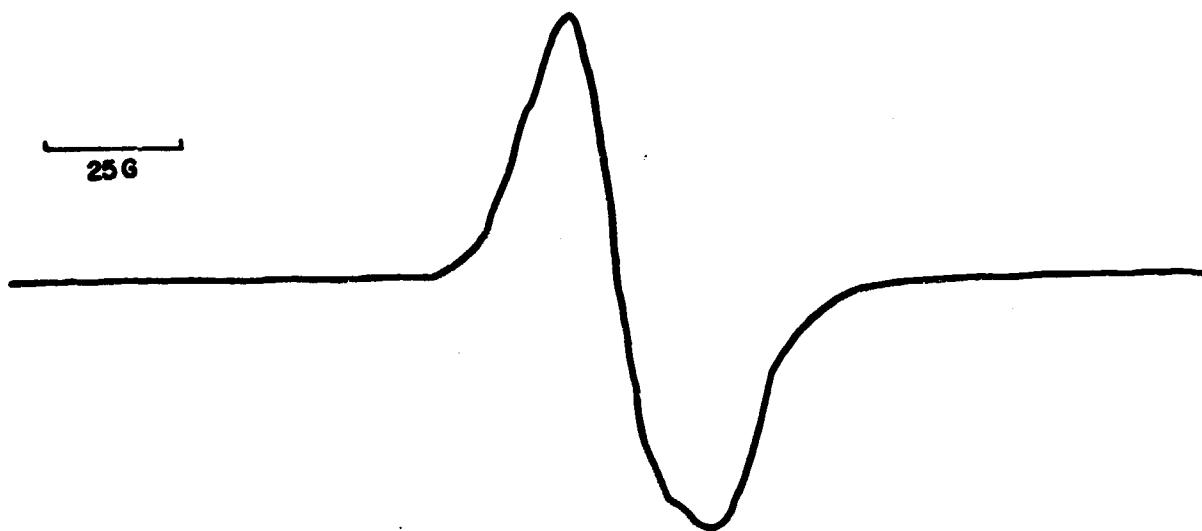


Figure 3. ESR spectrum of electron irradiated TGDDM/DDS sample.

gamma radiation is 2.4×10^{19} spins/g and the electron irradiated sample spin concentration is 1.7×10^{19} spin/g.

Figure 4 shows the spectrum of the gamma irradiated epoxy sample after 6 minutes of decay. Along with a significant decrease in overall intensity of the spectrum corresponding to a radical concentration of 1.2×10^{19} spins/g. The decay of the wings is essentially complete so that the spectrum resembles that of the electron irradiated sample in Figure 3. This seems to indicate a very quickly decaying species which may be trapped electrons, radical ions, or radical pairs (though there is no peak at g-4).

Figure 5 illustrates how the g value of 2.0046 of an electron irradiated can be obtained by a comparison with the g- value of a DPPH sample. The spectra exhibit no fine structure, though there is an assymetry present in which become more predominate as decay at room temperature was continued.

4.2 Radical Build-up

Figure 6 shows that the radical concentration versus gamma radiation dose (at 196°C) is a linear relationship. G (radical) has the value 0.59 radical/100eV for this irradiation. Because this curve is linear, it may be concluded there is a minimal amount of radical reaction at this temperature and thus all paramagnetic species are trapped.

Figure 7 shows the radical build-up curve for samples exposed to 1/2 MeV electrons and a curve showing the radical concentration at various doses after 200 minutes decay at room temperature ($\sim 25^\circ\text{C}$).

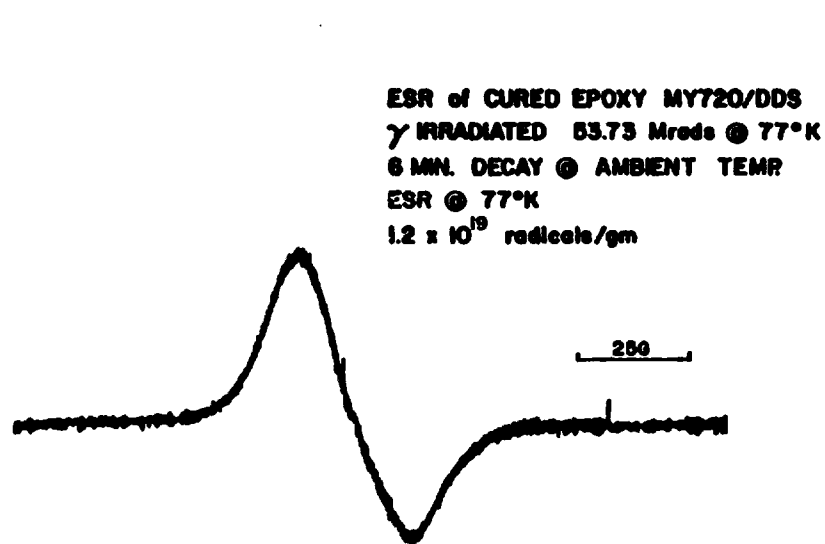


Figure 4. ESR spectrum of gamma irradiated sample after 6 minutes at ambient temperature.

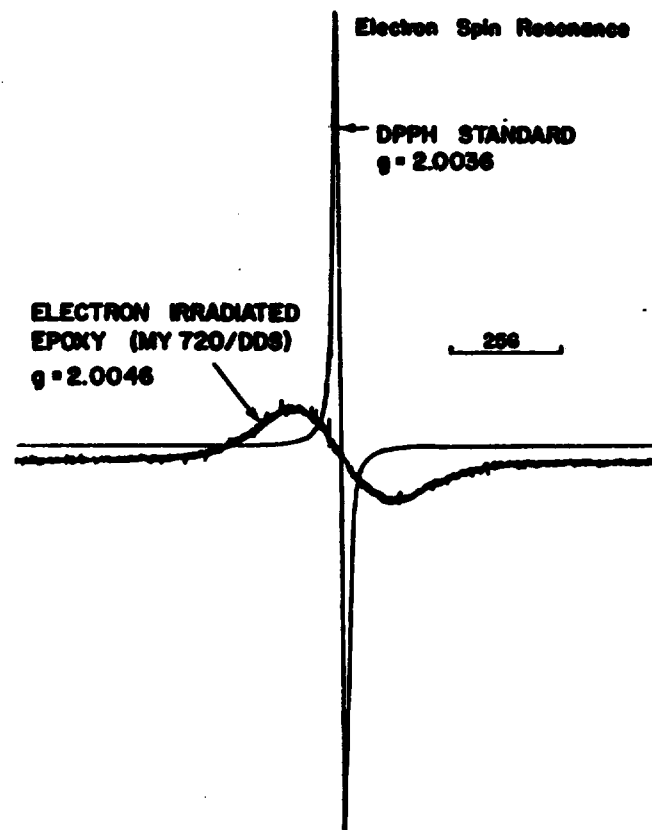


Figure 5. ESR spectrum of electron irradiated sample with superimposed spectrum of DPPH suspended in epoxy resin.

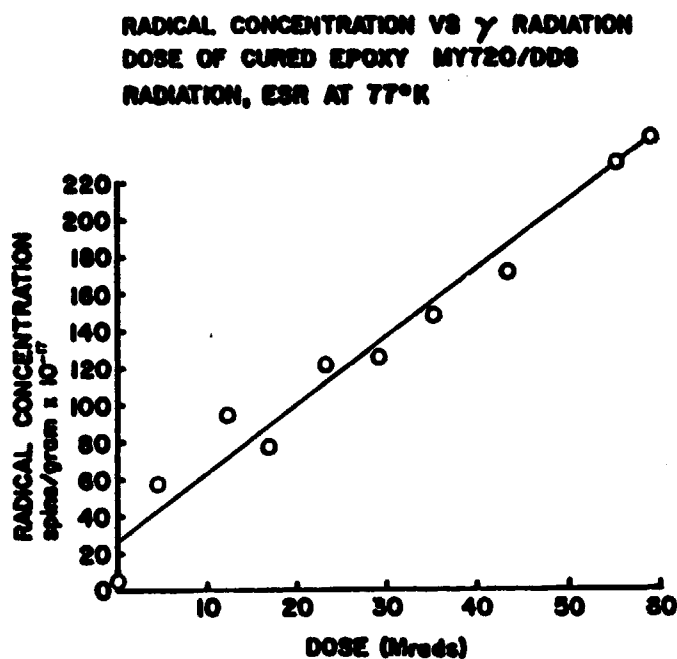


Figure 6. Build-up of radical concentration with dose of Cobalt 60 (1.33 and 1.17 MeV) in TGDDM/DDS samples.

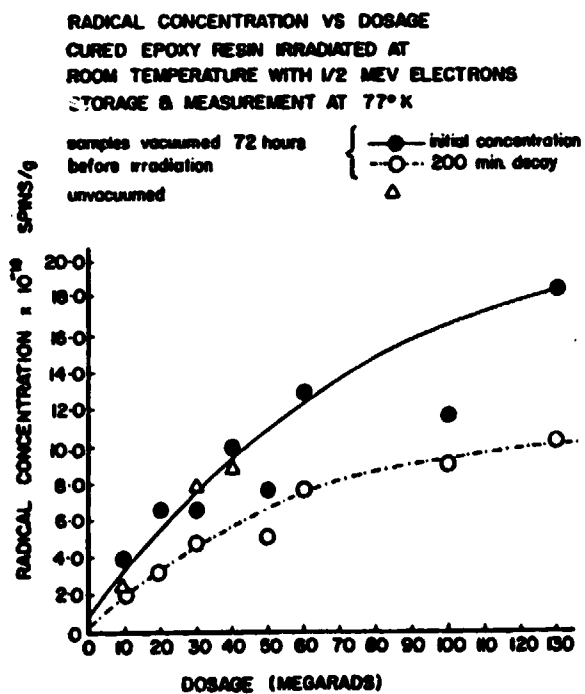


Figure 7. Build-up of radical concentration with dose of 1/2 MeV electrons in TGDDM/DDS samples.

4.3 Spur Size

Energy is deposited by the electrons in such a manner that spurs or groups of radicals are formed. One can assume that spur expansion due to diffusion of radicals is slow because of the immobility of the polymer chains. This assumption can be made confidently if one notes the glass transition temperature of a 73/27 (w/w) TGDDM/DD8 epoxy system has been reported to be 190°C (52) and 260°C (50), this value varying due to differences in sample preparation or rate and type of measurement.

If one also assumes the inhomogeneity of energy deposition illustrated in Figures 1A and 1B does not disrupt the presumption that spurs deposited in a random manner, then equation 42 (34) in Section 2.6.4 can be applied;

$$P_n = \frac{r^n e^{-r}}{n!}$$

Following Zimmerman's method (34), the first marked deviation from linearity in the radical build-up curve is at 20 Mrads, so this dose corresponds to a value of $r = 0.2$ in equation 42. The number of spurs would equal the number of boxes at 100 Mrads. The majority of spurs have 1 to 4 ion pairs (8), so assuming 25 electrons per spur and that the G (radical) is approximately 0.6 radical/100eV, the formation of a spur would be an event dissipating about 400 eV. Therefore,

$$\begin{aligned} 100 \text{ Mrads} \times \frac{100 \text{ erg/g}}{10^{-6} \text{ Mrad}} \times \frac{1.3 \text{ g}}{\text{cm}^3} \times \frac{1 \text{ eV}}{1.602(10^{-12}) \text{ erg}} \times \frac{1 \text{ spur}}{400 \text{ eV}} \times \frac{1 \text{ cm}^3}{\text{A}^3} \\ = 2.0 \times 10^{-5} \frac{\text{spur}}{\text{A}^3} \end{aligned}$$

of which the reciprocal would be a spur volume, $4.9 \times 10^4 \text{ \AA}^3$. A spur diameter can be calculated to be 45.5 Å, which is of the order, calculated by Zimmerman (34) for nylon 6, nylon 6,10, and polyoxamide.

The value for the diameter of a spur obtained by this calculation is higher than the actual value due to combination of radicals within the spurs. These radical reactions cause deviations from linearity in the build up curve at a lower dose than the dose at which nonlinearity would be caused simply by spur overlap.

4.4 Radical Decay

Figures 8 and 9 show radical concentration versus time at room temperature plots for electron and gamma irradiated samples, respectively. Both exhibit an initial fast decay followed by an apparently much slower decay region, indicating a relatively fast reacting species and slow reacting species are present.

4.4.1 The Q Function

Figure 10 shows a plot of the Q function derived by Dole (32) versus time. The linearity of the plot indicates the decay consists of two components, both second order reactions occurring in different zones. The equation that defines this line is a simplification of the general case (Equation 2.49 in Section 2.6.5.2) in which the slow decay component is assumed too slow for measurement.

Figure 11 gives a similar plot for the electron radiated samples of doses varying from 10 to 130 Mrads. The initial radical concentration, C_0 , is adjusted in this case by extrapolating a straight line through the origin and the 10 Mrad dose data point.

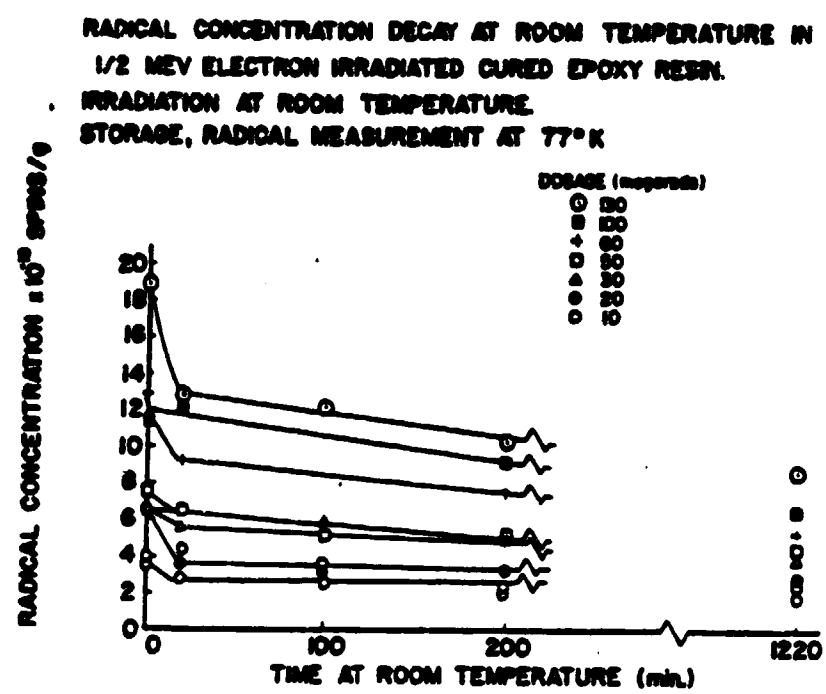


Figure 8. Radical concentration versus time at room temperature for TGDDM/DDS samples irradiated at various dosages with 1/2 MeV electrons.

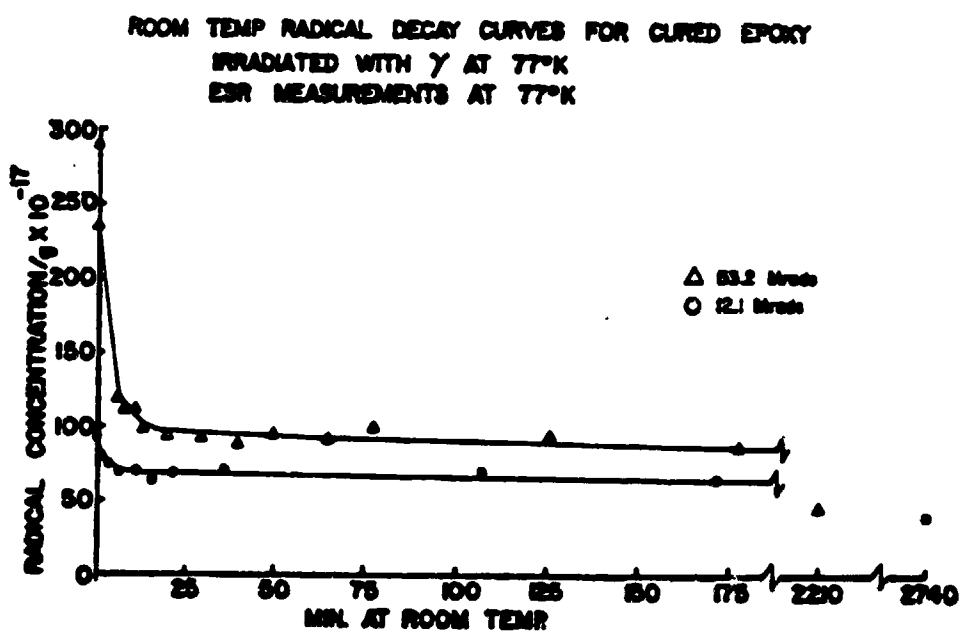


Figure 9. Radical concentration versus time at room temperature for TGDDM/DDS samples irradiated at various dosages with 1.33 and 1.17 MeV gamma rays.

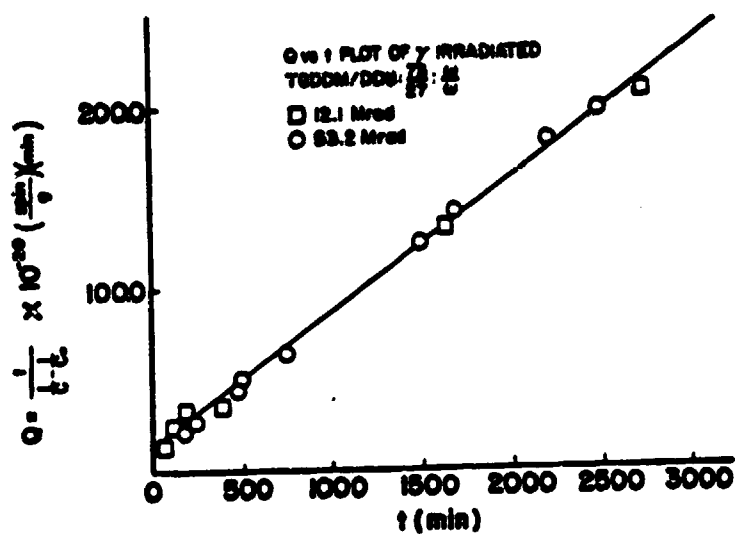


Figure 10. $Q = \frac{t}{C - C_0}$ versus time for radical decay data of Figure 9.

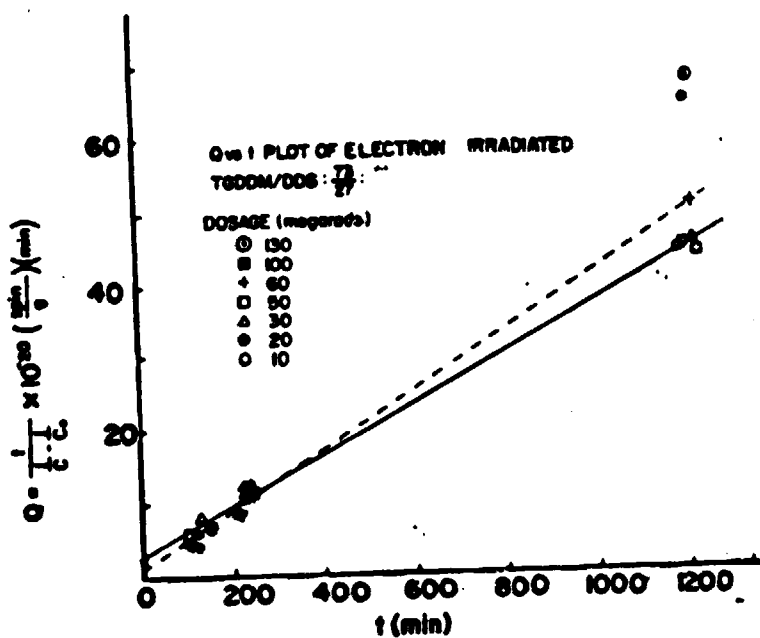


Figure 11. $Q = \frac{t}{C - C_0}$ versus time for radical decay data of Figure 8.

TABLE I
Calculated Values of the Q Function

$$Q = \frac{1}{X_f^2 K_f} X + Co \frac{X_s}{X_f} t$$

Dose Mrad	Co $\frac{\text{spin}}{g} \times 10^{-19}$	Slope $\frac{\text{spin}}{g} \times 10^{-19}$	Intercept $\frac{\text{spin/min}}{g} \times 10^{-20}$	X _s	X _f	$\frac{K_f}{g} \times 10^{21}$ min spin	$\frac{K_s}{g} \times 10^{21}$ min spin
12.1*	9.35	0.73	14.6	0.44	0.56	2.18	0.009
52.3*	29.00	0.73	14.6	0.20	0.80	1.07	0.034
10.0**	3.70	0.34	2.6	0.48	0.52	14.2	0.046
20.0**	7.80	0.34	2.6	0.38	0.70	7.8	0.172
30.0**	11.50	0.34	2.6	0.23	0.77	6.5	0.123
50.0**	19.00	0.34	2.6	0.15	0.85	5.3	0.093
60.0**	23.00	0.41	0.99	0.15	0.85	14.0	0.044
100.0**	38.00	0.52	-0.11	0.12	0.88	-117.0	0.009
130.0**	50.00	0.53	-0.87	0.10	0.90	-14.2	0.037

*gamma radiation (1.33 and 1.17 MeV)

**electron radiation (0.5 MeV)

At the lower doses the electron irradiated samples radical concentration decay data follow the same Q plot. Table I gives the equation and the values of the constants for various doses of the gamma and electron radiation. Discrepancies between the data of the two types of radiation could be due to the inhomogeneous placement of spurs and the error in estimation dosages and initial concentrations of radicals in the electron irradiated samples.

Furthermore, the Q function would not hold for higher doses as the data for electron irradiation suggest. At higher dosages, extensive spur overlap would result in the system no longer existing as separate zones. The decay data would exhibit simple second order behavior with one decay constant due to the homogeneous distribution of radicals. This effect would be expected to be more pronounced in the electron irradiated sample because the energy is deposited nonuniformly so spurs are more likely to overlap at relatively lower doses than with gamma radiation.

4.4.2 Radical Decay Constants

The free radical decay constants for the fast decaying species, k_f , are somewhat greater for the lower dose. The slow decaying species decay constants, k_s , were calculated from the longer times of decay and tend to increase with dose.

In the case of allyl radicals in polyethylene, the rate constants were found to decrease with dose and in the case of PET the rate constants increased with dose. Stannett et al (38) concluded this was due to crosslinking being the predominate reaction in polyethylene limiting polymer chain movement and chain scission predominating at low dose rates in PET, which should have a converse effect of increasing chain mobility. In Naranong's (3) thesis work an increase in stress and modulus of 12% compared with controls of an epoxy composite system with TGDDM/DDS as the matrix. The increase in these properties can be due to crosslinking reactions. The dosages used in Naranong's study were up to 5000 Mrads which are orders of magnitude greater than the doses used in this study. Decreases in the rate constant, k_f , might be due to added crosslinking in less crosslinked regions, causing a slowing of the reaction rate as crosslinking increases with dose.

The second order slow decay constants, k_s , indicate a trend of increasing with dose which would be characteristic of regions in which already have a high crosslink density. Due to the low chain mobility in high crosslinked regions, a higher rate of combination would be expected as radicals are placed closer to each other due to spur overlap.

The decrease of k_p with dose is also characteristic of second order kinetics during multiple zone reactions of which a model was developed by Dole and Inokuti (30) and reviewed in Section 2.6.3.2. When averaging over many small separated reactions, the observed reaction rate will always be greater than or equal to the ideal rate (the rate in which the radicals are homogeneously distributed in the medium).

As dose increases, the chance of spur overlap increases making some zones larger and the observed rate decreases approaching the value of the ideal rate in which there are no separate zones and the system is homogeneous.

The overall kinetics of the TGDDM/DDS system can be fit with a model describing two simultaneous second order reactions occurring in different zones. With increasing dose, the local concentrations in the slow decaying zones increase as a separation of the zones is maintained resulting with an increase of the observed decay rate constants. The decay constant of the fast decaying region decreases with increasing dose because the zones do not remain separate, for they are dispersed in regions in the epoxy that are interconnected. These conclusions are consistent with evidence that the polymeric network of cured epoxy resins contains regions of nonuniform crosslink density (53,54,55,56).

From electron microscopic work (54,55) and NMR studies (56) the sizes of the regions of high crosslink density (or nodules) range in size from 6 nm to 10 nm and are immersed in a lower crosslink density matrix. TGDDM (MY720) cured with N,N' dimethyl - 1,6 diaminohexane (DDH) rather than DDS has been found by Brown and Sandrecyki (53) and

Lind (56) in ESR spin probe and NMR studies, respectively, to contain inhomogeneities. The size of a spur (45 Å or 4.5 nm) is small enough to fit exclusively into regions of the size estimated for the nodules.

The decay of radicals located in a highly crosslinked nodule would be expected to be extremely slow due to restricted movement of chains.

Spurs located in more mobile regions would be expected to contain radicals or ion pairs that would combine at a faster rate.

The effect of oxygen has been neglected in the above arguments. Whether the degassing of the TGDDM and DDS before cure was extensive enough, if any oxygen present was reacted during cure, and if diffusion of oxygen into (or oxygen present in) the sample effects the radical decay is still in question.

5. Summary

Cured TGDDM/DDS $\frac{73}{27} \frac{w}{w}$ samples were subjected to Cobalt 60 gamma rays (1.33 and 1.17 MeV) and 1/2 MeV electrons at doses of 5 to 10 Mrads and a 10 to 150 Mrad ranges, respectively. Radical concentrations were determined by ESR spectrometer and a DPPH standard sample. From the radical concentration versus dose curve for the gamma irradiated samples a G (radical) of 0.59 radical/100eV was obtained. From the radical build-up curve an estimated spur diameter of 45.4 Å was determined for the 1/2 MeV electron irradiated samples.

The decay of radical concentration was observed at room temperature in samples irradiated with 12.1 and 52 Mrads doses of Cobalt 60 gamma rays and with doses ranging from 10 to 150 Mrads of 1/2 MeV electrons. The decay data from both samples fit a model which assumes two simultaneous second order reactions occurring in different zones. The decay constants ranged from 14.2×10^{-21} g/min spins to 1.07×10^{-21} g/min spin for the fast decay species and 0.009×10^{-21} g/min spin to 0.172×10^{-21} g/min spin for the slow decaying species. The results are consistent with electron microscopic, NMR, and ESR spin probe evidence of inhomogeneous distribution of regions of high and low crosslink density in epoxy resins.

6. Recommendations

For further research, decay studies of epoxy systems with different TGDDM/DDS ratios should be undertaken. The size of the crosslink nodules in epoxies is believed to vary with the epoxy/amine ratio. Also, an investigation if oxygen is enhancing the difference in decay of the different regions and if there are other effects due to oxygen. Also, a study of decay at longer times would obtain a more accurate estimate of the slow second order decay constant.

References

1. Jenkins, G. M. and K. Kawamura, Polymeric Carbons, Carbon Fibers, Glass, and Char, Cambridge University Press, 1976, p. 151-156.
2. McGrath, J. E., An Independent Assessment of the Need for NASA Research on the Durability of Materials in the Space Environments and for a New Nasa Facility to Accomplish the Research, VPI. & SU. Blackberg, VA24061.
3. Varanong, Naraporn, Effect of High Energy Radiation on Mechanical Properties of Graphite Fiber Reinforced Composites, NCSU, Raleigh, NC 27650.
4. Chapiro, Adolphe, Radiation Chemistry of Polymeric Systems, Interscience Publishers, New York, 1962.
5. Charlesby, Arthur, Atomic Radiation and Polymers Volume I, Pergamon Press, New York, 1960.
6. Ranby, B. and J. F. Rabek, ESR Spectroscopy in Polymer Research, Springer Verlag, Berlin, 1977.
7. Swallow, A. J., Radiation Chemistry of Organic Compounds, Pergamon Press, New York, 1960.
8. Spinks, J. W. and R. Woods, An Introduction to Radiation Chemistry, John Wiley and Sons, New York, 1964.
9. Henley, Ernest J. and Everett R. Johnson, The Chemistry and Physics of High Energy Reactions, University Press, Washington, D.C. 1969.
10. Charlesby, Arthur, Effect of Radiation on Materials, Harwood, J.J., editor, Rheingold Publishing Corporation, New York, 1958, Chapter 10.
11. Segre, E., Experimental Nuclear Physics, Volume I, John Wiley and Sons, Inc., New York, 1953, Part II.
12. Williams, Efrancon, The Radiation Chemistry of Macromolecules, Malcolm Dole, editor, Chapter 2, Academic Press, New York and London, 1972.
13. Burns, W. G. and R. Barker, Progress in Reaction Kinetics, Volume 3, G. Porter, editor, Chapter 7, Pergamon Press, Oxford, 1965.

14. Hauser, Karl H., Radiation Research, Supplement 2, 480-496 (1960).
15. Alger, Raymond, Electron Spin Resonance Techniques and Applications, Interscience Publishers, New York, 1968.
16. Casteleijn, G., J. J. ten Bosch, and J. Schmidt, Journal of Applied Physics, 39, 4375 (1968).
17. Ingram, D.J.E., Free Radicals as Studied by Electron Spin Resonance, Butterworth Scientific Publications, London 1968.
18. Portis, A. M., Physical Review, 91, 1071 (1953).
19. Slangen, H. J. M., Journal of Physics E: Scientific Instruments, 3, 775, (1970).
20. Burgess, V. R., Journal of Scientific Instruments, 38, 98 (1961).
21. Wyard, S. J., Journal of Scientific Instrumentation, 2, 769, (1965).
22. Dole, Malcolm, The Radiation Chemistry of Macromolecules, Volume I, Academic Press, New York, (1973) Chapter 1.
23. Parkinson, W. W. and O. Sisman, Nuclear Engineering and Design, 17, 247 (1971).
24. Charlesby, Arthur, Effect of Radiation on Materials, J. Harwood, editor, Reinhold Publishing Corporation, New York (1958), Chapter 10.
25. Dole, Malcolm, The Radiation Chemistry of Macromolecules, Volume II, Malcolm Dole, editor, Academic Press, New York, (1973), Chapter 6.
26. Brown, J. R. and J. H. O'Donnell, Journal of Applied Polymer Science, 19, 405 (1975).
27. Lyons, B. J. and F. E. Weir, Radiation Chemistry of Macromolecules, Volume II, Malcolm Dole, editor, Academic Press, New York (1973), Chapter 14.
28. Dole, Malcolm, The Radiation Chemistry of Macromolecules, Volume I, Malcolm Dole, editor, Academic Press, New York (1972), Chapter 14.
29. Waterman, D. C. and M. Dole, Journal of Physical Chemistry, 74, 1913 (1970).
30. Dole, Malcolm and Mitio Inokuti, Journal of Chemical Physics, 39, 310 (1963).

31. Iwasaki, Machio, Takahisa Ichikawa, and Toshi, Ohno, Journal of Chemical Physics, 50, 1984 (1969).
32. Dole, Malcolm, C. Hsu, V. M. Patel, and G. N. Patel, Journal of Physical Chemistry, 19, 2473, (1975).
33. Krasnansky, V. J., B. G. Ackhammers, and M. S. Parker, Society of Plastic Engineers, 1, 133 (1961).
34. Zimmerman, J., The Radiation of Macromolecules, Volume II, Malcolm Dole, editor, Academic Press, New York (1973), Chapter 7.
35. Krasnansky, V. J., M. S. Parker, and R. E. Forin, The Journal of Physical Chemistry, 70, 40 (1966).
36. Zimmerman, J. Journal of Polymer Science, 43, 193 (1960).
37. Flory, P. J., Journal of the American Chemical Society, 62, 1561, (1940).
38. Memetea, T. and V. Stannett, Polymer, 20, 469. (1979).
39. Araki, K., D. Campbell, and D. T. Turner, Journal of Polymer Science, A4, 2597 (1966).
40. Turner, D. T., The Radiation Chemistry of Macromolecules, Volume II, Academic Press, New York (1973), Chapter 8.
41. Stannett, V., T Memetea, M. Dole, J. Salik, Journal of Polymer Science, Letters Edition, 16, 63 (1978).
42. Patel, V. M., G. N. Patel, N. Gvozdec, C. S. Hsu, and M. Dole, Journal of Polymer Science, Polymer Physics Edition, 19, 467, (1978).
43. Brown, J. R. and J. H. O'Donnell, Journal of Applied Polymer Science, 23, 2165 (1979).
44. Lyons, A. R., M. C. Symons, J. K. Yandell, Makromolekulare Chemie, 157, 103(1972).
45. Colichman, E. L. and J. D. Strong, Modern Plastics, 35, 180, (1957).
46. Overall, Derrick, Polymer Letters, 1, 37 (1963).
47. Smith, W. V., and B. E. Jacobs, Journal of Chemical Physics, 37, 141 (1962).
48. Johnson, David R., Walter Y. Wen, and Malcolm Dole, Journal of Physical Chemistry, 77, 2174 (1973).

49. Poole, Charles P. Jr., Electron Spin Resonance, A Comprehensive Treatise as Experimental Technique, Interscience Publishers, New York (1967).
50. Morgan, R. J. and J. E. O'Neal, American Chemical. Division of Organic Coatings and Plastic Chemistry, 38, 485-490 (1977).
51. Walsh, W. K. and H. A. Rutherford, Textile Research Journal, 37, 89 (1967).
52. Carter, H. G., K. G. Kibler, and J. D. Reynolds, Fundamental and Operational Glass Transition Temperatures of Composites Resins and Adhesive, Advanced Composite Materials - Environmental Effects, ASTM STP 658, Vinson, J. R. Ed., American Society for Testing and Materials, 1978. pp. 84-97.
53. Brown, I. M. and T. C. Sandrecski, Polymer Preprints, 22, 284 (1981).
54. Morgan, Robert J. and James E. O'Neal, Journal of Materials Science, 12, 1966 (1977).
55. Mijovic, Jovan and J. A. Koutsky, Polymer, 20, 1095 (1979).
56. Lind, A. C., Polymer Preprints, 22, 333 (1981).

APPENDICES

TABLE A
Experimental Data for Radical Concentration Build-up and
Decay for 1/2 MeV Electron and 1.33, 1.17 MeV Gamma Irradiated Samples

Figure A-1			Figures 7 & 8			Figures 7 & 8			Figures 6 & 9			Figures 6 & 9		
dose*	time** (min)	spins/g x 10 ⁻	dose	time (min)	spins/g x 10 ⁻	dose	time (min)	spins/g x 10 ⁻	dose	time (min)	spins/g x 10 ⁻	dose	time (min)	spins/g x 10 ⁻
E(10)	0	6	E(10)	0	2.7	E(60)	0	11.3	0	0	0.1	G(53.4)	0	29
E(20)	0	8	E(10)	5	2.4	E(60)	5	5.3	G(4.7)	0	5.6	G(53.4)	6.2	12
E(30)	0	12	E(10)	100	2.0	E(60)	100	4.3	G(12.4)	0	9.4	G(53.4)	8.28	11
E(60)	0	17	E(10)	200	2.0	E(60)	200	4.4	G(12.4)	1.0	8.4	G(53.4)	10.89	11
E(70)	0	17	E(10)	1220	1.8	E(60)	1220	3.57	G(12.4)	3.8	7.7	G(53.4)	13.23	10
E(90)	0	17	E(20)	0	5.9	E(100)	0	10.2	G(12.4)	6.3	6.9	G(53.4)	19.23	9.5
E(100)	0	19.5	E(20)	5	3.7	E(100)	5	6.4	G(12.4)	11.6	7.0	G(53.4)	29.23	9.5
E(110)	0	20	E(20)	100	2.7	E(100)	100	4.3	G(12.4)	16.6	6.6	G(53.4)	39.58	9.2
E(150)	0	20.5	E(20)	200	2.7	E(100)	200	5.2	G(12.4)	22.6	6.8	G(53.4)	49.9	9.4
			E(20)	1220	1.8	E(100)	1220	4.5	G(12.4)	36.7	6.9	G(53.4)	67.3	9.3
			E(30)	0	5.7	E(130)	0	16.4	G(12.4)	64.7	6.4	G(53.4)	93.6	9.4
			E(30)	5	5.2	E(130)	5	7.4	G(12.4)	106.7	6.7	G(53.4)	77.5	9.9
			E(30)	100	4.8	E(130)	100	7	G(12.4)	172.7	6.4	G(53.4)	126.7	9.5
			E(30)	200	4.0	E(130)	200	5.9	G(12.4)	296.7	6.5	G(53.4)	176.7	8.7
			E(30)	1220	2.8	E(130)	1220	5.4	G(12.4)	417.9	4.5	G(53.4)	234.4	8.0
			E(50)	0	6.6				G(12.4)	735.9	5.7	G(53.4)	474.7	7.05
			E(50)	5	5.1				G(12.4)	1635.3	4.4	G(53.4)	747.7	6.6
			E(50)	100	4.3				G(12.4)	2740.3	4.2	G(53.4)	1697.0	6.5
			E(50)	200	4.2				G(16.6)	0	8.9	G(53.4)	2210.0	4.7
			E(50)	1220	3.0				G(23.4)	0	12			
									G(29.2)	0	13			
									G(34.5)	0	15			
									41.75	0	17			

*G: gamma radiation (1.33 and 1.17 MeV), E: 1/2 MeV electrons, dosage in Mrads in parenthesis.
 **time at ambient temperature (not including irradiation time for 1/2 MeV electron irradiated samples)

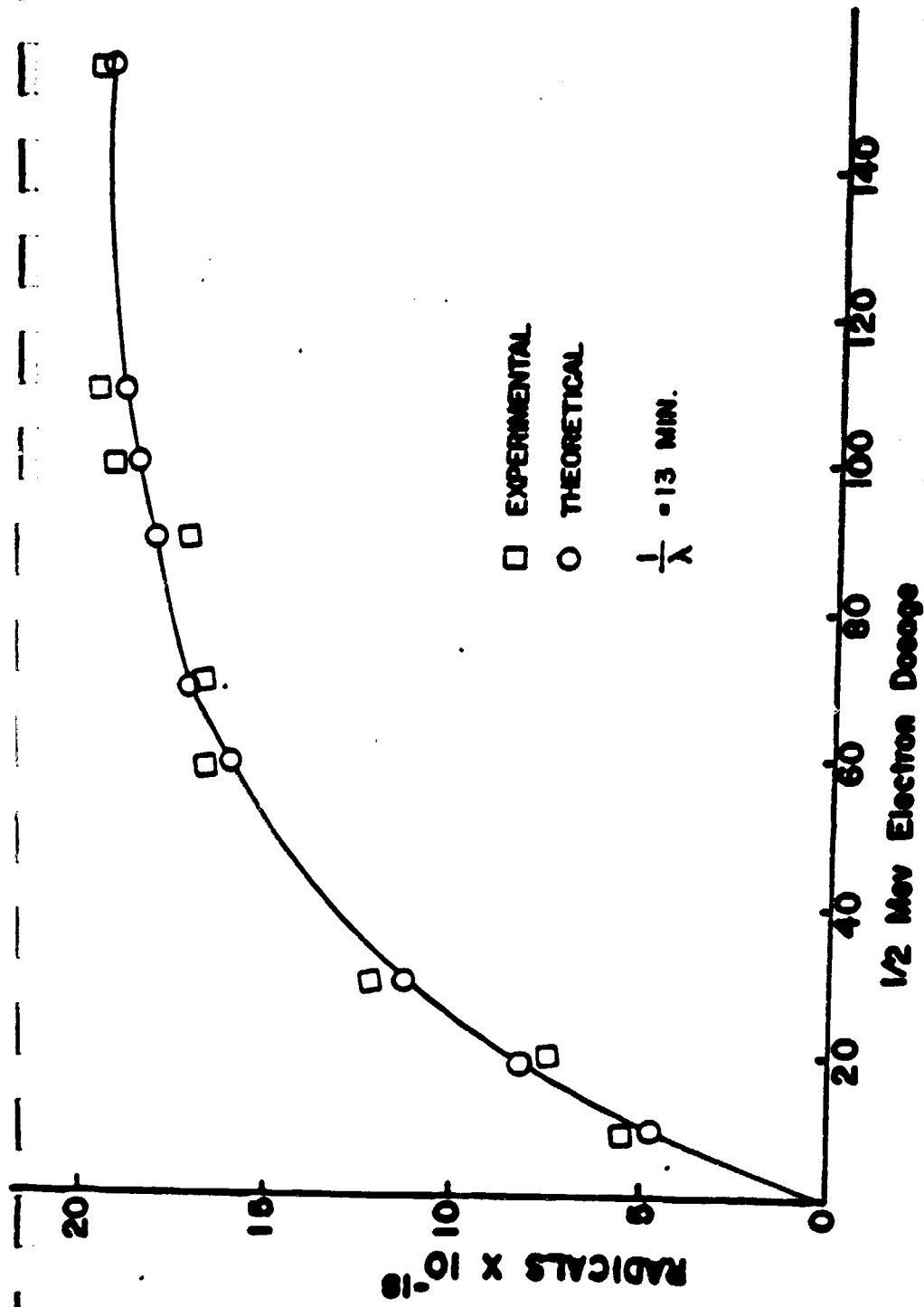


Figure A. Radical build-up curve for 1/2 Mev electron radiation an alternate experiment

Abstract Submitted
for the Phoenix Meeting of the
American Physical Society

March, 1981

Condensed Matter
Number 60

Polymer Physics

Electron Spin Resonance Studies of Epoxy Samples Exposed to 1/2 Mev Electrons. * K. SCHAFFER, R. D. GILBERT, J. D. MEMORY, and R. E. FORNES, N. C. State U. --Samples of cured epoxy resin (MY 720/DDS Ciba Geigy) have been irradiated at room temperature with 1/2 Mev electrons to dose levels up to 5×10^7 rads. These samples were stored at cryogenic temperatures following exposure until measurements were made on an x-band ESR spectrometer. Under the conditions of measurements, radical concentrations leveled off around 10^{19} radicals/cm³. Before irradiation, cured samples showed the presence of radicals with concentrations ranging from 10^{17} - 10^{18} radicals/cm³. The spectra of both cured and irradiated resins are asymmetric. Details of the results will be given. Estimates of radical decay rates will also be presented as well as ESR measurements at 77°K.
*Supported by NASA Grant NSG 1562.

Prefer Poster Session

R. E. Fornes
N. C. State University
School of Textiles
P. O. Box 5006
Raleigh, N. C. 27650